IMPACT OF CLIMATE CHANGE ON LOCAL HYDROLOGY: A CASE STUDY IN AGULA'E WATERSHED, TEKEZE BASIN, NORTH ETHIOPIA

MSc. THESIS

TSEGAY AREGAWI ATSBAHA

HAWASSA UNIVERSITY, HAWASSA, ETHIOPIA

NOVEMBER, 2017

IMPACT OF CLIMATE CHANGE ON LOCAL HYDROLOGY: A CASE STUDY IN AGULA'E WATERSHED, TEKEZE BASIN, NORTH ETHIOPIA

TSEGAY AREGAWI ATSBAHA

A THESIS SUBMITTED TO THE SCHOOL OF WATER RESORCE ENGINEERING, HAWASSA UNIVERSITY INSTITUTE OF TECHNOLOGY, SCHOOL OF GRADUATE STUDIES

HAWASSA UNIVERSITY, HAWASSA, ETHIOPIA

IN PARTIAL FULFILLMENT OF THE REQUIREMENTS FOR THE DEGREE OF MASTER OF SCIENCE IN WATER RESOURCE ENGINEERING (SPECIALIZATION: IRRIGATION AND DRAINAGE ENGINEERING)

NOVEMBER, 2017

SCHOOL OF GRADUATE STUDIES

HAWASSA UNIVERSITY

We, the undersigned, members of the Board of Examiners of the final open defense by TSEGAY AREGAWI ATSBAHA have read and evaluated his thesis entitled "Impact of Climate Change on Local Hydrology: A Case Study in Agula'e Watershed, Tekeze basin, North Ethiopia", and examined the candidate. This is, therefore, to certify that the thesis has been accepted in partial fulfillment of the requirements for the degree of Master of Science in Irrigation and Drainage Engineering.

_____.	_____	_____
Name of the Chairperson	Signature	Date
_____.	_____	_____
Name of Major Advisor	Signature	Date
_____.	_____	_____
Name of Internal Examiner	Signature	Date
_____.	_____	_____
Name of External examiner	Signature	Date
_____.	_____	_____
SGS Approval	Signature	Date

Final approval and acceptance of the thesis is contingent upon the submission of the final copy of the thesis to the School of Graduate Studies (SGS) through the School Graduate Committee (SGC) of the candidate's department.

Date: _____

Declaration

I, TSEGAY AREGAWI ATSBAHA, do hereby declare that this MSc. thesis is my original work and has not been presented for a degree in any other university, and all sources of material used for this thesis have been duly acknowledged.

Name: TSEGAY AREGAWI ATSBAHA Signature: _____

Acknowledgement

First and foremost, thanks to the Almighty God for granting me His limitless care, love and blessings all along the way.

I would like to express my greatest gratitude to the Ethiopia Minister of Water, Irrigation and Electricity (MoWIE), for awarding me the scholarship. I would like to extend my thanks to Tigray Regional State Bureau of Water Resource as well as Kilte Awla'elo Wereda Administration office for their contribution during the process of my scholarship award and for all their unlimited supports during my stay.

My sincere gratitude goes to my major advisor Dr. Mulugeta Dadi and my co-advisor Dr. Sirak Tekleab for all their regular advice and guidance from the starting until the completion of the work. I express my deepest appreciation for their encouragement and moral support throughout the study period. I am also so much thankful to Mr. Gebremedhin Gebremeskel Haile, who thought me the GIS, WetSpa and SDSM models from the grass root level and guided me throughout the progress of the work. Without his encouragement, guidance, and help; this work would have not taken this shape. I feel fortunate to have got this opportunity to work with him.

Last but not least, I would like to thank all my friends and family members back home who were spiritually with me, and gave me the strength to finalize my duties successfully. I am highly indebted to all my classmates and staff members of School of Water Resource Engineering for their ideal and technical supports and those who gave me their comments, ideas, shared love and happiness.

I am also thankful to the Ministry of Water and Energy Hydrology and GIS departments and the National Meteorological Service Agency Mekelle branch and then Ethiopian Mapping Agency who have been very helpful and cooperative in providing me the necessary data.

Abbreviations and Acronyms

AR5	Fifth Assessment Report
ASTER	Advanced Spaceborne Thermal Emission and Reflection Radiometer
BCM	Billion Cubic Meter
BoWRD	Bureau of Water Resource Development of Tigray Regional State
CGCM1	Canadian Global Coupled Model
CMIP5	Coupled Model Inter Comparison Project Phase 5
DDC	Data Distribution Center for IPCC
DEM	Digital Elevation Model
Eqn.	Equation
EMA	Ethiopian Mapping Agency
GCM	General Circulation Model
GHG	Greenhouse Gases
GIS	Geographic Information System
GPS	Geographic Positioning System
HadCM3	Hadley Center Coupled Model, Version 3
hpa	hectopascal
IPCC	International Panel on Climate Change
m.a.s.l	meters above sea level
MPIM	Max-Planck Institute for Meteorology
MoWIE	Ministry of Water, Irrigation and Electricity, Ethiopia
NMSA	Ethiopian National Meteorological Service Agency

NGO	Non-Governmental Organizations
P	Precipitation
PET	Potential Evapotranspiration
RCM	Regional Climate Model
SDSM	Statistical Downscaling Model
SRES	Special Report for Emission Scenario
SRTM	NASA Shuttle Radar Topographic Mission
TGCIA	Task Group on Scenarios for Climate and Impact Assessment
Tmax	Maximum Temperature
Tmin	Minimum Temperature
Tmn	Mean Temperature
USDA	United State Department of Agriculture
UTM	Universal Transverse Mercator coordinate system
WetSpa	Water and Energy Transfer between Soil, Plants and Atmosphere
WMO	World Meteorological Organization
WoWRME	Wereda office of Water Resource, Mining and Energy

Table of Content

Acknowledgement I
Abbreviations and Acronyms II
Table of Content IV
List of Tables VII
List of Figures VIII
List of Appendix Tables IX
List of Appendix Figures X
Appendix Equations X
ABSTRACT XI
1 INTRODUCTION 1
1.1 General 1
1.2 Statement of the Problem 2
1.3 Objective of the Study 3
1.3.1 General Objective 3
1.3.2 Specific Objectives 3
1.4 Research Questions 3
1.5 Scope of the Study 3
1.6 Significance of the study 3
2 LITERATURE REVIEW 4
2.1 Water Resources and Hydrologic Cycle 4
2.2 Hydrological Models and Their Classification 5
2.2.1 Hydrological Model Selection Criteria 7
2.2.2 WetSpa Hydrological Model 7
2.2.3 Climate Change 8
2.2.4 Impacts of Climate Change on Water Resources Availability 11
2.2.5 Climate Models Application 12
2.2.6 HadCM3/GCM Climate Model 13
2.2.7 Climate Data Downscaling Approach 14

2.2.8 Sensitivity Analysis, Calibration and Validation of Models 15
3 MATERIALS AND METHODS 17
3.1 Description of the Study Area 17
3.1.1 Location and Topography 17
3.1.2 Climate 19
3.1.3 Land Use Land Cover 20
3.1.4 Soil Type 21
3.1.5 Water Resources 22
3.1.6 Socio-Economic Activities 22
3.2 Data Sources 22
3.2.1 Meteorological Data 22
3.2.2 Hydrological Data 23
3.2.3 Spatial Data 23
3.2.4 Climate Scenario Data 23
3.2.5 Software Models and Other Materials 24
3.3 Methods 24
3.3.1 Filling Missed Data and Checking Data Consistency 24
3.3.2 Estimation of Potential Evapotranspiration 25
3.3.3 Thiessen Polygon Map Preparation 25
3.3.4 WetSpa Extension Model Input Parameters Preparation 27
3.3.5 WetSpa Extension Model Application Processes 31
3.3.6 HadCM3/GCM Model Application 38
3.3.7 SDSM Model Input Data and Downscaling 38
3.3.8 Statistical Downscaling Model (SDSM) 40
3.3.9 Estimation of Impact of Climate Change on Water balance Components 45
3.4 Sensitivity Analysis, Calibration and Validation of WetSpa Model 46
3.5 General Approaches of the Study 47

4 RESULTS AND DISCUSSION 49
4.1 Climate Change Scenario 49
4.1.1 Predictors and Predictand Relation 49
4.1.2 Baseline Scenarios 50
4.1.3 Future Period Scenario 53
4.2 WetSpa Model Results 57
4.2.1 Sensitivity Analysis for WetSpa Model Parameters 57
4.2.2 WetSpa Model Calibration and Validation 58
4.2.3 Simulation of Base Period Water Balance of Agula'e Watershed 62
4.3 Climate Change Impact on Future Water Availability 63
5 CONCLUSIONS AND RECOMMENDATIONS 66
5.1 Conclusions 66
5.2 Recommendations 67
REFERENCES 69
APPENDICES 75

List of Tables

Table 3. 1. Common Threshold Values of Gridded Maps' Parameters.....30
Table 3. 2. Monthly Mean Observed P, PET and Discharge (q), Value (1993-2003) 31
Table 3. 3 . List of NCEP Predictor Variables (Wilby and De Smedt, 2004) 42
Table4. 1.Selected Potential Predictors for Each Predictand of the Climate Station…….49
Table 4. 2. Observed and Downscaled Mean Annual Baseline Rainfall (mm).....53
Table 4. 3. Change in Climate for Future Periods A2a and B2a Scenarios.....56
Table4. 4.The WetSpa Model Global Parameters Calibration Results 58
Table 4. 5. Calibration and Validation Periods Water balance (mm).....59
Table 4. 6. Calibration and Validation Periods Model Performance Evaluation Results (%) 60
Table 4. 7.Base Period Measured and Simulated (A2a and B2a) Water Balance (mm) 62
Table 4. 8. Baseline and Future Period Mean Annual P, ET and SR for A2a and B2a Scenarios.....64

List of Figures

Figure 2. 1. Hydrologic Cycle (https://water.usgs.gov/edu/watercycle.html) 5
Figure 2. 2. Hydrological Model Types and Classification (Lenhart et al, 2002) 6
Figure 2. 3. WetSpa Model Schematic Structure at pixel Cell (Liu & De Smedt, 2004) 8
Figure 2. 4. The Four IPCC SRES Scenario Storyline (IPCC-TGICA, 2007) 11
Figure 3. 1.Location Map of Agula'e Watershed…….. 17
Figure 3. 2. Slope Map of Agula'e Watershed 18
Figure 3. 3. Mean Monthly Climatic Data of the Study Area. 19
Figure 3. 4. Land Use Land Cover Map of Agula'e Watershed.....20
Figure 3. 5. Soil Map of Agula'e Watershed.....21
Figure 3. 6. Grid Map of Meteorological Stations Thiessen Polygon 26
Figure 3. 7.WetSpa Model Local Parameters Parameterizations (Liu, 2004) 29
Figure 3. 8Africa Window from Which the Study Area Grid Box is Located. 39
Figure 3. 9. Climate Scenario generation (Wilby and Dowson, 2004).....44
Figure 3. 10. General Structural Set Up of the Study. 48
Figure4. 1. Observed and Downscaled Mean Monthly Tmax for Baseline (1992-2015)…..51
Figure4. 2.Observed and Downscaled Mean Monthly Tmin for Baseline (1992-2015) 52
Figure 4. 3. Observed and Downscaled Mean Monthly Precipitation (1992-2015).....52
Figure 4. 4. Change in Tmax for Future Time Horizons for A2a and B2a Scenarios. 53
Figure 4. 5. Change in Tmin for Future A2a and B2a Scenarios. 54
Figure4. 6. Change in Precipitation for Future A2a and B2a Scenarios.....56
Figure 4. 7. Change in PET for A2a and B2a of the Future Time Horizons 57
Figure 4. 8. (a) Model Calibration Hydrograph (1/1/1993 – 1/31/1999) and (b) Model Validation Hydrograph (1/1/2000 - 1/1/2003) for Agula'e Watershed. 61
Figure 4. 9: Change in (a) P, (b) ET, and (c) SR for A2a & B2a for Future Time Horizons. 65

List of Appendix Tables

Appendix Table1. Location and Data Availability of Hydro Meteorological Stations 75
Appendix Table2. Mean Monthly Observed Hydro Climatic Inputs for WetSpa (1993-2003) 75
Appendix Table3. Mean Monthly Observed Hydro Climatic Data for SDSM Inputs (1992-2015) 76
Appendix Table4. Mean Annual Baseline and Future Time Horizons Climatic Values for A2a and B2a Scenarios of Agula'e Watershed 77
Appendix Table5. Simulated Baseline and Future Period Water Balance Components (mm) for A2a Scenario of Agula'e Watershed 78
Appendix Table6. Simulated Baseline and Future Period Water Balance Components (mm) for B2a Scenarios of Agula'e Watershed 79
Appendix Table7. Default Values of Land Use Land Cover Parameters (Wilby and Dawson, 2004) 80
Appendix Table 8. Watershed Land Use Classification Determination 81
Appendix Table9. Default Values of Soil Parameters (Wilby and Dawson, 2004) 81
Appendix Table 10. Watershed Soil Classification Determination 82
Appendix Table11. Model Performance Evaluation Criteria 82

List of Appendix Figures

Appendix Figure1. Double Mass Curve of Precipitation of Atsbi and Wukro. 82
Appendix Figure 2. (a) Calibration (1992-2006) and (b) Validation (2007-2015) Graph of SDSM for Tmax and Tmin for Wukro and Mekelle Airport Stations.....83
Appendix Figure 3. Observed and Downscaled Climatic Data (1992-2015).....84
Appendix Figure4. Trends of (a) Precipitation, (b) Tmax and (C) ET for A2a and B2a Emission Scenarios for 1992-2099.....85
Appendix Figure5.USDA Triangular Soil Texture Classification (George et al, 2013)).....86

Appendix Equations

Appendix Equation1. Estimation of Extraterrestrial Radiation (FAO56, 1998) 86

ABSTRACT

Climate change, nowadays, has significant impact on the water resource system of an area. This study was conducted in Agula'e watershed, Tekeze river basin, Ethiopia, using Water and Energy Transfer through Soil, Plants and Atmosphere (WetSpa) hydrological model and General Circulation Model (GCM) aiming at estimating the impact of climate change on water availability of the study area. By making proper calibration, precipitation and temperature outputs of HadCM3 coupled atmosphere-ocean GCM model for A2a (medium to high) and B2a (Medium to low) SRES emission scenarios were downscaled using Statistical Downscaling Model (SDSM). In 2020s, precipitation, maximum temperature, minimum temperature and potential evapotranspiration will increase by 1.03%, 0.55%, 0.09% and 2.08% for A2a emission scenario and 1.84%, 0.42%, 0.1% and 2.14% for B2a emission scenario respectively. In 2050s, it will be expected an increment trend in precipitation, maximum temperature, minimum temperature and potential evapotranspiration by 0.8%, 1.63%, 0.12% and 3.13% for A2a emission scenario and 3.06%, 1.19%, 0.10% and 2.95% for B2a emission scenario. In 2080s, precipitation, maximum temperature, minimum temperature and potential evapotranspiration will increase by 1.05%, 3.17%, 0.15% and 4.63% % for A2a emission scenario and 1.35%, 1.97%, 0.13% and 3.65% for B2a emission scenario. In the future period, the overall trend in aerial mean maximum temperature, precipitation, and potential evapotranspiration show positive increment by 2.5%, 0.96%, and 3.28% under A2a and 2.05%, 2.12% and 2.91% for B2a emission scenario respectively. Minimum temperature will not show significance change for both emission scenarios. The model showed that precipitation and actual evapotranspiration results in average increment trend by 1.03%, 0.78% and 1.03% for A2a scenario and 1.93%, 3.05% 1.34% for B2a scenario in 2020s, 2050s and 2080s time horizons respectively. In the future time horizons, actual evapotranspiration will be increased by 6.96%, 7.01% and 7.42% under A2a scenario and by 8.49%, 9.91% and 8.25% for the B2a scenario. The overall trend of precipitation and actual evapotranspiration value will increase by 0.95% and 7.13% under A2a emission scenario and 2.11% and 8.88% under B2a emission scenario respectively. Surface runoff will generally has decrement trend in all the future periods and will averagely decrease by 71% for A2a and70% for B2a emission scenarios.

Key Words: Climate Change, GCM, HadCM3, SDSM, Water balance, WetSpa

1 INTRODUCTION

1.1 General

Water is the most important natural resource required for the survival of all living species. As the available amount of water is limited and not spatially and uniformly distributed in relation to the population needs, proper management of water resources is essential to satisfy the current demands as well as to maintain sustainability. Water resources planning and management now a days is becoming difficult due to the conflicting demands from various stakeholders, increasing population, rapid urbanization, climate change shifts hydrologic cycle, the use of high-yielding but toxic chemicals in various land use activities, and increasing incidences of natural disasters (Yakob, 2009).

Climate change can cause significant impacts on water resources by changing the hydrological cycle. The change on temperature and precipitation components of the cycle can have a direct consequence on the evapotranspiration component quantity, and on quality and quantity of the runoff component. Consequently, the spatial and temporal availability of water resource, or in general the water balance, can be significantly affected, which clearly influences its impact on sectors like agriculture, industry and urban development, etc (Hailemariam, 1999).

Ethiopia is considered as the water tower of ‘’East Africa’’ due to the availability of abundant water resources. The country has an estimated potential of 2.6 BCM groundwater (Awulachew et al., 2007) and 111 BCM surface water (Yazew, 2005) which indicates that there is ample amount of water with regard to its geographical positions. Ethiopia has 12 river basins and most of the basins are suitable both for Irrigation and hydropower developments. But the country was not using its water resource potential as needed for development (Awulachew et al., 2007).

However, this water potential has threatened by the climate change impact. Soliman, 2009; Melesse, 2011 indicated that climate change in the Upper Blue Nile basin of Ethiopia would occur and would shift and reshape the annual and seasonal climate patterns and variation in rainfall, reduced reservoir yield and erratic rainfall. Similarly, Kebede et al., (2013) indicated that an increasing trend of annual maximum temperature and annual future rainfall with seasonal variations was observed in Baro-Akobo Basin and Nile Basin. Variations in frequency, distribution and intensity of rainfall are now a common phenomenon in the country. Furthermore, the country’s economy is mainly dependent on rain-feed agriculture,

as a result people remains food insecure and the country is not possibly to achieve the millennium development goals in all sectors if it likely to continue.

For proper planning, development and utilization of water resource projects, a good understanding and accurate estimation of the watershed water balance is a basic issue. This can be achieved by properly studying the response of a basin for a given quantity of rainfall falling on the upstream area. A good estimation of the transformation of rainfall in to the different forms of water resource need an adequate and properly recorded historical data, such as stream flow and rainfall gauging stations. The provision of such recording instruments and stations at every proper site is capital intensive and difficult specially for developing countries like Ethiopia.

In Tigray, significant achievements were made on the development of agriculture through irrigation by using seasonally harvested runoff using earth dams, river stream diversion structures and by pumping from ground water. However, most of the implemented schemes are not serving their function well because of over flooding and under inflow problems (Zenebe, 2009).

This research aims at estimating the impact of climate change on water balance components like surface runoff and evapotranspiration over Agula'e watershed which is a tributary of Geba catchment using WetSpa (Water and Energy Transfer between Soil, Plants and Atmosphere) hydrological model. Besides, the research assesses the climate change impact on the catchment hydrological response using GCM climate models.

1.2 Statement of the Problem

The change in climate causes a significant impact on the water resources by disturbing the normal hydrological processes. One of the most significant potential consequences of changes in climate may be alterations in regional hydrological cycles and subsequent changes in river flow regimes and evapotranspiration. Climate change can affect multiple features of water resources like quantity and quality, high and low flow extremes, timing of events, water temperature (Kim et al., 2008).

Due to underdevelopment of the water resources, the Ethiopian people have been exposed to major problems such as impacts of drought and flood, shortage of clean water supply and inadequate energy supply (Hailemariam, 1999).

Agula'e watershed shows large temporal and spatial variation in river discharge due to variation of climatic characteristics of rainfall and other bio-physical characteristics in the area. The main problem of the watershed is water shortage during the dry season and higher

water discharge during the rainy season which needs proper prediction, planning and management systems.

1.3 Objective of the Study

1.3.1 General Objective

The general objective of the study is to estimate the impact of climate change on hydrological response in Agula'e watershed, Tekeze basin, north Ethiopia.

1.3.2 Specific Objectives

- To develop climate change scenarios using Statistical Downscaling Model (SDSM)
- To simulate water balance components in selected period at watershed level using WetSpa hydrological model.
- To estimate the impact of climate change on hydrological response (evapotranspiration and surface runoff) of the watershed by comparing the present and future water availability.

1.4 Research Questions

So as to meet the above objectives the research questions for this study were:

- What are the climate change scenarios of a watershed?
- What is the water resources potential of the selected watershed?
- What is the effect of climate change (temperature and precipitation increase or decrease) on surface runoff and evapotranspiration of the watershed?

1.5 Scope of the Study

The study focused on the estimation of impact of temperature and precipitation parameters change on surface runoff and evapotranspiration water balance components in Agula'e watershed.

1.6 Significance of the study

It is believed that this study focuses in Agula'e watershed but the result will benefit the local community and districts, NGOs and the policy makers as well. Moreover, the application of hydrological and climate models involved in this study were verified, so that it could be considered for other related future studies in other similar regions.

2 LITERATURE REVIEW

2.1 Water Resources and Hydrologic Cycle

Water the most powerful substance for living things has a 1.36 BCM of water resources globally, from this 97.2% is salt water mainly found in oceans and 2.8% is available as freshwater worldwide (Raghunath, 2006). Even if the water available in water bodies, such as ocean and great lakes stores plenty of water in amount, it is not directly useful for human beings. The immediate use of water for human being is the one stored as groundwater and the remaining water found in land surfaces, lakes and streams as fresh water.

Ethiopia is quite rich in water resources and its drainage pattern is of great importance for its neighboring countries. The country has 12 river basins with a total annual surface water resources estimated at 111 BCM, of which 68% is in the Nile basin (Yazew, 2005).Again, the country annually releases 122 BCM of water as runoff volume (Awulachew et al., 2007). Abay, Baro-Akobo, Omo-Gibe and Tekeze are the main river basins in Ethiopia contributing runoff to the neighboring countries.

The hydrologic cycle is a circulation of water in the lithosphere, hydrosphere, biosphere, cryosphere and atmosphere. It is defined as the pathway of water as it moves in its various phases through the atmosphere to the earth, over and through the land, to the ocean, and back to the atmosphere (Karamouz, 2003). Hydrologic cycle can be considered as a closed water circulation system for earth as there is no loss or gain of water in the cycle. The hydrological cycle is also defined as a water transfer cycle occurs continuously in nature; at which the phenomena of evaporation and evapotranspiration, precipitation and runoff takes place during the water transfer system (Raghunath, 2006). Water first evaporates from the surfaces of water bodies and transpires from surface of vegetation as a vapor. Then the vapor rises up to the atmosphere, condenses and forms clouds and then through process of condensation, results precipitation back to the earth surface. This precipitation flows as runoff to oceans or infiltrates into the soil to be a groundwater or evaporates from the surface. This system of water circulation starts its cycle again and again and will not be stop at one time (Figure 2.1).

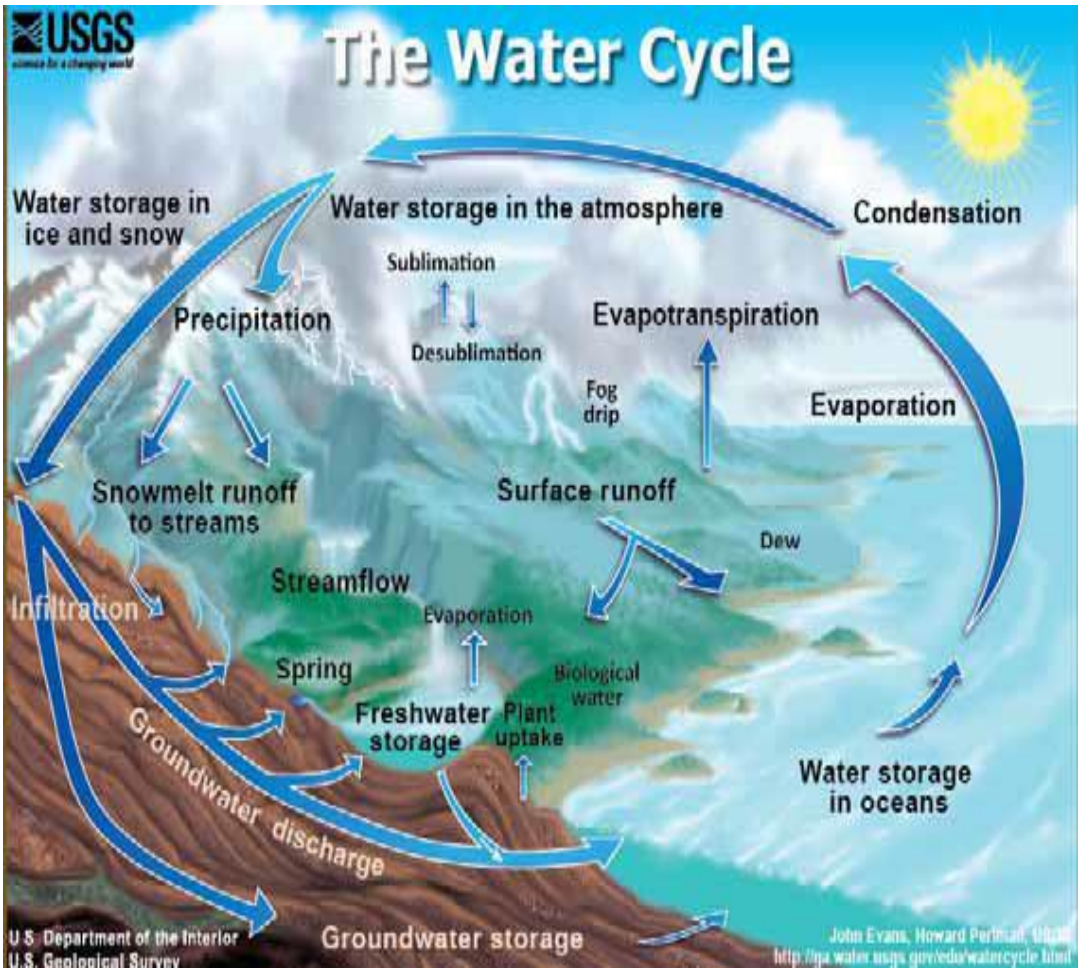

Figure **2. 1**. Hydrologic Cycle (https://water.usgs.gov/edu/watercycle.html)

2.2 Hydrological Models and Their Classification

Hydrologic models are simplified and conceptual representations of a part of the hydrologic cycle. They are primarily used for hydrologic prediction and for understanding hydrologic processes.

According to (Lenhart et al, 2002), models are used to establish a baseline when data is not available and to estimate long term impacts that are not easy to calculate. Hydrological model are classified in different aspects. These classification methods can be defined as short term and long term, small scale and large scale, forecasting and predictive, physical and mathematical, continuous and discrete, descriptive and conceptual, lumped and distributed, deterministic and stochastic. Classifications are generally based on the method of representations of the hydrological models. Physical based models are based on our understanding of the physics of the hydrological process.

Generally, physical based models are used to simulate wide range of complex process. Depending on the character of the result obtained, model are classified as stochastic, if one

or more of the variables in a mathematical model are regarded as random variables having distributions in probability and deterministic, when all the variables are considered to be free from random variation (Lenhart et al, 2002).

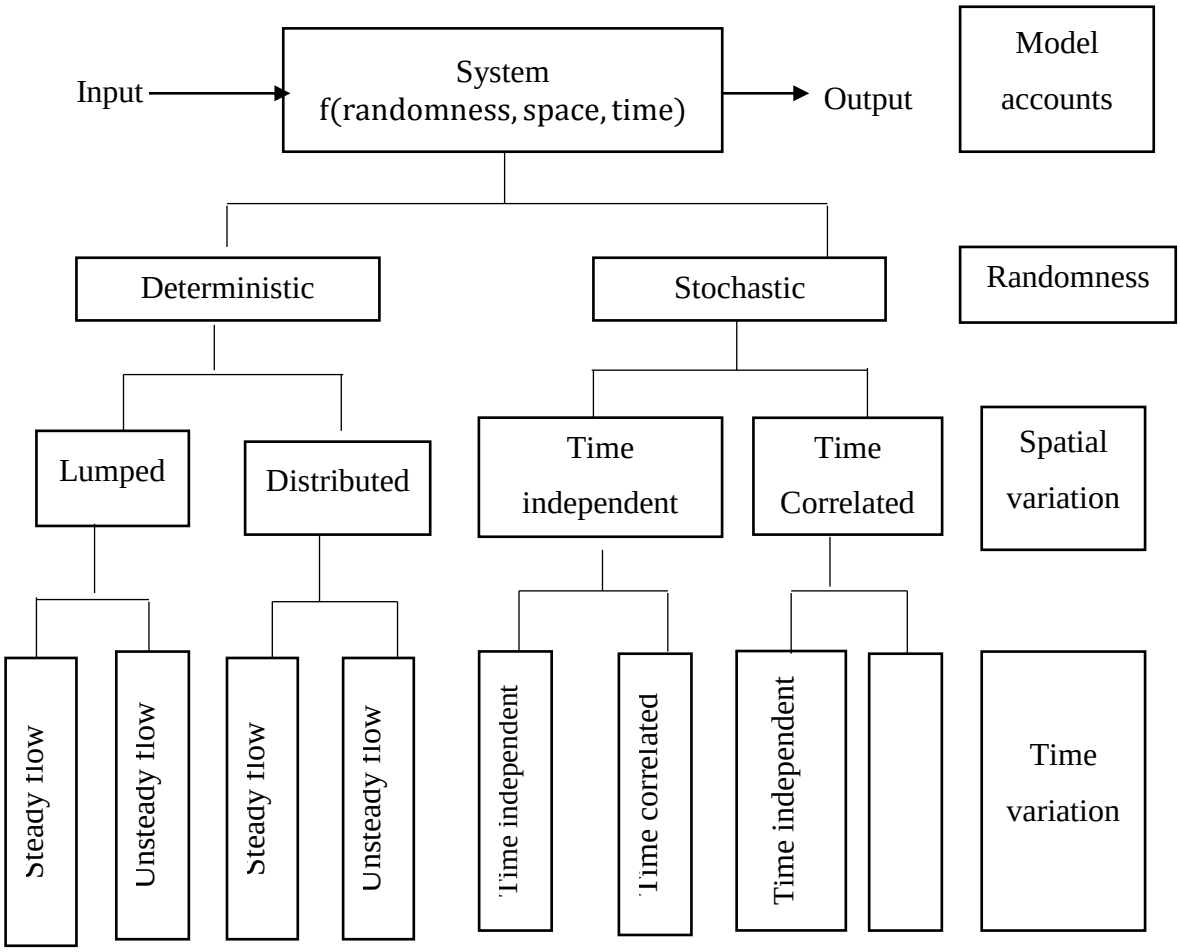

Figure 2. 2. Hydrological Model Types and Classification (Lenhart et al, 2002)

Without going into too much detail, deterministic hydrologic models can be classified into three main categories (Cunderlik 2003).

1. Lumped Models: - parameters of lumped hydrologic models do not vary spatially within the basin and thus, basin response is evaluated only at the outlet, without explicitly accounting for the response of individual sub-basins. The impact of spatial variability of model parameters is evaluated by using certain procedures for calculating effective values for the entire basin. The most commonly employed procedure is an area weighted average (Haan et al., 1982).

2. Semi-distributed Models: - parameters of semi-distributed (simplified distributed) models are partially allowed to vary in space by dividing the basin into a number of smaller sub-basins.

3. **Distributed Models**: - parameters of distributed models are fully allowed to vary in space at a resolution usually chosen by the user. Distributed modeling approach attempts to incorporate data concerning the spatial distribution of parameter variations together with computational algorithms to evaluate the influence of this distribution on simulated precipitation-runoff behavior. Distributed models generally require large amounts of data for parameterization in each grid cell. However, the governing physical processes are modeled in detail, and they can provide the highest degree of accuracy if properly applied.

2.2.1 Hydrological Model Selection Criteria

There are a number of criteria which can be used for choosing the right hydrologic model. These criteria are mainly dependent on the use of the model. Furthermore, some criteria are also user dependent such as: personal preference; computer operation system; input/output management and structure etc. Cunderlik (2003) suggested four criteria for the selection of hydrological models. These are: (1) Required model outputs for the needed purpose, (2) different hydrological processes that are required to be modeled for the desired purpose, (3) availability of input data and (4) Price and/or availability of the model.

Depending upon the above selection criteria for this research Water and Energy Transfer between Soil, plants and atmosphere (WetSpa) hydrological model was selected.

2.2.2 WetSpa Hydrological Model

WetSpa is an acronym for Water and Energy Transfer between Soil, Plants and Atmosphere. It is a physically based and distributed hydrological model for predicting the Water and Energy Transfer between Soil, Plants and Atmosphere on regional or basin scale and daily time step, developed in the Vrije Universiteit Brussels, Belgium (Wang et al., 1997 and Batelaan et al., 1996). The model is physically based and simulates hydrological processes of precipitation, interception, depression, surface runoff, evapotranspiration, infiltration, percolation, interflow, groundwater flow (Liu and De Smedt, 2004). It simulates continuously both in time and space, for which the water and energy balance are maintained on each raster cell (Figure 2.3).

The model uses an input data of historical climate data (precipitation and potential evapo-transpiration, minimum and maximum temperatures) and discharge data and grid maps of

elevation, land use and soil type of higher resolution on each pixel. According to Liu and De Smedt (2004) and Nyenje and Batelaan (2009), river flow hydrographs, soil moisture, infiltration rates, groundwater recharge, surface water retention and runoff are the main outputs of the WetSpa model.

Different authors (Jaroslaw and Batelaan, 2011; Nyenje and Batelaan, 2009; Bahrem and De Smedt, 2008; Adem and Batelaan, 2006) have studied hydrological processes and associated impacts of climate change using the WetSpa distributed hydrological model. As a result, these researches were shown remarkable results through using this model. The model is user friendly and easily compatible with ArcView GIS software. This is the reason why WetSpa model was selected in this research for the estimation of water resource potentials.

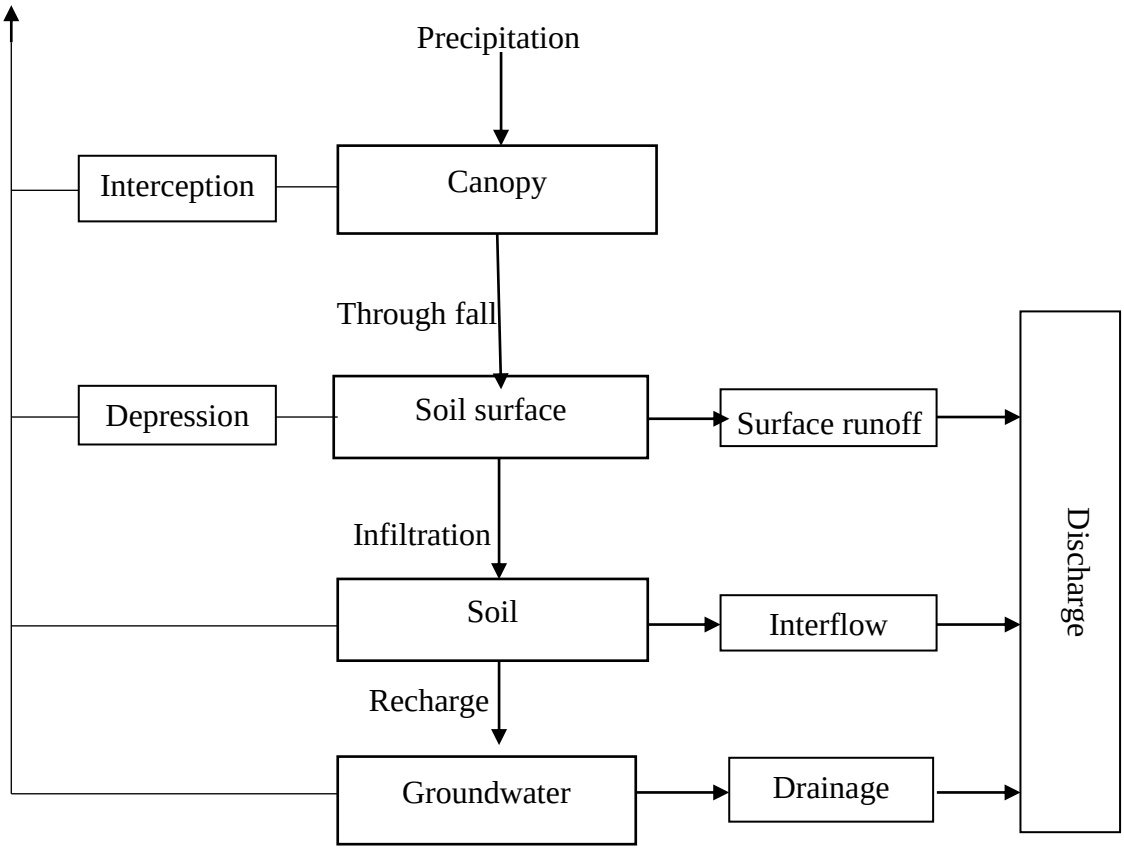

Figure **2. 3**. WetSpa Model Schematic Structure at pixel Cell (Liu & De Smedt, 2004)

2.2.3 Climate Change

Climate change, now a day, is an overwhelming global issue. Everything, living or non-living in one or another way relates with the subject of climate change. The main

symptoms of global warming are increase in temperature of the atmosphere, oceans, and landmasses of planet earth. At present earth appears to be facing a rapid warming, which mostly believed as results of human-induced activities. The chief cause of this warming is thought to be the burning of fossil fuels, such as coal, oil, and natural gas from which greenhouse gases are released into the atmosphere (IPCC, 2013).

Global warming is caused by a collective evident that, it is due to a distinct anthropogenic influence (Bates et al., 2008; Casper, 2010; IPCC, 2013). Even though the natural hazards are contributing to the climate change, human-induced climate changes are tremendously higher and complex.

Since the 1990s the Intergovernmental Panel for Climate Change (IPCC, 1990, 1996, 2001, 2007 and 2013) released different climate change related assessment reports. These reports have forced policy makers to take action on the climate change that threatens the earth. Meanwhile, based on the new evidence of climate change from different independent scientific analyses, from observations of the climate system, paleoclimate archives, theoretical studies of climate processes and simulations using climate models, the IPCC has released a new assessment report. As a result, the Working Group I of the IPCC's released its Fifth Assessment Report (AR5) outlined and has projected the climate change that could be occurred on the globe during the twenty first century.

Therefore, according to IPCCs Fifth Assessment Report (IPCC, 2013), warming of the climate system is unequivocal, and since the 1950s, many of the observed changes are unprecedented over decades to millennia. The atmosphere and ocean have warmed, the amounts of snow and ice have diminished, sea level has risen, and the concentrations of greenhouse gases have increased. Moreover, each of the last three decades has been successively warmer at the Earth's surface than any preceding decade since 1850. In the Northern Hemisphere, 1983–2012 was likely the warmest 30-year period of the last 1400 years. Ocean warming dominates the increase in energy stored in the climate system, accounting for more than 90% of the energy accumulated between 1971 and 2010. The rate of sea level rise since the middle ninetieth century has been larger than the mean rate during the previous two millennia. Over the period 1901 to 2010, global mean sea level rose by 0.19m.

The Special Report for Emission Scenarios (SRES) are climate change projections developed by IPCC starting from 1990s (IPCC-TGICA, 2007; IPCC, 2013). These scenarios are due to emissions from greenhouse gases, aerosol precursor which produces

global warming. The emission scenarios were developed based on population, economy, technology, energy and land use as deriving forces.

According to IPCC, (IPCC-TGICA, 2007; IPCC, 2013) the emission scenarios are categorized in to four families based on their unique characteristics for the twenty first century.

A1 Scenario: Globalization

This family is characterized by very rapid economic growth with new and efficient technology use and global population will peaks in middle century and declines afterwards. There is convergence among regions capacity building, increase in social and cultural interactions. The A1 scenario family develops into three groups that describe alternative directions of technological change in the energy system. These are: Fossil intensive (A1FI) that emphasis on fossil fuels, Non - fossil energy sources (A1T), or Balance across all energy sources (A1B).

A2 Scenario: Regionalization

The storyline and scenario describes a very heterogeneous world with a self-reliance and preservation of local identities. It is characterized by continuously increasing population and regionally oriented economic development.

B1 Scenario: Globalization, sustainability and equity globalized and extensive (sustainable development).

It has similar trends of global population increment with A1 storylines. The scenario is characterized with rapid changes in economic structures towards a service and information economy and resource-efficient technologies.

B2 Scenario: **Regionalization,** sustainability and equity regional, extensive (mixed green bag). This scenario family describes the world emphasizes on local solutions to economic, social, and environmental sustainability. Global population increases at a rate lower than A2 storylines with intermediate levels of economic development. It has less rapid and more fragmented change in technology than A1 and B1 scenarios.

These emission scenarios are used as indicating future likely impacts of climate change ranged from the relatively less effect of climate change to the very worst effect of climate change conditions that would possibly appear in the future.

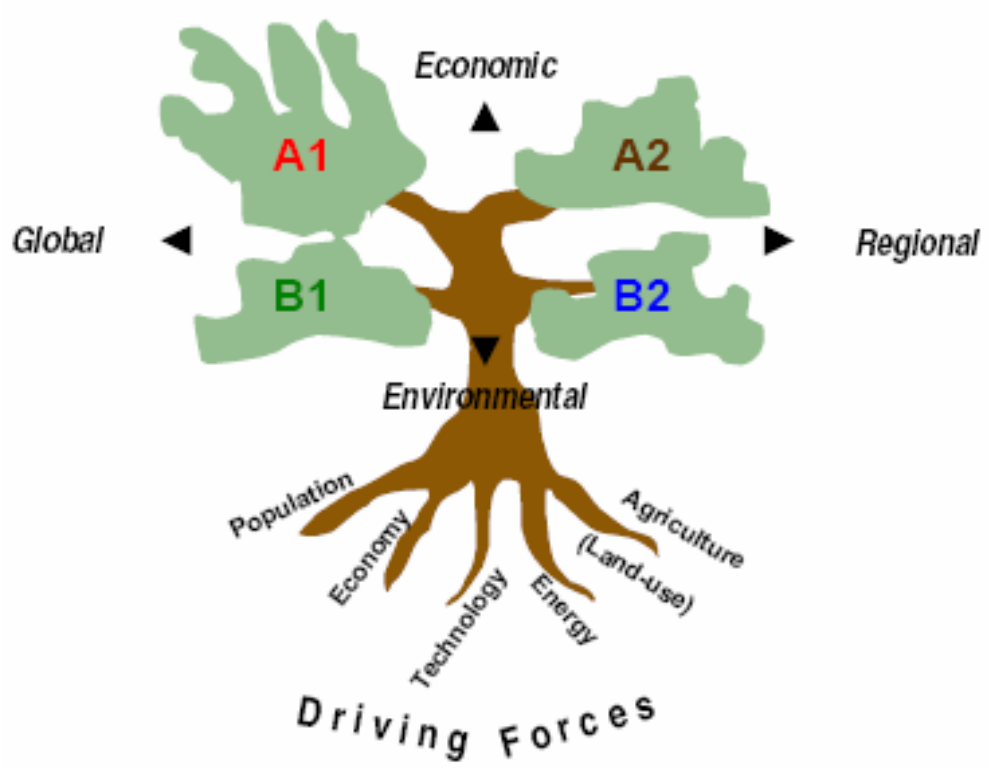

Figure **2. 4**. The Four IPCC SRES Scenario Storyline (IPCC-TGICA, 2007)

2.2.4 Impacts of Climate Change on Water Resources Availability

The hydrologic cycle is highly sensitive to climate change because the components of the hydrologic cycle are vulnerable to changing climate. Findings of the IPCC (2013), strongly suggests that climate change has the potential to deteriorate the water resources availability, water quality and water supplies. Being the most potable water for mankind, if groundwater severely affected by the climate change, it goes to threaten the survival of life on earth.

In many countries of the world the use of water resources for public water supply constitutes important potable water. However, many factors affect future surface water and groundwater resources as changes in precipitation and temperature regimes, coastal flooding, urbanization, land use changes and changes in cropping system (Holman, 2006). Similarly, Herrera-Pantoja and Hiscock (2008) concluded that future climate may present a decrease in potential water resources that will increase stress on local and regional water resources. As a result attention to the water resources remains inevitable to overcome the problem with some solutions.

Many studies have been conducted to investigate the impact of climate change in water resources, stream flow and land use/land cover changes in the upper Blue Nile of Ethiopia. In the upper Blue Nile of Ethiopia, climate change has observed to shift the time of rainfall patterns and of the groundwater recharge and temperature has observed increasing trends in the mean annual, rainy and dry seasons (Tekleab et al., 2013). These changes contributed tremendous effects on the water potentials in Ethiopia.

Therefore, water is a vital resource and awareness needs to be raised on its vulnerability to overexploitation, pollution and most importantly, climate change (Nyenje and Batelaan, 2009). The change in climate and weather conditions in the atmosphere and hydrosphere leads to changes in precipitation patterns and this leads to changes in hydrologic cycle and finally causes changes in catchment hydrologic response. As surface and groundwater recharge has direct relationships with rainfall, the more rainfall rains the more water run on surface and infiltrates the soil to the groundwater and hence the more water stored in the water table.

2.2.5 Climate Models Application

Models are physical or mathematical simplifications of natural systems used for analyzing physical parameter data. Model also describes equations of physical systems and techniques that provide a means for quantitative explorations or predictions that will help in decisions making. Projections of changes in the climate system are made using a hierarchy of climate models ranging from simple climate models, to models of intermediate complexity, to comprehensive climate models and Earth System Models (IPCC, 2013). Moss et al.,(2010) described climate models as there are a wide variety and complexity of models which are numerical representations of the earth's natural systems used to study how climate responds to changes in natural and human-induced perturbations.

These climate models help to project future likely impacts of climate change in the planetary system. Hydrologic cycle is one among others that is highly influenced by climate change as a result of effects on the atmospheric and rainfall patterns. Consequently, there are improvements on the climate models in time and space in predicting future climate change impacts that may occur. According to IPCC (2013) Climate models have improved since the fourth assessment report for future prediction and for studying preceding climatic situations. In the climate system models are known to reproduce observed continental and local scale atmospheric patterns and trends over many decades.

2.2.6 HadCM3/GCM Climate Model

Climate models, both global and regional, are the primary tools that aid in our understanding of the many processes that govern the climate system (S. Jeremy et al., 2007). Climate is one of the most challenging geophysical systems to simulate because of the number of interacting components and the wide range of time and spatial scales of relevant processes and their complexity (Laprise R., 2008). Global climate models also known as general circulation models (GCMs) are the most complex of climate models, since they attempt to represent the main components of the climate system in three dimensions. According to many research GCMs are the vital resource used to perform climate change experiments regionally, globally and very fine scale up to point climate pattern from which climate change scenarios are derived; but they have main drawbacks because of their course resolution. Most of the time they lack producing of current climate trend including the most important statistical parameters like mean and variance.

GCMs depict the climate using a three dimensional grid over the globe, typically having a horizontal resolution of between 250 and 600 km, 10 to 20 vertical layers in the atmosphere and sometimes as many as 30 layers in the oceans. Their resolution is thus quite coarse relative to the scale of exposure units in most impact assessments. Moreover; many physical processes, such as those related to clouds, also occur at smaller scales and cannot be properly modeled. Instead, their known properties must be averaged over the larger scale in a technique known as parameterization. This is one source of uncertainty in GCM-based simulations of future climate (IPCC-TGICA 2007). A few years ago, GCMs only included a representation of the atmosphere, the land surface, sometimes the ocean circulation, and a very simplified version of the sea ice. Nowadays, GCMs take more and more components into account, and many new models now also include sophisticated models of the sea ice, the carbon cycle, ice sheet dynamics and even atmospheric chemistry (Goosse H. et al., 2013).

HadCM3 is a coupled atmosphere-ocean GCM developed at the Hadley Centre of the United Kingdom's National Meteorological Service that studies climate variability and change. It includes a complex model of land surface processes, including 23 land cover classifications; four layers of soil where temperature, freezing, and melting are tracked; and a detailed evapotranspiration function that depends on temperature, vapor pressure, vegetation type, and ambient carbon dioxide concentrations (Palmer et al., 2004).

The atmospheric component of the model has 19 levels with a horizontal resolution of 2.5° latitude by 3.75° longitude, which produces a global grid of 96 x 73 cells. This is equivalent to a surface resolution of about 417 km x 278 km at the equator, reducing to 295 km x 278 km at 45° latitude. The oceanic component of the model has 20 levels with a horizontal resolution of 1.25° latitude by 1.25° longitude. HadCM3 has been run for over a thousand years, showing little drift in its surface climate. Its predictions for temperature change are average; and for precipitation increase are below average (IPCC, 2001).

The HadCM3 GCM output data can be downscaled to the local level data using latitudinal locations of a target site. Hence, the HadCM3 outputs can be used for studies in Ethiopia. Due to this, Kebede et al., (2013) has used this HadCM3 climate model to model climate system in Baro-Akobo river basin of Ethiopia and revealed successful work. Zeray Abraham, (2006) also used the GCM climate model to assess climate change impact on water resource potential in Lake Zeway of Awash river basin, Ethiopia. Based on this, for this study HadCM3 GCM was used as a source of large scale data for the determination of future climate change projections and likely water resources impacts by downscaling these large scale HadCM3 GCM outputs in to the basin of interest.

2.2.7 Climate Data Downscaling Approach

Downscaling of climate scenarios refers to a process of taking global information on climate response to changing atmospheric composition, and translating it to a finer spatial scale that is more significant in the context of local and regional impacts. There are software available today for downscaling of General Circulation Model (GCM) and Regional Climate Model (RCM) datasets and makes ready to use for future climate change predictions. According to Wilby et al., (2004) and Wilby and Dawson, (2007), Dynamical and Statistical downscaling approaches are the two general approaches used in downscaling regional climate models.

Dynamical downscaling approach is a method of extracting local scale information by developing and using regional climate models (RCMs) with the coarse general circulation models (GCM) data used as boundary condition. It simulates climate processes over the region of locality or basin with a high resolution regional climate model. Dynamical downscaling involves the nesting of a higher resolution Regional Climate Model (RCM) within a coarser resolution GCM. The RCM uses the GCM to define time varying atmospheric boundary conditions around a finite domain, within which the physical dynamics of the atmosphere are modeled using horizontal grid spacing's of 20–50

km (Wilby and Dawson, 2007). RCMs have been developed that as it can attain horizontal resolution finer and finer as compared to GCMs resolution. The advantage of dynamical downscaling method is that a regional climate model can simulate local fine scale feedback processes which are not verified with statistical methods. Performance of this downscaling is, however, highly dependent on the quality data input.

Statistical downscaling approach, assures development of statistical relationships between local climate variables (predictands) and large scale climate variables (predictors) (Wilby et al., 2004). It also provides an application of predictands-predictor relationships to the output of GCM and RCM experiments to simulate local climate characteristics. The most common method of statistical downscaling is when predictands are simulated as a function of predictors. This kind of downscaling is useful especially for impact assessment modeling studies for reproducing different climatic statistics at basin or local level. Therefore, statistical downscaling models are used as a decision support tool to know whether or not the historical climate data available and the downscaled climate data have relationships through calibration and validation of the models.

According to Wilby et al., (2004), Wilby and Dawson (2007), Xu et al., (2005) and Kebede et al., (2014) the statistical downscaling model provides a consistent estimates of temperature extremes and precipitations in seasonal and site level, is easily computational, can easily be crafted and used for specific uses, direct regional incorporations of observational records, and uses basic standard statistical procedures.

Therefore in this study, the Statistical Downscaling Model (SDSM) was used to downscale future climate change scenarios, which was obtained from the output of General climate model in the watershed. Results of the SDSM were used as input to analyze the impact of climate change to water resources potentials.

2.2.8 Sensitivity Analysis, Calibration and Validation of Models

Sensitivity Analysis

Sensitivity analysis is a technique of identifying the responsiveness of different parameters involving in the simulation of a hydrological process. A hydrological model like WetSpa, which involves a wide range of data and parameters in the simulation process, calibration is quite a cumbersome task.

Sensitivity analysis is a method of minimizing the number of parameters to be used in the calibration step by making use of the most sensitive parameters largely controlling the

behavior of the simulated process. Sensitivity is expressed by a dimensionless index I, which is calculated as the ratio between the relative change of model output and the relative change of a parameter.

Calibration and Validation

Calibration is tuning of model parameters based on checking results against observations to ensure the same response over time. This involves comparing the model results, generated with the use of historic meteorological data, to recorded stream flows. In this process, model parameters varied until recorded flow patterns are accurately simulated.

Hydrological Models calibration like WetSpa run can be divided in to several steps. Among these Water balance and stream flow generation are the most important part. Refsgaard and Storm (1996) distinguished three types of calibration methods: the manual trial-and-error method, automatic or numerical parameter optimization method; and a combination of both methods.

Manual calibration is the most common and especially recommended in cases where a good graphical representation is strongly demanded for the application of more complicated models. However, it is very cumbersome, time consuming, and requires experience. Automatic calibration makes use of a numerical algorithm in the optimization of numerical objective functions. The method undertakes a large number of iterations until it find the best parameters. The third method makes use of combination of the above two techniques regardless of which comes first. For this study, this approach was considered.

For this study, one of the water balance component, stream flow, was used for calibration and validation purpose. Using independent discharge data, models are validated and the goodness of fit is quantified by the model bias (MB). Coefficient of determination (R2) and Nash-Sutcliff efficiency (NSE) between the observations and the final best simulations. Besides, Relative root mean square error (RRMSE) (Van Rompaey et al., 2001), mean absolute error (MAE) and Relative volume error (RVE) are calculated.

3 MATERIALS AND METHODS

3.1 Description of the Study Area

3.1.1 Location and Topography

Agula'e watershed covers an area of about 690 km^2 and has a perimeter of 236 km. Geographically it extends from 13^{0}32'N to 13^{0}53'N latitude and 38^{0}42'E to 39^{0}45'E longitude and situated in eastern and southern eastern zones of Tigray Regional State. Agula'e watershed is one main tributary of Geba catchment, which in turn is one tributary of the Tekeze river basin and it is bounded by Genfel(north and west), Ilala (south) sub catchments of Geba catchment, and by Danakil basin in east directions (Figure 3.1).

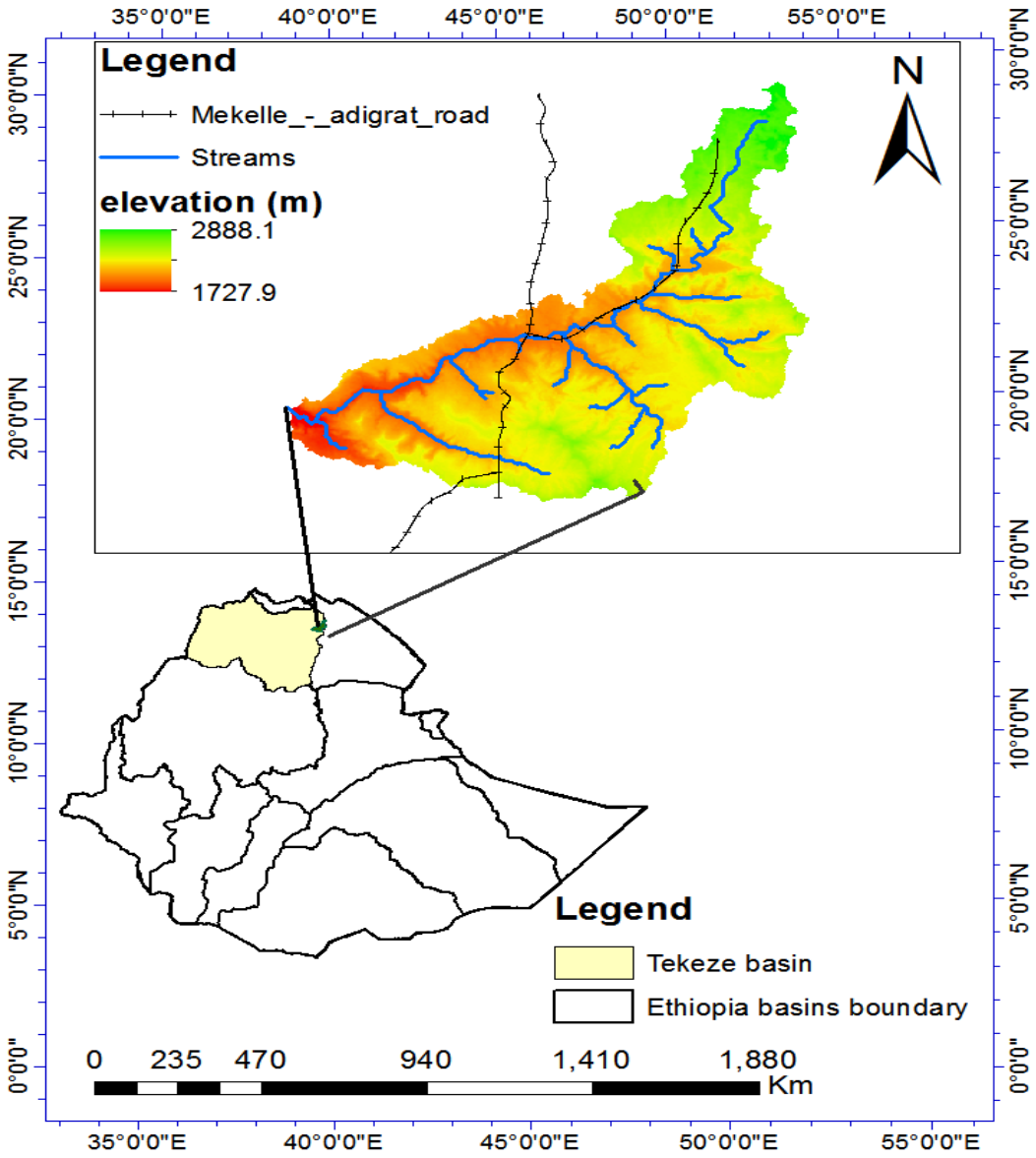

Figure **3. 1**.Location Map of Agula'e Watershed

The elevation of the watershed ranges from 1727.9 to 2888.9 m.a.s.l with the mean elevation of 2275.1 m.a.s.l. The longest flow path that stretches from the top upstream of the watershed to the gauging station along the watershed outlet is 72.6km in length. The slope of the watershed ranges from 0.01 to 149.2% with mean slope of 14.82% (Figure 3.2)

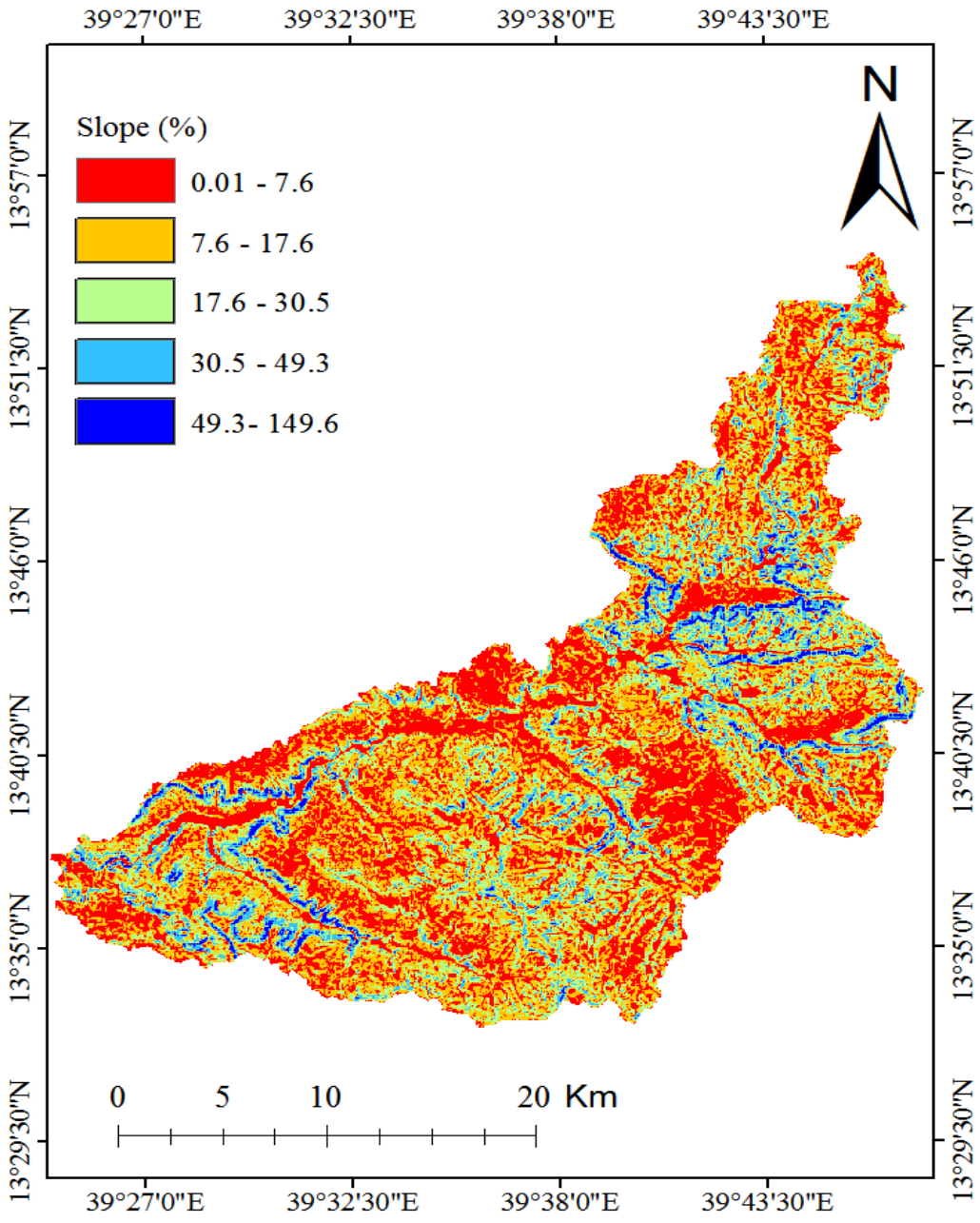

Figure 3. 2. Slope Map of Agula'e Watershed

3.1.2 Climate

From the statistical analysis of the climatic data taken from the four meteorological stations (Appendix Table 3), the annual rainfall amount of Agula'e watershed ranges from 300 to 800mmwith average annual precipitation of about 582mm.The highest amount of rainfall usually observed during July to August and the lowest is during October to January. Almost 78% of the annual rainfall amount occurs during the rainy season (Figure 3.3).

The rainfall of the study area shows pronounced annual as well as seasonal fluctuation, torrential and erratic in its nature. Variation in spatial and temporal distribution of rainfall often affects the agricultural sustainability of the area (Zenebe, 2009).

The result obtained from the statistical analysis of the data of the meteorological stations shows that the annual mean minimum, mean maximum and mean temperature of the study area are about 11.1℃, 25.5 ℃ and 18.8 ℃ respectively. The mean monthly minimum temperature of the area varies from 8.2℃ to 13.2 ℃ and mean monthly maximum temperature varies from 23.8 ℃ to 27.9 ℃. The minimum temperature is observed from November to January and April to June are the months that maximum temperature is observed.

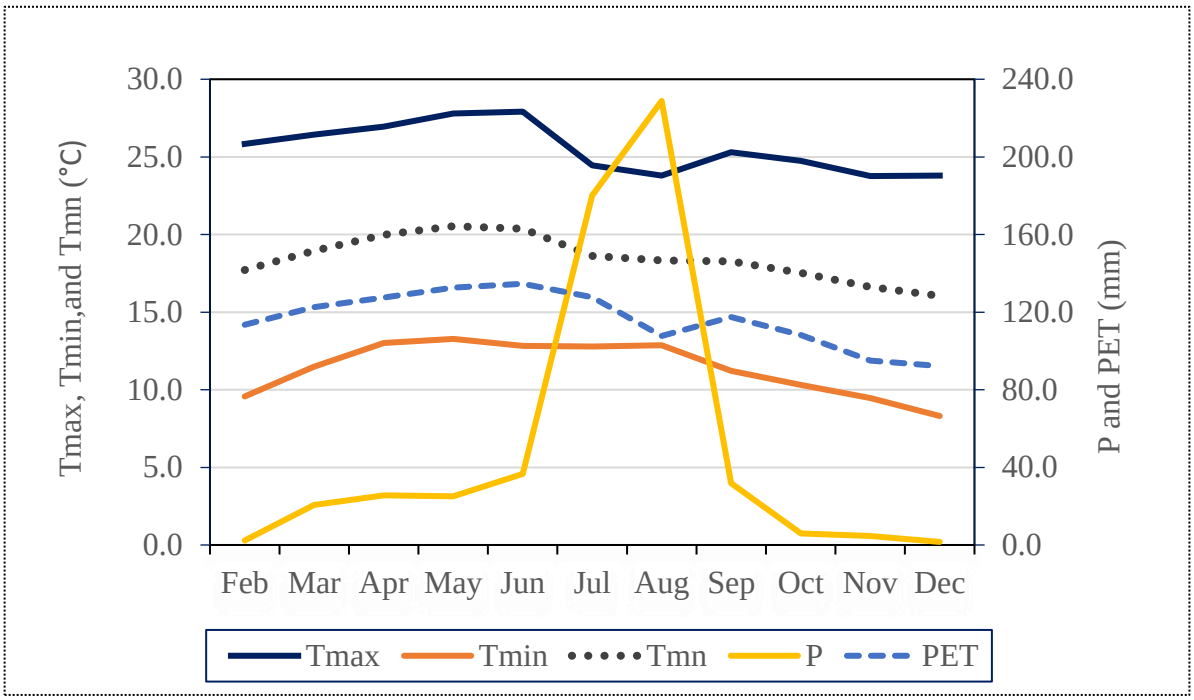

Figure **3. 3**. Mean Monthly Climatic Data of the Study Area.

The mean monthly potential evapotranspiration of Agula'e watershed ranges from95mm to 135mm with average value of 113mm (Appendix Table 4).The mean monthly potential evapotranspiration and mean monthly maximum temperature have maximum value from April to June and minimum value on November and December (Figure 3.3).

3.1.3 **Land Use Land Cover**

Based on the International Geographic-Biosphere Program (IGBM) land classification described in WetSpa model (Wilby and Dawson, 2004), the land use land cover of the area is classified as croplands, grasslands, closed shrublands, barren or sparsely vegetation forest lands and deciduous broadleaf forest (Appendix Table 10).

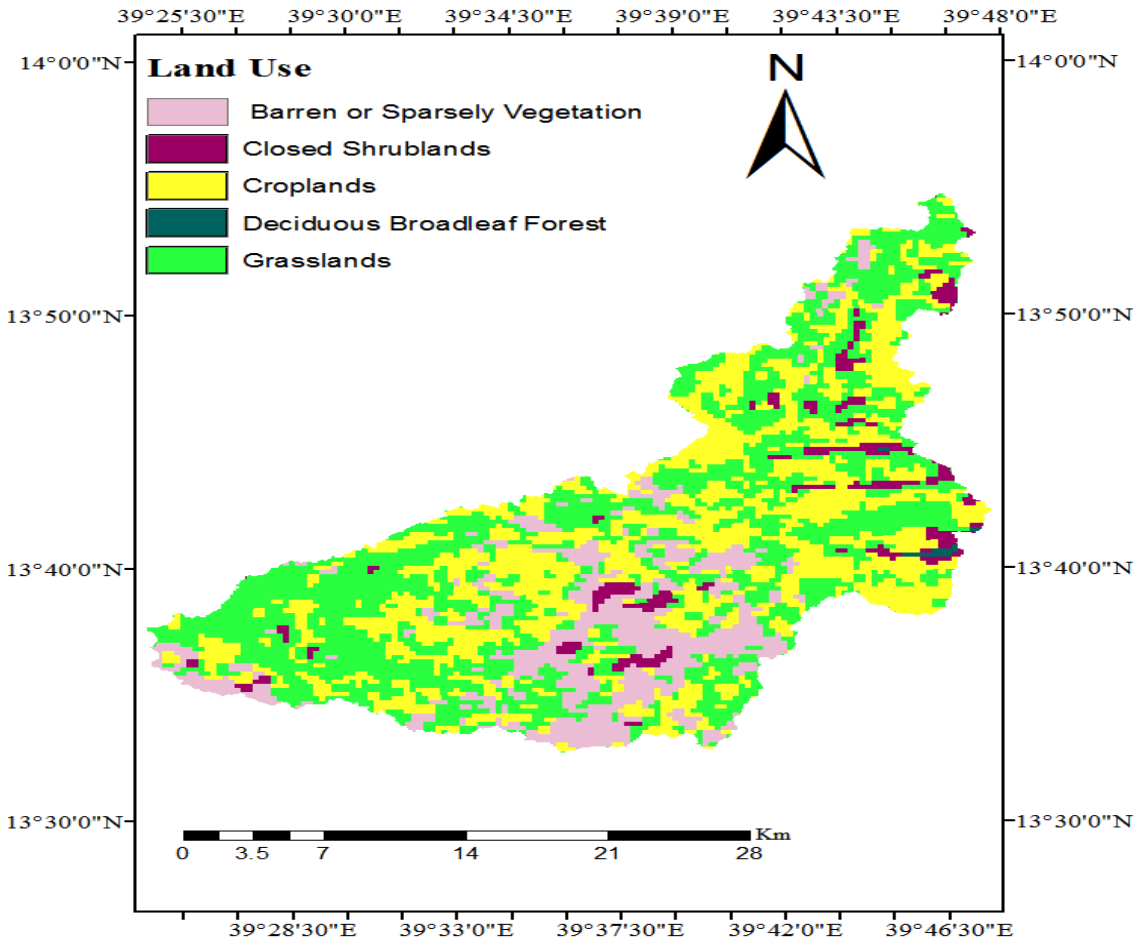

Figure **3. 4**. Land Use Land Cover Map of Agula'e Watershed

A large portion of the study area is covered by grasslands and croplands which covers about 304.38km^2 (44.07 %) and 247.304 km^2(35.76%) of the catchment area respectively. There are also barren or sparsely vegetation, closed shrublands, and deciduous broadleaf

forest that covers 107.82$km^2$29.91km^2 and 1.54km^2which all together covers about 20% of the total area (Figure 3.4).

3.1.4 Soil Type

The soil type of the study area was identified based on the Food and Agriculture Organization (FAO, 1998) of the United States Department of Agriculture soil texture classification system. The FAO soil type class was translated to textural soil class using the soil texture percentage (coarse, medium and fine) from the universal soil texture class (Appendix Table 9).

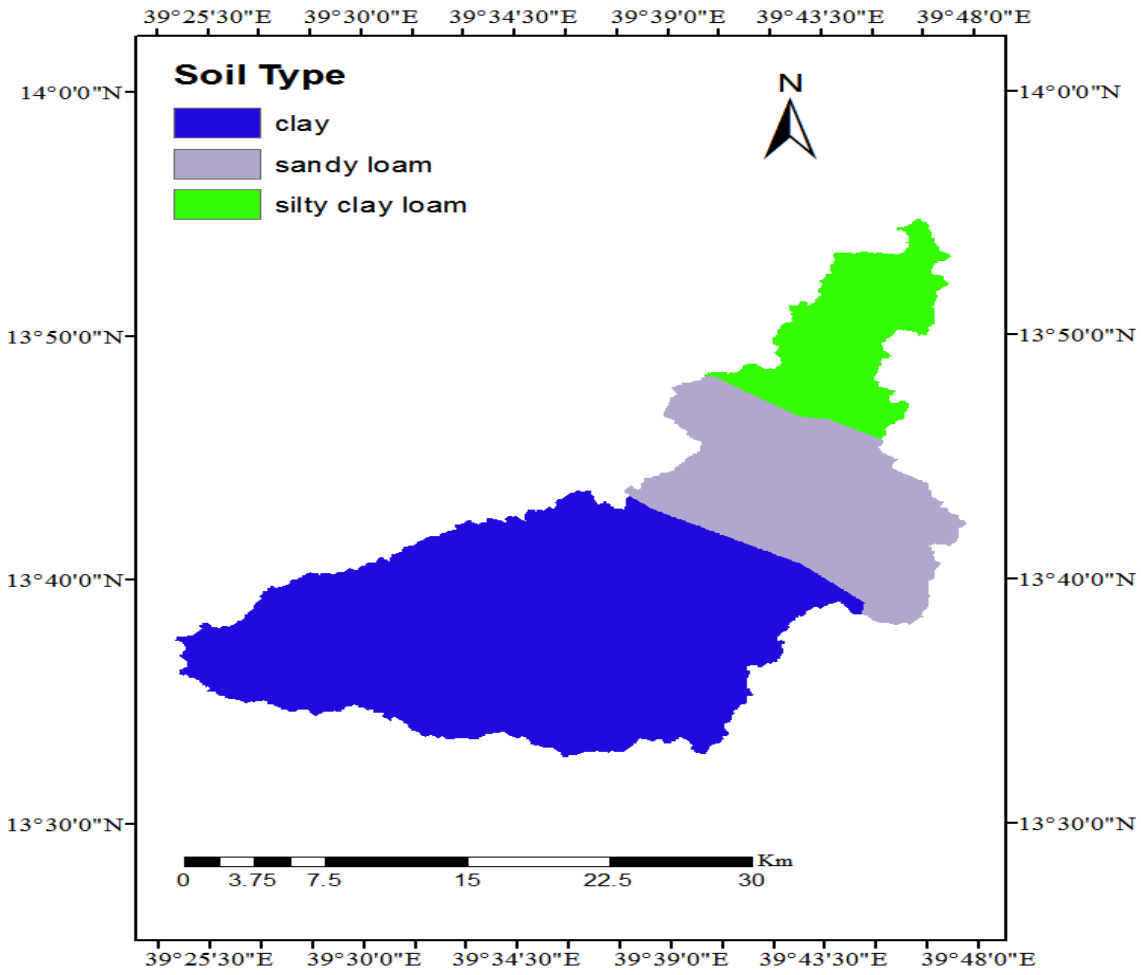

Figure **3. 5**. Soil Map of Agula'e Watershed

Accordingly, three dominant soil types were identified in the watershed. These soil types are silt clay loam (24.1%), sandy loam (13.0%) and clay (62.9%). Clay, sandy loam and silt clay loam soils are found in the lower, middle and upper part of the watershed respectively (Figure 3.5).

3.1.5 Water Resources

According to Ezana (1999) the area has different groundwater and surface water potentials. Shallow and deep groundwater exists in different aquifers which may be developed by means of hand dug wells and bore holes. Groundwater potential is generally high either in valley along water course or in plateau. A number of bore holes and hand dug wells have been constructed for water supply as well as irrigation purpose.

Recently, surface water harvesting structures like small earth dams and steam flow diversions have also been constructed for small scale irrigation purpose. Berki and Maimekden are larger main streams of Agula'e watershed.

Based on the analyzed value, the watershed has average annual discharge of about534m^3/s, with mean monthly value ranges from 2.8 m^3/s to 302 m^3/s (Table 3.2).The river discharge of the study area is highly dependent on seasonal rainfall variability. Hence, highest river discharge is measured during main rainy season of the year, which is from July to end of September. The average annual stream flow varies from about minimum of 200 m^3/s to the maximum discharge of 800 m^3/s

3.1.6 Socio-Economic Activities

According to Zenebe (2009), the main economic activities in the catchment are subsistence farming (mixed farming). Maize, bean, potato, onion, cabbage, wheat, teff, tomato, swiss chard, barley and lettuce are grown mainly in the area. Vegetable crops are grown through irrigation during the dry season in the lower cultivated area; since the lower catchment is the only area where cultivation in the dry season is possible. The average land holding of the farmers is estimated about 0.5ha per household. Livestock rearing is another important activity in the catchment and includes cattle, goat, sheep, donkey, chicken and bees. Bees and sheep are the main important production sectors to support the crop production.

3.2 Data Sources

3.2.1 Meteorological Data

Daily precipitation, maximum and minimum temperature data series of 1992-2015 were collected from National Metrological Service Agency (NMSA) of Mekelle branch office. These data were collected from four stations found in and around the study area. Atsbi station is found within the watershed and Wukro, Hagereselam and Mekelle Airport stations are located outside but near the watershed (Figure 3.6). These daily historical data from

1993-2003were used as input for the WetSpa hydrological model and that of 1992-2015 were used for SDSM climate model.

Daily potential evapotranspiration rates, used as input for WetSpa extension model, were estimated using the Hargreaves method. Meteorological stations are geo-referenced (latitude, longitude and elevation). Coordinate locations of the gauging stations were collected at field using the Geographical Positioning System (GPS) as described in Appendix Table 1.

3.2.2 Hydrological Data

Hydrological data of daily stream flow (1993-2003), required for performing sensitivity analysis, calibration and validation of the hydrological model, was obtained from the Ministry of Water, Irrigation and Electricity of Ethiopia (MoWIE). In Agula'e watershed there is only one discharge flow gauging station located at the out let of the catchment with longitudinal and latitudinal coordination of 544099E and1506599N respectively (Appendix Table1).

3.2.3 Spatial Data

Spatial data inputs for the models employed in this study such as landscape data including tabular and spatial land use information, and digital elevation data were gained from the Ethiopian Mapping Agency (EMA). The soil data were taken from MoWIE of Ethiopia. The soil and land use maps were originally obtained from FAO Africover data base website (http://www.africover.org./index.htm). This mapping was based on the satellite imagery data with a scale of 1:200,000. These values were then integrated into look up tables and linked to the map in the ArcGIS ArcView interface.

DEM (30m resolution), obtained from the elevation data bases of the Advanced Spaceborne Thermal Emission and Reflection Radiometer (ASTER)from website(http://aster.usgs.gov), was used to delineate the watershed and to analyze the drainage patterns of the land surface terrain. Sub basin parameters (slope gradient, slope length of the terrain) and the stream network characteristics (stream slope, stream length, and width) were derived from DEM.

3.2.4 Climate Scenario Data

The large scale present NCEP predictors and future climate scenario data of HadCM3 GCM outputs for the A2a and B2 SRES emission scenarios were downloaded from the website (http://www.cics.uvis.ca/scenarios/sdsm/select.cgi). Of the many GCM predictors, only HadCM3 has grid boxes, from where the data can be downloaded, for the study area. The

predictor variables of HadCM3 are provided on grid box basis of size 2.5° by 3.75° resolution. Therefore, by using the geographical coordinates of local predictands (centroid of the study area) the exact point of grid box has been known and used to download the predictor variable of the selected scenarios.

The predictand variables, taken from meteorological stations which were selected for this study, were located within one grid box. These climate scenario data were used to investigate the relative change between the current and future study period. The output of the future climate data was then used to estimate the hydrological impacts in the WetSpa extension model.

3.2.5 Software Models and Other Materials

ArcMap 10.1, (used for grid map preparation), ArcView GISV3.2 (used for grid parameters preparation), WetSpa Extension2009 (used for water balance simulation), and SDSM V4.2.9 (used for downscaling large scale predictors to local scale predictands) were employed in this study. Similarly, the materials GPS (for taking geographic-coordinate values in UTM, Latitude, and Longitude) and Laptop computer (for processing the models and writing the document) were used.

3.3 Methods

During the estimation of the water balance components of the study area and assessment of climate change on water availability on the area, the following basic steps were followed.

3.3.1 Filling Missed Data and Checking Data Consistency

Data was checked if there was missed data. The missed daily precipitation data were interpolated from the corresponding data available from nearby stations using Normal Ratio Method. This approach enabled an estimation of missing rainfall data by weighting the observation at N gauges by their respective annual normal rainfall using the following equation (Singh, 1994).

$$P_x = \frac{N_x}{M}\left[\frac{P_1}{N_1} + \frac{P_2}{N_2} + \frac{P_3}{N_3} + \cdots + \frac{P_m}{N_m}\right] \quad eqn.\ 3.1$$

Where: P_x = Daily precipitation of the target station. N_x = Average normal annual precipitation value for station X. N_1 , N_2 , N_3 …….. N_m = Average normal annual precipitation at the adjacent stations. P_1,P_2,P_3, …..,P_m = Daily storm precipitation at the adjacent stations. m= is the number of stations sites.

The same procedure was applied for the estimation of the missed data of temperature. Whereas the stream flow missed data was filled by using the average data from the same date of the past and next year's available records as there is only one recording station.

To check the data consistency of rainfall values from the rain gauge stations, double mass curve method was adopted to correct and adjust the reported rainfall values. The correction factor (C_f)was estimated by the ratio of the gradient of line before change (ΔS_1)to line gradient after change(ΔS_2). Hence, the result indicated as the data are consistent (Appendix Figure1).

3.3.2 Estimation of Potential Evapotranspiration

Even though Penman Monthieth equation is assumed as the best method for potential evapotranspiration (PET) estimation, all the other selected stations except Mekelle Airport station do not have the complete data required as input for the Penman Monthieth equation. Relative humidity, wind speed and sunshine hour data are incomplete in Hagereselam and Atsbi meteorological stations and completely not available in Wukro station. To select the best of the other methods, PET was calculated for Mekelle Airport station using different PET estimation methods. The Hergreave method, which uses the minimum and maximum temperatures and extraterrestrial radiation as input data has relatively nearest value to the result of Penman Monthieth method. Hence, the PET time series data were calculated through use of the Hargreaves equation (Allen et al., 1998) as shown below.

$$PET = 0.0023 \times (T_{mean} + 17.8) \times (T_{max} - T_{min})^{0.5} \times R_a \quad ---------- eqn.3.2$$

where, PET is the potential evapotranspiration (mm/day);T_{mea}, T_{max} and T_{min} are the daily mean, maximum and minimum temperatures (℃) respectively.R_a is extraterrestrial radiation (mm/day), computed based on latitudinal location of the site and the day of the year (FAO56, 1998) using the relation expressed in Appendix equation 1.

The weighted daily PET series for the watershed is estimated by applying the weighting factor for the daily PET series obtained for the land uses (Drogue et al, 2002).

$$PET_w = \sum_{i=1}^{n} (w_i \times LU_i) \quad ---------- eqn.3.3$$

Where,$w_i$is weighting factor (the ratio of area of LU_i to the total area), LU_i is land use of a specified target area.

3.3.3 Thiessen Polygon Map Preparation

To use the stations climatic data to the watershed modeling process in WetSpa, a Thiessen polygon grid map of precipitation and potential evapotranspiration were developed using Atsbi, Hagereselam, Mekelle Airport and Wukro meteorological stations. These stations were selected based on data availability and proximity to the Agula'e watershed. Atsbi is found within the watershed where as Wukro, Hagereselam and Mekelle Airport stations are located outside but around the watershed. This map was prepared in the ArcGIS software to determine how much part of the watershed is covered by each of the meteorological stations (Figure 3.6). The Thiessen polygon method clearly identifies areal weight coverage of each meteorological station.

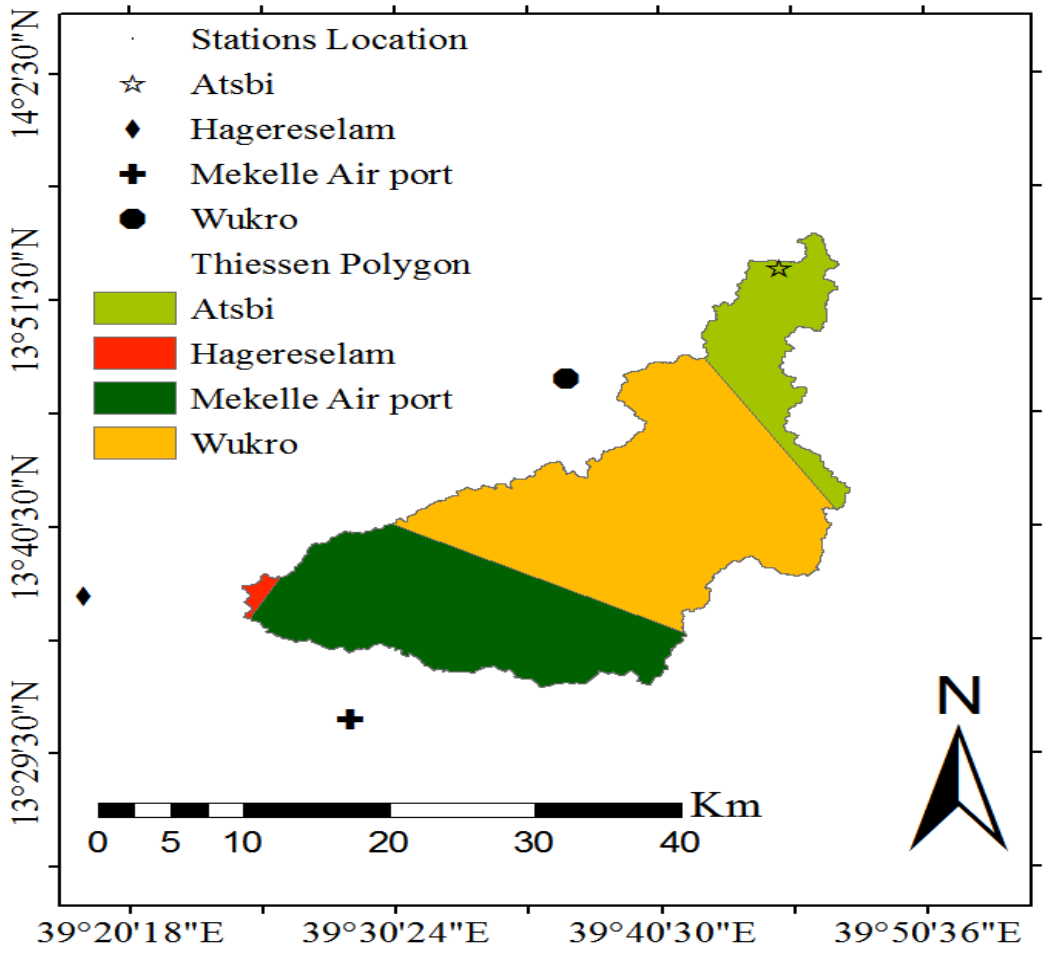

Figure **3. 6**. Grid Map of Meteorological Stations Thiessen Polygon

Accordingly, the areal coverage of Atsbi, Hagereselam, Mekelle Airport and Wukro meteorological stations is13.80%, 0.61%, 35.33% and 50.26% respectively. Wukro and Mekelle Airport stations cover more than 85 % of the watershed area whereas Hagereselam covers very small part of the watershed. This areal classification helps to capture the grids

for daily precipitation and potential evapotranspiration during the modeling process WetSpa.

3.3.4 WetSpa Extension Model Input Parameters Preparation

For the estimation of watershed water balance using the distributed hydrological model, WetSpa, the non-spatial hydro meteorological data sets (precipitation, potential evapotranspiration and stream discharge) and spatial biophysical features (topography map, soil type map, land use map, and precipitation and PET stations Thiessen polygon map) of the watershed were needed as main inputs.

A distributed spatial features of topography, land use, soil type and stations Thiessen polygon maps of the watershed were prepared using ArcMap10.1 (Figures 3.1, 3.4, 3.5 and 3.6) respectively.

Surface Parameters

Surface parameter grids of flow length, flow accumulation, stream network, slope, hydraulic radius and others like sub watershed were prepared in the view topography of the ArcView project. The DEM was made to depression-less using the fill sinks function so that positive drainage will occur throughout the basin, which creates an accurate representation of flow direction and therefore accumulated flow *(*Liu and De Smedt, 2004).

The spatial model parameters necessary for WetSpa extension were then created using the functions in ArcView. Flow direction and flow accumulation grids were calculated based on the flow path of steepest decent from the filled elevation. The vector stream network is extracted from the result of flow accumulation using a threshold cells value of 10. This means cells receiving a flow from above 10 different cells have got a value of one and considered as stream while those getting below it are not.

In deriving the slope, the threshold of minimum slope 0.01% was set so as to avoid the problem of zero slopes in specific areas. The catchment has average slope of 14.55% and a minimum of 0.01% and a maximum of 149.58%, which shows the highly variable topographic scene of the area which in turn take a responsibility for the highly varied hydrological phenomena of surface runoff and infiltration.

The grid of hydraulic radius was calculated using the power law relationship with a network constant a = 0.07 and a geometry scaling exponent b = 0.47, corresponding a flood frequency of 2-year return period was chosen since flooding of the measured discharge data seems normal. Finally, a map of sub catchment was extracted from the master filled DEM

with a cells threshold value of 1000. As a result 153 sub catchments were distinguished corresponding to a minimum, maximum and average sub catchment area of 0.0125km^2, 18.87$km^2$and 4.482km^2respectively.

Land Use Parameters

The land use based parameters used in the model include root depth, interception capacity, and the Manning‘s coefficient and the WetSpa model parameters of potential runoff coefficient and depression storage capacity have been derived. The Manning‘s roughness coefficient for river channels are derived using the value assigned in the look up table of WetSpa extension.

Soil Parameters

The soil hydraulic properties such as conductivity, porosity, field capacity, residual moisture, pore distribution index and wilting point were derived from the soil map. The initial relative saturation grid of the soil was created by the function ‘Initial Moisture’ using the Topographical Wetness Index method, even though it is not important for long term simulation. The minimum relative saturation was set to be 0%.

Potential runoff coefficient and depression storage capacity parameter

Potential runoff coefficient and depression storage capacity parameter maps were created from previously created slope, land use and soil type maps in their respective views. Then the program load these grid themes directly from their views and these parameter grids were created and displayed ‘Runoff coefficient and depression’ in order to give a clear view of them. To create the runoff coefficient grid, the impervious percentage for urban cells is set to be default value (30%).The potential runoff coefficient highly varies depending on slope, soil type and land use. All the three factors play an important role in determining it.

Flow Routing Parameters

The flow routing parameters include flow velocity, average travel time and its standard deviation from cells to the catchment outlet and to the sub catchment outlet were calculated in the view ‘Routing Parameter‘. The function velocity creates a flow velocity grid from the Manning‘s coefficient, hydraulic radius and slope grid. The default flow velocity limits 3.0m/s for upper and 0.005m/s for lower were assigned. The average flow velocities of the area is fairly slow due to the very low hydraulic radius (most part is between 0.004 to 0.171m) and the relatively law‘s roughness coefficient of the catchment.

A flow travel time and standard deviation grids in hours from each cell to the catchment outlet are created using the weighted ‘Flow length’ routine, and flow travel time and

standard deviation grids in hours from each cell to its sub catchment outlet were created and ASCII files to all these parameters were saved in the ASCII file of the project. The concentration time, defined as the time it takes for water from the furthest point to reach the outlet of the catchment is around 59hours. The mean travel time for the entire catchment is about 23 hours and the maximum flow length is about 72.6 km.

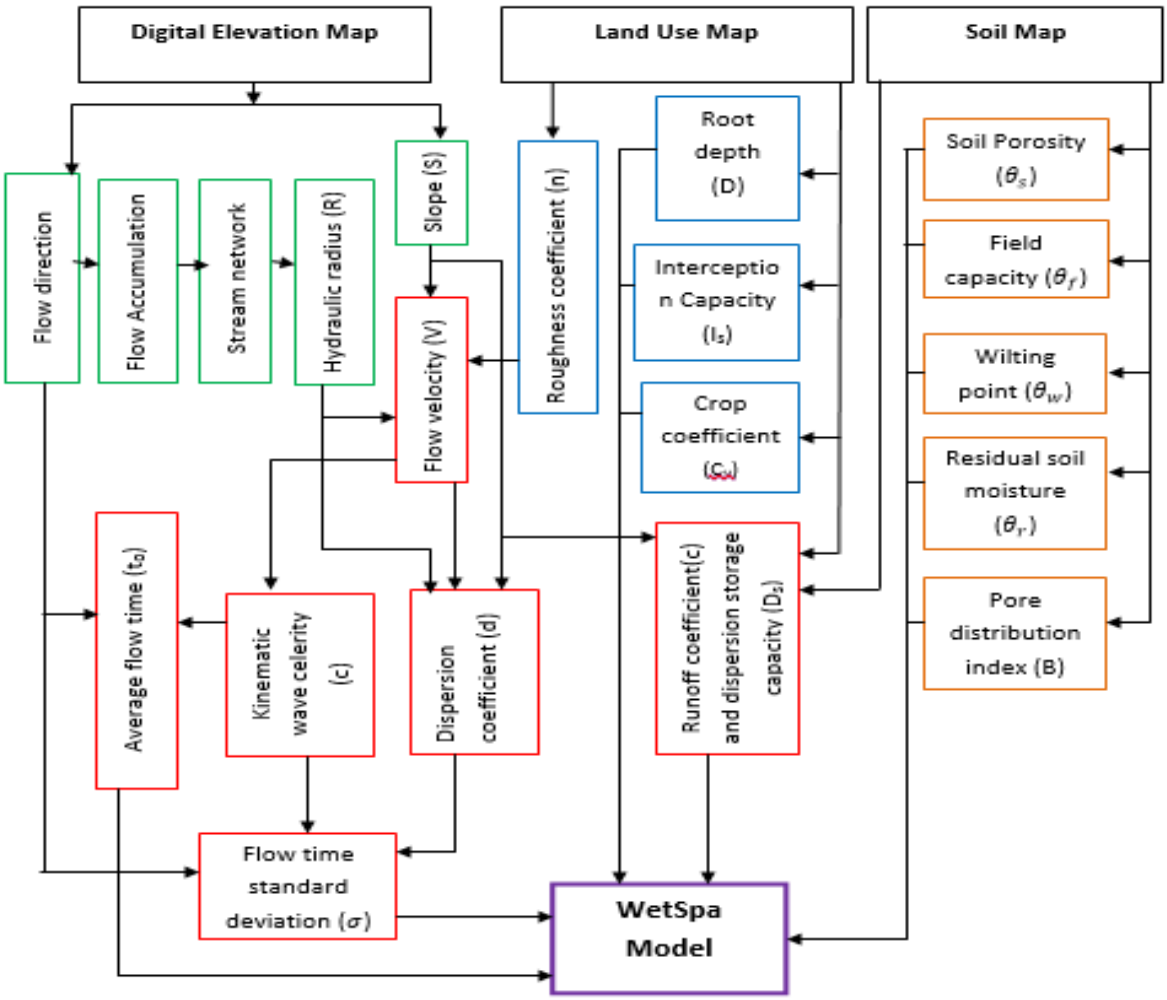

Figure 3. 7.WetSpa Model Local Parameters Parameterizations (Liu, 2004)

The parameter tables are time series data that have an attribute data for the model which contains land-use type parameters (rooting depth, leaf area index, vegetation height), soil type parameters for each textural soil class (soil porosity, field capacity, wilting point, residual soil moisture and pore size distribution index), and the runoff coefficient and depression storage capacity parameters for all combinations of land uses, slopes, and soil types. Average flow time and flow time standard deviation parameters of the digital elevation model are also among the WetSpa model tabular parameter inputs. The average flow time depends on the flow direction and kinematic wave celerity (that is influenced by

the flow velocity) parameters. The kinematic wave celerity, flow velocity and dispersion coefficient are the input for the flow time standard deviation estimation (Figure 3.7).

Table **3. 1.** Common Threshold Values of Gridded Maps' Parameters

Parameters with common threshold values	Unit	Value
Stream network delineating threshold	cell	10
Sub catchments determining threshold value	cells	1000
Upstream drained area by a particular cell	km^2	> 0.1
Sub catchments	total	153
Maximum sub catchment area	km^2	18.7
Average sub catchment area	km^2	4.48
Average hydraulic radius at upland cells	meter	0.005
Average hydraulic radius at outlets	meter	1.5
Maximum flow length of the watershed	km	72.6
Time of concentration	hour	59
Mean travel time for entire watershed	hour	23
Manning's coefficient for lowest order	$m^{-1/3}s$	0.055
Manning's coefficient for highest order	$m^{-1/3}s$	0.025
Impervious area within an urban cell	%	30

In order to run the WetSpa model, the input base maps have to be made to have similar area and cell size. The topography, land use, soil type and meteorological stations' grid maps were made to have same area and cell size of the watershed. Accordingly, these base maps of area 690.65km^2 , were made to have grid cell size of 50m by 50m, 436 rows and 415 columns. This situation helps the WetSpa model to perform proper simulations.

The other non-spatial input data were the minimum and maximum temperature, precipitation, potential evapotranspiration and discharge data. Temperature and precipitation data were available from Atsbi, Hagereselam, Mekelle Airport and Wukro stations. Potential evapotranspiration data of each station was estimated by Hargreaves equation using the temperature data as input (eqn.3.2). Measured discharge data was available from one recording station found at the outlet of Agula'e watershed. The maximum and minimum temperature data were used for PET estimation but not directly used as input for WetSpa model since snow melting is not present in the watershed. These

all climatic input data were provided in daily time series and prepared in text format when used as input for WetSpa Extension model.

Table **3. 2**. Monthly Mean Observed P, PET and Discharge (q), Value (1993-2003)

Month	P (mm)		PET(mm)		q ($m3/s$)	
	monthly	daily	monthly	daily	monthly	daily
January	3.6	0.1	99.30	3.30	4.3	0.14
February	2.3	0.1	113.51	3.76	2.8	0.10
March	20.6	0.7	122.46	4.07	7.2	0.23
April	25.6	0.9	127.53	4.23	9.4	0.31
May	25.0	0.8	132.61	4.47	7.3	0.23
June	36.6	1.2	134.90	5.30	13.6	0.45
July	180.2	6.0	112.67	3.74	128.4	4.14
August	228.8	7.6	107.81	3.57	302.5	9.76
September	31.9	1.1	117.54	3.92	40.7	1.36
October	6.0	0.2	108.14	3.61	10.3	0.33
November	4.7	0.2	95.12	3.17	4.4	0.15
December	1.6	0.1	92.2	3.07	3.6	0.12
Average	47.26	1.58	113.5	3.78	44.5	1.44

3.3.5 WetSpa Extension Model Application Processes

1. Root Zone Water Balance

For each grid cell, the root zone water balance is modeled continuously by equating inputs and outputs (Wilby and Darwin, 2004)):

$$\frac{D \times \Delta\theta}{\Delta t} = P - I - S - R - F \quad eqn.\ 3.4$$

Where D[mm] is root depth, $\theta[m^{-3}m^{-3}]$ is soil moisture, P $[ms^{-1}]$ is precipitation, I $[ms^{-1}]$ is the initial loss including interception and depression storage, S $[ms^{-1}]$ surface runoff, E $[ms^{-1}]$ is actual evapo-transpiration from the soil & vegetation, R$[ms^{-1}]$ is percolation out of the root zone or groundwater recharge, and F$[ms^{-1}]$ is interflow, and Δt is duration of simulation time[s].

2. Interception

Interception is that portion of the precipitation, which is stored or collected by vegetal cover and subsequently evaporated to the atmosphere. Interception is affected by the storm

characteristics, the species of vegetation, percentage of canopy cover, growth stage, season, and wind speed, etc. Interception loss is higher during the initial phase of a storm and approaches zero thereafter. The equation can be expressed as:

$$I(t) = \begin{cases} I_{i,o} - SI_{(t-1)}. & \text{for } P_{i(t)} > I_{i,o} - SI_{i(t-1)} \\ P_{i(t)}, & \text{for } P_{i(t)} < I_{i,0} - SI_{i(t-1)} \end{cases} \quad ----------eqn.3.5$$

Where $I_{i(t)}$ is the interception loss at cell i over the time interval (mm), $I_{i,o}$ is the cell interception storage capacity (mm), $I_{i(t-1)}$ is the cell interception storage at time step t-1 (mm), and $P_{i(t)}$ is the cell precipitation amount (mm).

The cell interception storage capacity is estimated by the empirical relation based on statistical analysis of long-term measurements (De Smedt, D., 1997), and is written as.

$$I_{i,o} = I_{i,min} + \left(I_{i,max} - I_{i,min}\right)\left[\frac{1}{2} + \frac{1}{2}\sin\left(2\pi\frac{d-87}{365}\right)\right]^b \quad ----------eqn.3.6$$

In which $I_{i,min}$ is the minimum interception storage capacity at cell i (mm), $I_{i,max}$ is the maximum interception storage capacity (mm), and d is the day of the year. The exponent 'b' controls the shape of the variation curve, and can be adjusted according to the local conditions during calibration.

3. Depression Storage

Depression Storage is the precipitation that reaches the ground that get trapped into several small depressions, which is retained in puddles, ditches, and on the ground surface. As soon as rainfall intensity exceeds the local infiltration capacity, the rainfall excess begins to fill depression.

In WetSpa Extension, a simple empirical equation suggested by Linsley (1982) is used to estimate depression storage:

$$SD_{i(t)} = SD_{i,o}\left(1 - \exp\left(-\frac{PC_i}{SD_{i,o}}\right)\right) \quad ---------- \text{ eqn. } 3.7$$

Where $SD_{i(t)}$ is the cell depression storage at time t (mm), $SD_{i,o}$ is the cell depression storage capacity (mm), and PC_i is the accumulative excess rainfall on the soil surface (mm).

4. Surface Runoff (S)

The surface runoff is calculated using a moisture-related modified rational method with a runoff coefficient depending on land cover, soil type and slope (Bahrem and De Smedt, 2008):

$$S = C(P - I) \times r\left(\theta/\theta_s\right)^{\alpha} \quad ----------eqn.3.8$$

Where θ and $\theta_s[m^3m^{-3}]$ are root zone water content at time t and saturation, C [–] is potential runoff coefficient, and α[–] is a parameter reflecting the effect of rainfall intensity. C is derived from a lookup table, linking values to slope, soil type and land use classes (Liu, 2004). The value of 'α' is evaluated as follows:

$$\alpha = \max\left[1, \mathrm{K_{run}} + (1 - \mathrm{K_{run}})\left({}^{\mathrm{P}}/_{\mathrm{P_o}}\right)\right] \text{ eqn. 3.9}$$

Where $\mathrm{K_{run}}$ [–] is a surface runoff exponent, p is precipitation and $\mathrm{P_o}$ [ms-1] is rainfall intensity scaling parameter that can be adjusted during global parameter calibration.

5. Actual Evapotranspiration (E)

Actual evapotranspiration from the soil and vegetation is calculated based on the relationship developed by Thornthwaite and Mather (1955), as a function of potential evapotranspiration (EP), vegetation type, stage of growth, and soil moisture content(θ).

$$\mathrm{E} = \begin{cases} \mathrm{C_v K_{ep}} \mathrm{EP} - 1, & \text{for } \theta \geq \theta_\mathrm{f} \\ \mathrm{C_v K_{ep}} \mathrm{EP} - 1\left(\dfrac{\theta_\mathrm{i} - \theta_\mathrm{w}}{\theta_\mathrm{f} - \theta_\mathrm{w}}\right), & \text{for } \theta_\mathrm{w} \leq \theta_\mathrm{i} \leq \theta_\mathrm{f} \\ 0, & \text{for } \theta_\mathrm{i} \leq \theta_\mathrm{w} \end{cases} \text{ eqn. 3.10}$$

Where $\mathrm{C_v}$[–] is a vegetation coefficient, which varies throughout the year depending on growing stage and vegetation type, $\mathrm{K_{ep}}$ [–] is a correction factor for adjusting potential evapotranspiration (EP)$\theta[ms^{-1}]$, $\theta_\mathrm{i}[m^3m^{-3}], \theta_\mathrm{w}[m^3m^{-3}]$ and $\theta_\mathrm{f}[m^3m^{-3}]$are the soil moisture content of cell i at time t, permanent wilting point, and field capacity respectively. When the water content (θ_i) is lower than the wilting point ($\theta_i < \theta_w$), evapotranspiration is only possible by capillary rise from the groundwater, which is controlled by the groundwater storage G [m] and a scaling parameter G0 [m] calculated with the next relation:

$$E_G = (C_v K_{ep} EP - 1)\left({}^{G}/_{G_o}\right), \quad for \theta_i < \theta_w \text{ } eqn. 3.11$$

Where $E_g[ms^{-1}]$ is the evapotranspiration from the groundwater. The other components are the same as described above.

6. Percolation (R)

The rate of percolation, R, or groundwater recharge is the natural process by which water is added from soil water zone to the saturation zone of the aquifer and is derived by the Brooks and Corey relationship (Eagleson, 1970; Famiglietti and Wood, 1994) of 1966:

$$\mathrm{R_{i(t)}} = \mathrm{K}\left(\theta_{\mathrm{i(t)}}\right)\Delta\mathrm{t} = \mathrm{K_s}\left(\frac{\theta_{\mathrm{i(t)}} - \theta_\mathrm{r}}{\theta_\mathrm{s} - \theta_\mathrm{r}}\right)^{\frac{2+3\mathrm{B}}{\mathrm{B}}} * \Delta\mathrm{t} \text{ eqn. 3.12}$$

Where K ($\theta_{i(t)}$) $[ms^{-1}]$ is the effective hydraulic conductivity, $K_s[ms^{-1}]$ is the saturated hydraulic conductivity, $\theta_s[m^3m^{-3}]$ andθ_r $[m^3m^{-3}]$ are the saturation and residual soil moisture content, and B [–] is the soil pore size distribution index, tabulated value, and Δt(s) is time interval. K_s, θ_s, θ_r and B of each cell are obtained from spatial distributed grid parameters prepared in ArcView.3.2.

7. Interflow (F)

Interflow is assumed to occur when the soil moisture is higher than field capacity and is determined based on the Darcy's Law and the kinematic approximation, as a function of hydraulic conductivity, moisture content, slope angle, and root depth (D):

$$F = D \times S_o \times K_i \times K(\theta)) \times \Delta t \ / \ W_i \quad \text{eqn. 3.13}$$

Where S_o $[mm^{-1}]$ is the surface slope, K_i [–] is a scaling parameter to adjust the horizontal hydraulic conductivity in the soil layer, K (θ) $[ms^{-1}]$ is effective hydraulic conductivity over time interval and W_i is the cell width (m).

8. Groundwater flow ($\mathbf{Q_g}$)

Groundwater flow is defined as the quantity of water that discharges from the groundwater storage into the stream for each time step. Groundwater flow is simplified as a lumped linear reservoir for each sub watershed and a non-linear reservoir method is an optional in the model with storage exponent of 2 (Wittenberg and Sivapalan, 1999). The ground water flow is estimated by the equation:

$$Q_G = K_g[\frac{SG_{s(t)}}{1000}]^m \quad \text{eq. 3.14}$$

Where $Q_G[ms^{-1}]$ is the groundwater drainage in the sub catchment outlet, $K_g[m^2s^{-1}$for linear, $m^{-1}s^{-1}$for non-linear reservoir] is the groundwater recession coefficient, m (-) is an exponent [m=1 for linear reservoir and m= 2 for non-linear reservoir] and $SG_{s(t)}$[m] is the groundwater storage of sub catchment at time t, derived as:

$$\frac{\partial G}{\partial t} = R - Q_G - E_G \quad \text{eqn. 3.15}$$

Where R = percolation (ms^{-1}), E_G= Evapotranspiration from ground water (ms^{-1})

The evapotranspiration from the groundwater is expressed by:

$$E_{G(t)} = C_d[C_v EP - EI_{(t)} - ED_{(t)} - ES_{(t)}] \quad \text{eqn. 3.16}$$

The groundwater balance of each sub catchment is estimated as:

$$SG_{s(t)} = SG_{s(t-1)} + (\sum [RG_{i(t)} \times (A_i)])/A_s - E_{Gs(t)} - QG_{s(t)}(\frac{\Delta t}{1000A_s}) \quad \text{eqn. 3.17}$$

Where $SG_{s(t)}$ and $SG_{s(t-1)}$ are groundwater storage of the sub catchment at time step t and t-1 (mm), A_i is the cell area (m^2), A_s is the sub catchment area (m^2), $EG_s(t)$ is the average evapotranspiration from groundwater storage of the sub catchment (mm), and$QG_{i(t)}$ is the groundwater discharge ($m^3 s^{-1}$)

9. Overland Flow and Channel Flow Routing

The routing of overland flow and channel flow is implemented by the method of the diffusive wave approximation of the St. Venant equation (Miller and Cunge, 1975):

$$\frac{\partial Q}{\partial t} + c\frac{\partial \theta}{\partial x} - d\frac{\partial^2 \theta}{\partial x^2} = \text{---------- eqn. 3.18}$$

Where Q [$m^3 s^{-1}$] is the discharge, x [m] is the distance along the flow direction, C[ms^{-1}] is the kinematic wave celerity, interpreted as the velocity by which a disturbance travels along [$m^{-1}s^{-1}$] the flow path, and d [$m^2 s^{-1}$] is the location dependent dispersion coefficient, which measures the tendency of the disturbance to disperse longitudinally as it travels downstream.

Assuming the water level gradient equals the bottom slope and the hydraulic radius approaches the average flow depth for overland flow, C_i and d_i can be estimated by (Henderson, 1966) ;

$$C_i = \frac{5}{3} \times V_i \text{ ---------- eqn. 3.19}$$

$$d_i = \frac{V_i \times R_i}{2 \times S_i} \text{ ---------- eqn. 3.20}$$

Where R_i [m] is the hydraulic radius or average flow depth, $S_i$is the cell slope (m/m) V_i [ms^{-1}] is the flow velocity.

The hydraulic radius is determined by a power law relationship with an exceeding probability (Molnar and Ramirez, 1998), which relates hydraulic radius to the controlling area and is seen as a representation of the average behavior of the cell and the channel geometry

$$R_i = a(A_i)^b \text{ ---------- } eqn. 3.21$$

where A_i is the drained area upstream of the cell (km²), which can be easily determined by the flow accumulation routine in ArcView GIS, a (-) is a network constant and b (-) a geometry scaling exponent, both depending on the discharge frequency, and their values are taken from lookup tables.

The flow velocity is calculated by the Manning equation as;

$$V_i = \frac{1}{n_i} \times R_i^{\frac{2}{3}} \times S_i^{\frac{1}{2}} \text{ ---------- } eqn.3.22$$

Wheren_i = the Manning's roughness coefficient ($m^{-1/3}s$), which depends upon land use categories and the channel characteristics obtained as default value. The flow velocity is predetermined by limits as$V_{min}$and V_{max} during model calculation. To reflect the property that hydraulic radius increases as water deepens, the channel roughness coefficient is set between predetermined limits n_{max}andn_{min}, depending upon the GIS derived stream orders in the WetSpa Extension.

Hence, the model implies a velocity field that does not vary as a function of flow, so it is similar to the unit hydrograph approach.

An approximate solution to the diffusive wave equation in the form of a first passage time distribution is applied (Liu et al., 2003), relating the discharge at the end of a flow path to the available runoff:

$$u_{(t)} = \frac{1}{\sigma_i \sqrt{2\pi t^3 / {t_i}^3}} \exp\left[\frac{(t_i - t)^2}{4{\sigma_i}^2 t / t_i}\right] \text{ ---------- } eqn.3.23$$

Where $u_{(t)}$[s^{-1}] is the flow path unit response function, serving as an instantaneous unit hydrograph (IUH), which makes it possible to route water surplus from any grid cell to the basin outlet or any downstream convergent point, t_i[h] is the average flow time, and σ_i[h] is the standard deviation of the flow time.

The parameters t_i and ${\delta_i}^2$ are spatially distributed, and can be obtained by integration along the topographically determined flow paths as a function of flow celerity (c) and dispersion coefficient (d).

$$t_i = \sum_{i=1}^{N} \left(\frac{1}{c_i}\right) l_i \text{ ---------- } eqn.3.24$$

$${\sigma_i}^2 = \sum_{i=1}^{N} \left(\frac{2 \times d_i}{{c^3}_i}\right) l_i \text{ ---------- } eqn.3.25$$

Where N is number of cells, $l_i$is the cell width (m).

Hence, flow hydrographs at the basin outlet or any downstream convergent point are obtained by a convolution integral of the flow response from all contributing cells.

The main advantage of WetSpa extension model is that it allows spatially distributed hydrological parameters of the basin to be used as inputs to the model simulated within a GIS framework. Inputs to the model include digital elevation data, soil type data, land use

data, with their parameter lookup tables in database file (dbf) format and climatologically data like precipitation, evapotranspiration, discharge data (optional for model calibration).

10. Watershed Water Balance

Water balance for the entire catchment is used to keep track of water changes in the hydrological system, and also a measure of model performance by comparing the simulation results with the field observations. When modeling for a relatively long time period, changes in the storage of interception, depression and channel can be neglected, and the general watershed water balance can be expressed as;

$$\mathrm{P} = \mathrm{RT} + \mathrm{ET} + \Delta\mathrm{SS} + \Delta\mathrm{GS} \quad \text{eqn. 3.26}$$

Where P is the total precipitation in the watershed over the simulation period (mm), RT and ET are total runoff and total actual evapotranspiration (mm),ΔSS and ΔSG are the change in soil moisture and groundwater storage for the watershed between the start and the end of the simulation period (mm). Changes in the storage of interception, depression and channel flow are neglected when dealing with simulation of relatively longer time period. For a given simulation period T(s) and initial soil moisture and groundwater storage conditions, the components in equation 3.26can be expressed as;

$$P = \sum_{t=0}^{T}\sum_{i=1}^{N_w} P_{i(t)} \quad eqn.3.27$$

$$RT = \sum_{t=0}^{T}\sum_{i=1}^{Nw}[RS_{i(t)} + RI_{i(t)}] + \sum_{t=0}^{T}\sum_{s=1}^{N_r}[\frac{QG_{s(t)}}{A_s}\Delta t] \quad eqn.3.28$$

$$ET = \sum_{t=0}^{T}\sum_{i=1}^{N_w}[EI_{i(t)} + ED_{i(t)} + ES_{i(t)}] + \sum_{t=0}^{T}\sum_{s=1}^{N_r}[EG\ i(t)] \quad eqn.3.29$$

$$\Delta SS = \sum_{t=0}^{N_w}[\theta_{i(T)} - \theta_{i(0)}] \quad eqn.3.30$$

$$\Delta SG = \sum_{t=0}^{Nw}[\theta SGs_{i(T)} - \theta SGs_{i(0)}] \quad eqn.3.31$$

where $\theta_{i(T)}$ and $\theta_{i(0)}$ are cell soil moisture content at the end and the start of the simulation period (m^3/m^3), $\theta SGs_{i(T)}$and $\theta SGs_{i(0)}$ are sub catchment groundwater storage at the end and the start of the simulation period (mm), $N_w$and N_{wr} are the number of cells and stream links upstream of the outlet respectively and the others have been described in above descriptions.

3.3.6 HadCM3/GCM Model Application

The main concern of this research is to estimate the impact of climate change on the local water availability and its hydrologic counterparts in the watershed using climate data sets available from HadCM3 GCM output. HadCM3 is a climate model developed, to forecast climate changes, at the Hadley center of the United Kingdom's National Meteorological service. HadCM3/GCM is a dataset from which climatic projections are downscaled that can be calibrated and validated based on the observed and simulated data for selected predictand variables (Paeth et al., 2007; Kebede et al., 2013).

In order to estimate the impact of climate change on water availability, a time series data at present and a future scenarios were used. Observed data were collected from secondary data sources and based on boundary condition, predictor data from GCM outputs were downscaled through using Statistical Downscaling Model (SDSM) for SRES emission scenarios (IPCC, 2013). In this study, all GCM simulations were driven from recent HadCM3 global coupled climate model simulations. SDSM is a decision support tool which derives large scale climatic variables (predictors) to local/station variables (predictands) (Wilby et al., 2004).

3.3.7 SDSM Model Input Data and Downscaling

The A2a and B2a SRES emission scenarios were selected for this study assuming the basin would experience such emission and socio economic scenarios in the future. In A2a and B2a experiments, A2 and B2 stands for medium to low and medium to high emission scenarios respectively. Letter 'a' refers to a different initial point of climate solution for ensemble members along the reference period.

These were downloaded from the Canadian Institute for Climate Studies (CICS) website http://www.cics.uvic.ca/scenarios/sdsm/select.cgi. Even though there was a possibility of selecting predictors from different available GCMs like HadCM3 and CGCM1, only the HadCM3 GCM has grid boxes representing the study area. CGCM1 model currently has not have predictor files for Africa Window but only for the North American Window. Hence, the data files downloaded were only for the HadCM3 model. The predictor variables of HadCM3 are provided on a grid box by grid box basis of size 2.5° latitude x 3.75° longitude. As the study area falls in between 13°32'43"N to 13°54'50"N (average 13.73°N) latitude and 39°24'35''E to 39°47'50"E (average 39.41°E) longitude, the nearest grid box for the HadCM3 model, which represents the study area, is the one with origin of 12.5°N

latitude and 37.5°E longitude coordinates. This box is represented by latitudinal box number of Y=30 and longitudinal box number of X=11 (Figure 3.8).

The grid box data downloaded consist of three directories:

- NCEP_1961-2001: this contains 41 years of 26 daily observed predictor data, derived from the NCEP reanalyses, normalised over the complete 1961-1990 period.
- H3A2a_1961-2099: this contains 139 years of 26 daily GCM predictor data, derived from the HadCM3 A2a experiment, normalised over the 1961-1990 period.
- H3B2a_1961-2099: this contains 139 years of 26 daily GCM predictor data, derived from the HadCM3 B2a experiment, normalised over the 1961-1990 period.

NCEP data are re-analysis data sets from the National Centre for Environmental Prediction, which were re–gridded to conform to the grid system of HadCM3. These were the data used in the model calibration and both the NCEP and HadCM3 data have daily predictor values of twenty six parameters (Table 3.3), which were used in the determination of the predictands. According to Wilby and Dawson (2004), the predictors selected with regard to each predictand should be physically and conceptually sensible, strongly and consistently correlated with it, and accurately modelled by GCMs.

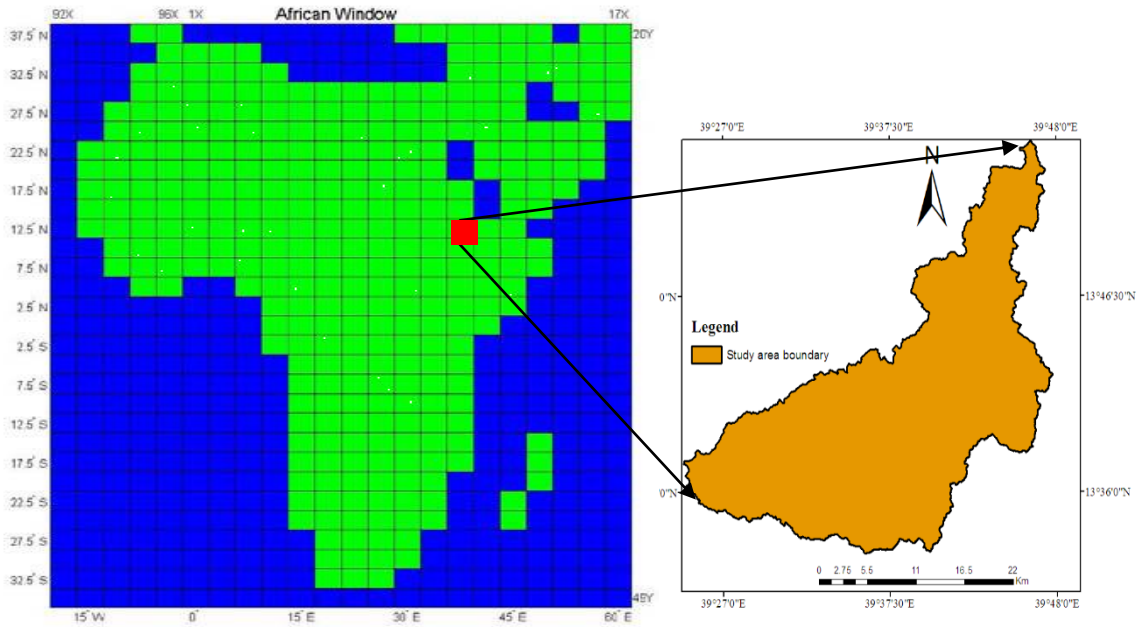

Figure 3. 8Africa Window from Which the Study Area Grid Box is Located.

Observed daily data of precipitation, minimum and maximum temperature of the period from 1992 to 2015, collected from four stations namely Atsbi, Hagereselam, Mekelle Airport and Wukro stations, were used for downscaling global predictor to local scale. All

stations are found in one grid cell of GCM/HadCM3 of 2.5° latitude by 3.75° longitude where the study area is located. To overcome the problem with precipitation downscaling, which is more of conditional type affected by local climate rather than global predictors, future climate variables of all stations were compared (Wilby and Dawson, 2004).Precipitation, maximum and minimum temperature history data of (1992-2015) of the selected meteorological stations were used as a base line because all stations except Mekelle Airport do not have recorded data more than the selected period. The observed meteorological time series data of 1992 - 2006 were used for calibration and the data from 2007 - 2015 were used for validation of the Statistical Downscaling Model.

3.3.8 Statistical Downscaling Model (SDSM)

The Statistical Downscaling Model Version 4.2.9 was used for downscaling the large scale climate (Predictors) data to the local scale (predictands) data. SDSM is advantageous as it is easy to implement, and generation of the downscaled values involves observed historic daily data. The latter advantage ensures the maintenance of local spatial and temporal variability in generating realistic time series data.

SDSM have additional tasks of data quality control and transformation, predictor variable pre-screening, automatic model calibration, basic diagnostic testing, statistical analysis and graphing of climate data. In the downscaling process, shown in Figure 3.8, with the bold boxes represents the main discrete processes of the SDSM model. The following sections discuss on the descriptions of the model processes separately (Wilby and Dawson, 2004).

I. Setting of Model Parameters

For weather generation task, ***Year Length*** was set to the default "Calendar (366)" that allows 29 days in February every Leap years and used with observed data. For scenario generation, the year length was set to 360 since the HadCM3 have model years consisting of 360 days.

The ***start and end date*** for all input data were arranged as needed. ***Missing Data Identifier***, the code assigned to identify missing data in all inputs, was set to default value -999. Whenever SDSM encounters this code the value will be skipped (e.g., during model calibration, or calculation of summary statistics) but can generate a value during scenario generation.

Allow Negative Values: The default allows simulation of negative values by unconditional processes in the downscaling model (e.g., for temperature). Conditional processes (example, rainfall amounts) are unaffected by this button.

For some conditional variables it is necessary to specify an event threshold. For example, when calibrating daily precipitation models, the parameter was set to 0.03 mm/day to treat trace rain days as dry days and 0 for temperature.

Default File Directory that allows to select a default directory that is accessed by all screens when first searching for files.

II. Quality Control and Data Transformation

To come up with good model output, climatic input data were checked for missing and unrealistic values. The quality control function of SDSM also provides the minimum, maximum, and mean of the input data. All the input data were checked for missing data codes and data errors before the calibration process. Data transformation was not used in this model.

III. Screening the Downscaling Predictor Variables

The central concept behind any statistical downscaling method is the recognition of empirical relationships between the gridded predictors and single site Predictand. This is the most challenging part of the work due to the temporal and spatial variation of the explanatory power of each predictor (Wilby and Dawson, 2004). The selection was done at most care as the behavior of the climate scenario completely depends on the type of the predictors selected. Annual analysis period was used which provides the predictor-predictand relationship all along the months of the year. The significance level, which tests the predictor and predictand significance relationship, was set to be equal to the default value ($p<0.05$). Moreover, the process type that identifies the presence of an intermediate process in the predictor-predictand relationship was defined.

For daily temperature, which is not regulated by an intermediate process, the unconditional process was selected. However, the conditional process was selected for daily precipitation because of its dependence on other intermediate process like on the occurrences of humidity, cloud cover, and/or wet-days. Several analyses were made till best predictor-predictand correlations were found. Out of the group selected from the twenty six predictors (Table 3.3), those predictors which have high explained variance were selected. The partial correlation analysis was done for the selected predictors to see the level of correlation with each other. This enables to drop the predictor which has very highly correlation with another predictor. Finally the potential usefulness of downscaling relationship was checked by scatter plotting.

Table 3. 3 . List of NCEP Predictor Variables (Wilby and De Smedt, 2004)

	Description of predictors	symbol	Description of predictor	symbol
1	Mean see level pressure	mslp	Divergence at 500hpa	p5zhaf
2	Surface airflow strength	p_faf	850 hpa airflow strength	P8_faf
3	Surface zonal velocity	p_uaf	850 hpa zonal velocity	P8_uaf
4	Surface meridional velocity	p_vaf	850 hpa meridional velocity	P8_vaf
5	Surface vorticity	p_zaf	850 hpa vorticity	P8_zaf
6	Surface wind direction	p_thaf	850 hpa geopotential height	P850af
7	Surface divergence	p_zhaf	850hpa wind direction	P8thaf
8	500hpa airflow strength	p5_faf	850hpa divergence	P8zhaf
9	500hpa zonal velocity	p5_uaf	500hpa relative humidity	r500af
10	5000hpa meridional velocity	p5_vaf	P850 hpa relative humidity	r850af
11	500hpa vorticity	p5_zaf	Near surface relative humidity	rhumaf
12	500hpa geopotential height	p500af	Surface specific humidity	shumaf
13	500hpa wind direction	p5thaf	Mean temperature	tempaf

IV. Selection of Potential Predictor Variable

This selection process involved the identification of appropriate predictor variables that have strong correlation with the predictand variable. Next use these empirical predictor-predictand relationships of the observed climate to downscale ensembles of the same local variables for the present and future climate. This is based on the assumption that the predictor-predictand relationships under the current condition will remain valid under future climate conditions too. The most relevant predictor variables were selected for each predictand through linear correlation analysis, partial correlation analysis and scatter plots between the predictors and the predictand variables.

Accordingly, the best correlated potential predictor variables were selected for minimum temperature, maximum temperature and precipitation for Atsbi, Hagereselam, Mekelle Airport and Wukro meteorological stations as listed in Table 4.1

V. Model Calibration

This operation is normally carried out based on the selected predictor variables that uses the NCEP data base of the selected grid box. The mathematical relation between a specific

predictand and the selected predictor variables is estimated and the parameters of a multiple linear regression equation were determined.

Setting was done based on the SDSM manual (Wilby and Dawson, 2004). Accordingly, the temporal resolution of the downscaling model was selected by choosing the model type as monthly. In Monthly models, model parameters are estimated for each month of the year. For this study, the calibration was done for the period of 1992-2006 for all stations at a monthly model type in order to see the monthly temporal variations. The unconditional and conditional processes were selected for temperature and precipitation values respectively. From the advance setting the model transformation was set to 'none' for temperature and 'fourth root' for precipitation calibration. Stochastic conditional selection and ordinary least squares optimization algorithm were set. During the calibration of temperature, the inflation variation and bias correction values were set to the default value of 12.0 and 1.0 respectively. But for precipitation, to adjust the high variation in mean and variance of the observed and downscaled value, the bias correction values for Mekelle Airport and Hagereselam were adjusted to1.053 and 1.12 respectively and the variance inflation for Atsbi station was adjusted to 11. The rest was set to the default value.

VI. Weather Generator and Validation

Weather Generator task of SDSM produces synthetic current daily weather data based on inputs of the observed time series data and the multiple linear regression parameters produced during the calibration step using the present large scale NCEP predictor data. Each time-serious-data of the observed climate variable is linked to the regression model weights to generate the synthetic time series data into a serious of ensembles. The results among the ensembles differ based on the relative significance of the deterministic and stochastic components of the regression models and mainly due to the stochastic component of the downscaling. As indicated in the SDSM manual, larger differences can be observed in precipitation ensemble members than that of temperature. Because precipitation series display more "noise" arising from local factors but local temperature variables are largely determined by regional forcing.

The result of the weather generator, obtained by averaging the twenty ensemble results, was used to validate the calibrated model using independent observed data not used during the calibration procedure and the synthesized artificial weather time series data representing the present condition. During weather generation, the data series from 1992-2006 were used for the calibration and from 2007-2015 was selected for validation process for all stations.

To check the appropriateness of the selected potential predictors, the monthly mean of the observed and generated values of the calibration and validation period of each climatic parameters were compared for graphical fitness comparison (Appendix Figure 2).

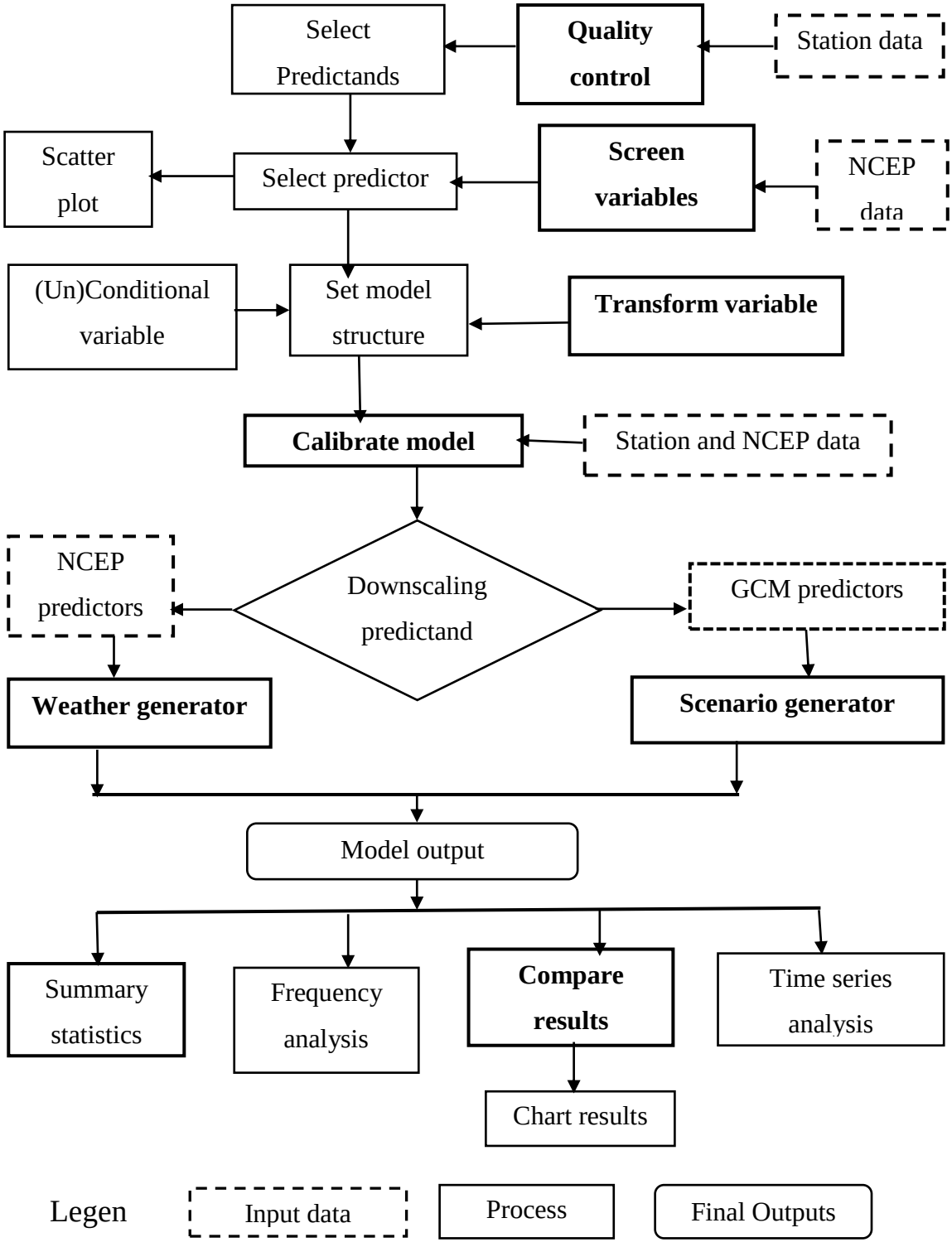

Figure **3. 9**. Climate Scenario generation (Wilby and Dowson, 2004)

VII. Scenario Generation

SDSM used input from HadCM3 GCM model output with the SRES emission scenarios with grid boxes containing the study area. Hence for this study, the HadCM3A2a and HadCM3B2a were used as input for the scenario generation. The regression weights produced during the calibration process were applied to the time series outputs of the GCM model.

This is based on the assumption that the predictor-predictand relationships under the current condition will remain valid under future climate conditions too. Twenty ensembles of synthetic daily time series data were produced for each of the two SRES emission scenarios for a period from 1961 to 2099. The final product of the statistical downscaling method was then found by averaging the twenty independent stochastic GCM ensembles. Wilby and Downson, (2004) suggested that it is adequate to consider the average of the ensembles as the target here is only to see the general trend of the climate change in the future and to preserve inter-variable relationships

The monthly mean of the downscaled and observed climate values of the base period parameters were compared for graphical fitness to check the best agreement of the parameters (Appendix Figure 3).

3.3.9 Estimation of Impact of Climate Change on Water balance Components

These synthesized average out puts of the A2a and B2a emission scenario generations' data of the selected time horizons were used as input for the WetSpa model during water balance components simulation.

The base period water balance was simulated using the baseline observed and downscaled (A2a and B2a) precipitation and estimated potential evapotranspiration. From the future downscaled precipitation and estimated potential evapotranspiration for A2a and B2a scenarios, the time series data of three time horizons 2020 -2043 (2020s), 2048 -2071 (2050s) and 2076 – 2099 (2080s) were selected to make comparable with the baseline parameters. These values were, then, used as input for WetSpa model to simulate the consecutive water balance of the watershed. The future (2020s, 2050s and 2080s) water balance components were then compared with the baseline water balance components to evaluate the impact of climate change on water availability for A2a and B2a scenarios occurred in the watershed.

3.4 **Sensitivity Analysis, Calibration and Validation of WetSpa Model**

After discharge and climate historical data were collected from the gauging station and meteorological stations respectively, different techniques were used for calibration and validation of the model. The data obtained during the first years of the data series were used for calibration and the remaining data series were used for validation.

A) Sensitivity Analysis

Sensitivity analysis is a method of minimizing the number of parameters to be used in the calibration step by making use of the most sensitive parameters largely controlling the behavior of the simulated process. Sensitivity is expressed by a dimensionless index, which is calculated as the ratio between the relative change of model output and the relative change of a parameter.

B) Model Performance Evaluation

Statistical measures provide quantitative estimates for the goodness of fit between observed and predicted values, and are used as indicators of the extent at which model predictions match observation (Liu and De Smedt 2004). While calibrating, it is useful to have a good method of evaluating the results. Finally the model performance was evaluated for both calibration and validation in different ways including visual comparison between observed and predicted parameter values or evaluation of peak flow rate and time to the peak (Gebremeskel et al, 2003).

The goodness of fit in the peak discharge and time to the peak can be evaluated by their relative absolute error and mean absolute error respectively. While other evaluation criteria, like model bias, model determination confidence, and the model efficiency, for the models were used.

1. Model Bias

Model bias is a relative mean difference between predicted and observed stream flows for a sufficiently large simulation sample, reflecting the ability of reproducing water balance. It is an important criterion for comparing whether a model is working well or not through measuring under or over prediction for a set of predictions systematically. Model bias (C_1) value is given by the equation.

$$C_1 = \frac{\sum_{i=1}^{n} Q_{si-}Q_{o.l)}}{\sum_{i=1}^{n} Q_{oi}} \quad \text{eqn. 3.32}$$

Where C_1= the model bias, Q_{si} and Q_{oi} are the simulated and observed stream flows at time step i (m^3/s) and N is the number of time steps over the simulation period. Model bias

measures the systematic under or over prediction for a set of predictions. A lower C_1 value indicates a better fit, and the value 0.0 represents the perfect simulation of observed flow volume. Positive and negative values indicate over and under predictions respectively.

2. Model Confidence

Model confidence expressed by its determination coefficient is one of the important criteria in assessment of continuous model simulation. It is calculated as the rate of the sum of the squares of the deviations of the simulated and observed discharges from the average observed discharge.

$$C_2 = \frac{\sum_{i=1}^{N}\left(Q_{s_i} - \bar{Q}_o\right)^2}{\sum_{i=1}^{N}\left(Q_{o_i} - \bar{Q}_o\right)^2} \text{ eqn. 3.33}$$

Where C_2 = the model determination coefficient, $\bar{Q}_o$ = the mean observed stream flow over the simulation period. C_2 Represents the proportion of the variance in the observed discharges that are explained by the simulated discharges. Value varies between 0 and 1, with a value close to 1 indicating a high level of model confidence.

3. Nash-Sutcliffe Efficiency

(Nash and Sutcliffe, 1970) pointed out model evaluation criteria called Nash-Sutcliffe coefficient which is used so as to describe how well discharges were simulated by the model. This efficiency criterion is commonly used for model evaluation. The equation can be described as

$$C_3 = 1 - \frac{\sum_{i=1}^{N}\left(Q_{s_i} - Q_{o_i}\right)^2}{\sum_{i=1}^{N}\left(Q_{o_i} - \bar{Q}_o\right)^2} \text{ eqn. 3.34}$$

WhereC_3 = the Nash-Sutcliffe efficiency used for evaluating the ability of reproducing the time evolution of stream flows or discharges. The C_2 value can range from a negative value to 1, with 1 indicating a perfect fit between the simulated and observed hydrographs.

3.5 General Approaches of the Study

In order to effectively implement the study, structural skeleton of the approach (input/output relationships) is likely shown in Figure 3.9 below. It was designed to show how the parameters were interlinked each other in the flow of the system for estimating water resource and the climate change impact on water resources availability.

Initially, a quality hydro meteorological data were collected and missing data were filled and data consistency was checked using the appropriate methods. Next, Digital maps of meteorological stations and physical maps of the watershed were prepared in ArcMap 10.1.

Besides the present and future climate scenario data related to the study area were obtained. The digital maps and daily data set of hydro climatic data were used as input for the WetSpa model, after calibration, for present water balance component estimation. The present and future climatic scenario data were downscaled using SDSM V4.2.9 to get local scale present and future scenario data.

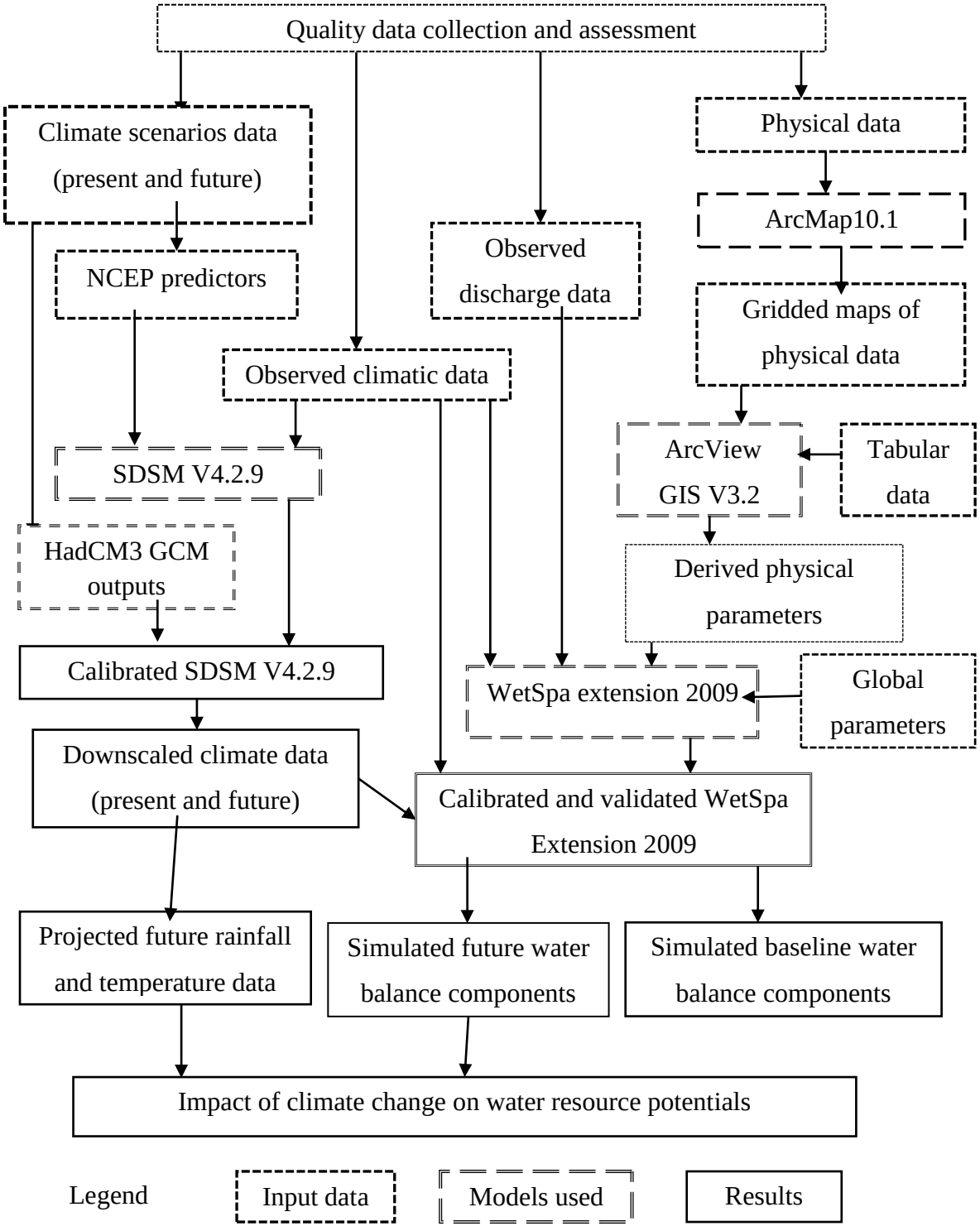

Figure **3. 10**. General Structural Set Up of the Study.

4 RESULTS AND DISCUSSION

4.1 Climate Change Scenario

4.1.1 Predictors and Predictand Relation

Accordingly, the best correlated potential predictor variables were selected for minimum temperature, maximum temperature and precipitation for Atsbi, Hagereselam, Mekelle Airport and Wukro meteorological stations as listed in Table 4.1.

Table**4. 1.**Selected Potential Predictors for Each Predictand of the Climate Station

Parameters	Selected calibration predictors	symbol	Partial r	P value
Atsbi Station				
Maximum Temperature	Meridional velocity component near surface	p_v	-0.182	0.0000
	Divergence near surface	p_zh	-0.137	0.0000
	Near surface temperature	temp	0.365	0.0000
Minimum temperature	Zonal velocity component at 850hpa	p8_u	0.505	0.0000
	Geopotential height at 500hpa	p500	0.262	0.0000
	Near surface temperature	temp	0.151	0.0000
Precipitation	Divergence near surface	p_zh	0.058	0.0246
	Zonal velocity component at 850hpa	p8_v	-0.101	0.0000
	Relative humidity at 500hpa	r500	0.062	0.0374
Hagereselam Station				
Minimum temperature	Vorticity near surface	p_z	-0.366	0.0000
	Divergence near surface	p_zh	0.043	0.0000
	Zonal velocity component at 850hpa	p8_u	0.069	0.0000
	Vorticity at 850 hpa	P8zh	0.275	0.0000
	Near surface specific humidity	shum	0.319	0.0000
	Near surface temperature	temp	0.344	0.0000
Maximum temperature	Mean sea level pressure	mslp	-0.117	0.0000
	Vorticity near surface	p_z	-0.072	0.000
	Geostrophic air flow velocity at 850 hpa	P8_f	-0.1330	0.0000
	Near surface temperature	temp	0.3740	0.0000
Precipitation	Mean sea level pressure	mslp	0.097	0.0000

	Divergence near surface	p_zh	0.079	0.0007
Mekelle Airport Station				
Maximum temperature	Geopotential height at 500hpa	p500	0.146	0.0000
	Zonal velocity component at 850hpa	p8_u	0.176	0.0000
	Near surface temperature	temp	0.349	0.0000
Minimum temperature	Zonal velocity component near surface	p_u	0.304	0.0000
	Geopotential height at 500hpa	p500	0.234	0.0000
	Geopotential height at 850hpa	p850	-0.223	0.0000
Precipitation	Meridional velocity near surface	p_v	0.069	0.0051
	Vorticity near surface	p_z	-0.063	0.0115
	Divergence near surface	p_zh	0.075	0.0022
	Relative humidity at 500hpa	r500	0.061	0.0153
Wukro Station				
Maximum temperature	Zonal velocity component near surface	p_u	0.093	0.0000
	Zonal velocity component at 500hpa	p5_u	-0.352	0.0000
	Geopotential height at 500hpa	p500	0.036	0.0170
	Near surface temperature	temp	0.331	0.0000
Minimum temperature	Zonal velocity component near surface	p_u	0.040	0.0005
	Vorticity near surface	p_z	-0.352	0.0000
	Divergence near surface	p_zh	0.070	0.0000
	Zonal velocity component at 850hpa	p8zh	-0.049	0.0000
	Near surface temperature	temp	0.359	0.0000
Precipitation	Mean sea level pressure	mslp	0.168	0.0000
	Divergence near surface	p_zh	0.123	0.0000
	Geopotential height at 500hpa	p500	0.062	0.0374

Where hpa = hectopascal = 100 pascal or 1 millibar, r = correlation, p = probability

4.1.2 Baseline Scenarios

In all stations, the downscaled baseline mean monthly maximum and minimum temperature show good agreement with that of the observed data. In the case of precipitation, even though there were little variations in individual months which are due to local effects, the downscaled values have good concurrence with observed data. In general, in all stations the

downscaled present climate variables (precipitations, maximum and minimum temperatures) have good fit with observed data, which is very important for future climate generations as indicated in Figure 4.1, 4.2, and 4.3.

Maximum Temperature

The projected maximum temperature for the baseline period shows good agreement between observed and downscaled values for all stations except a little variation in month of July, August and October at Wukro station, in October to December at Hagereselam station and in June, August and December at Atsbi (Appendix Figure3). Mekelle Airport station result has almost the same observed and downscaled baseline value (Figure4.1). The result shows no underestimation in maximum temperature in any of the stations.

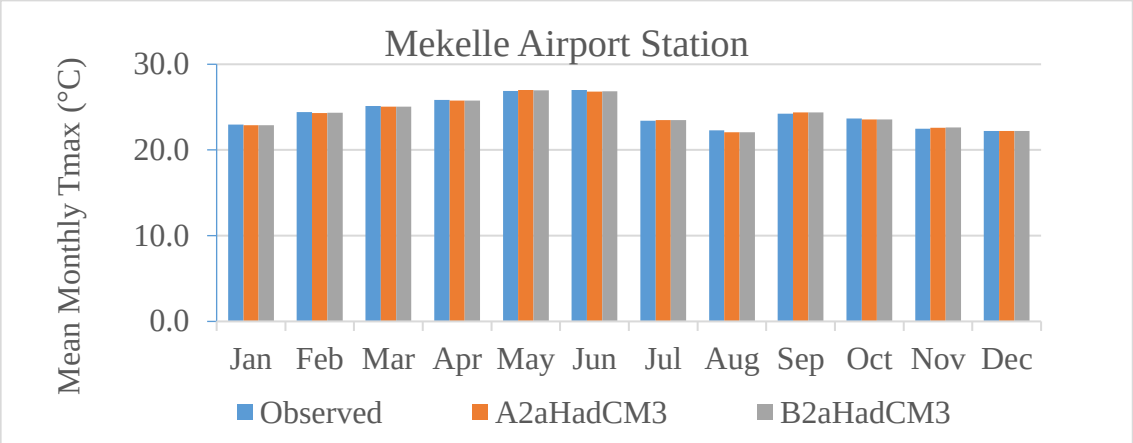

Figure**4. 1**. Observed and Downscaled Mean Monthly Tmax for Baseline (1992-2015)

Minimum Temperature

Except little variation in certain months, the projected minimum temperature of all stations for baseline period for A2a and B2a emission scenarios show good agreement with observed data. The monthly minimum temperature downscaled for both emission scenarios in the baseline period show overestimation and a model variation with the observed data on July, August, October at Wukro (Figure 4.2), in October at Mekele and July and August at Hagereselam stations and slight underestimation in June at Atsbi and in January in Hagereselam, as shown in (Appendix Figure 4).

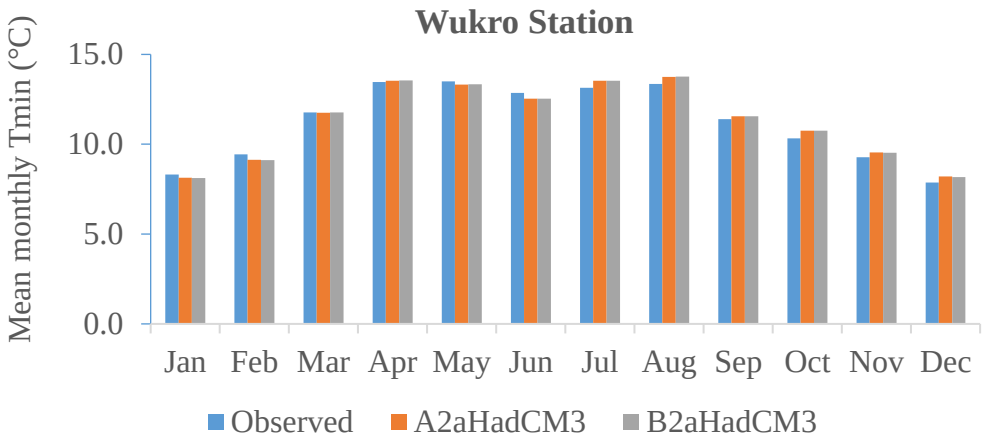

Figure**4. 2**.Observed and Downscaled Mean Monthly Tmin for Baseline (1992-2015)

Precipitation

As shown in figure 4.3, the SDSM model performs reasonably well in estimating the mean monthly precipitation in many months but there is a relatively little overestimation in the month of March and July in Hagereselam (Figure 4.3) station. There are also overestimation in months of May and July at Mekelle and in August in Atsbi station. Downscaled precipitation has slightly lower value in July at Wukro, in September at Mekelle Airport and in June and September at Atsbi (Appendix Figure 5).

The result, however, can be taken as satisfactory given that precipitation downscaling is necessarily more problematic than temperature because daily precipitation amounts at individual sites are relatively poorly resolved by regional scale predictors, rather it depends on local factors like topography.

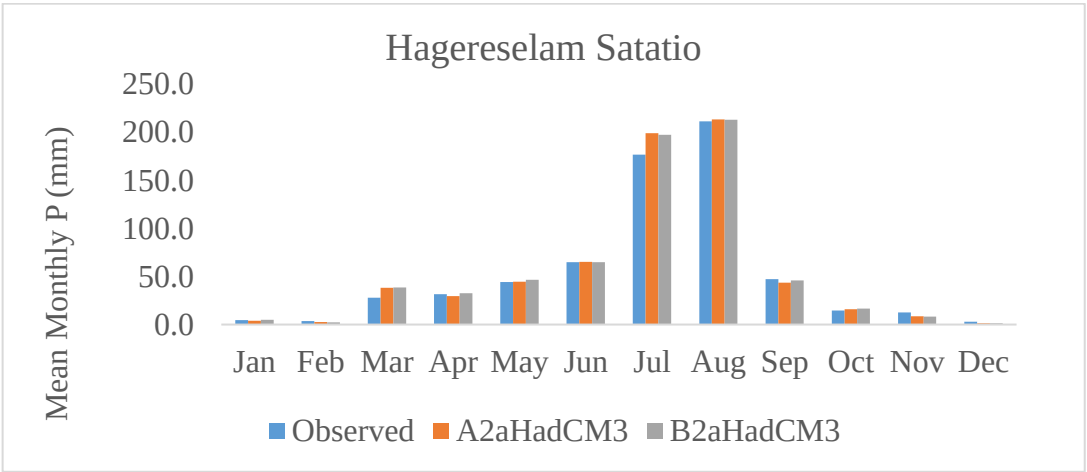

Figure **4. 3**. Observed and Downscaled Mean Monthly Precipitation (1992-2015)

Table 4. 2**.** Observed and Downscaled Mean Annual Baseline Rainfall (mm)

Stations name	Observed values	Downscaled values		Error (%)	
		A2a	B2a	A2a	B2a
Wukro	589.5	594.7	588.9	0.88	0.10
Mekelle Airport	550.4	548.6	556.0	-0.33	1.02
Hagereselam	642.5	651.4	647.9	1.39	0.84
Atsbi	525.4	540.6	526.4	2.89	0.19

4.1.3 Future Period Scenario

Maximum Temperature

For all stations, the overall analysis for the future periods of maximum temperature will show an increasing trend for both A2a and B2a emission scenarios (Figure 4.4).Atsbi station showed less increasing trend for both A2a and B2a Emission scenarios than the other stations.

The average annual maximum temperature in 2020s in Wukro, Mekele Airport, Hagereselam and Atsbi will be increased by 0.46 ºC, 0.19 ºC, 0.75 ºC and 0.12 ºC for A2a and 0.46 ºC, 0.21 ºC, 0.74 ºC and 0.13 ºC for the B2a emission scenarios respectively.

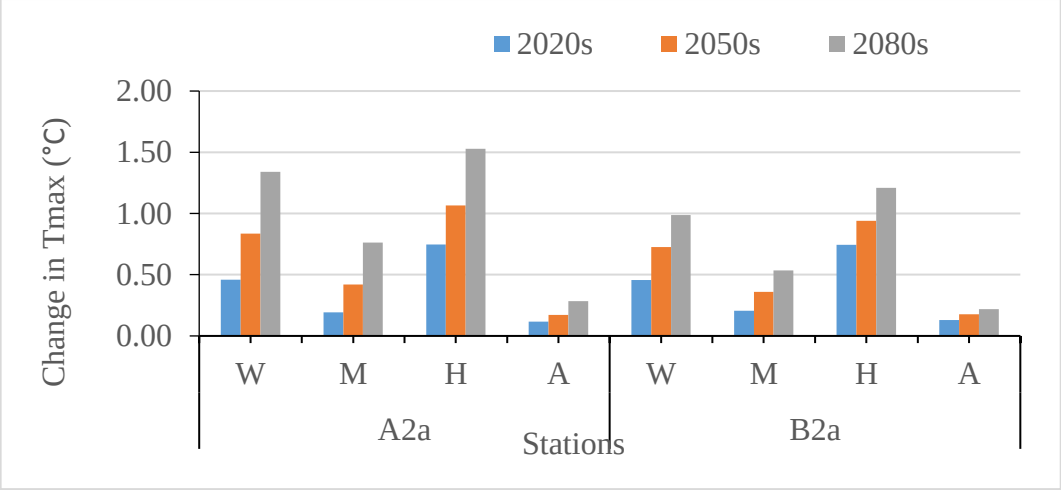

W=Wukro, M=Mekelle, H=Hagereselam, A=Atsbi

Figure **4. 4**. Change in Tmax for Future Time Horizons for A2a and B2a Scenarios.

For the 2050s the average annual maximum temperature at Wukro, Mekele Airport, Hagereselam and Atsbi will be increased by 0.83ºC, 0.42ºC, 1.07ºC and 0.17ºC for A2a and 0.73 ºC, 0.36ºC, 0.94ºC and 0.18ºC for B2a emission scenarios respectively.

For the 2080s the average annual maximum temperature increase by 1.34 ºC, 0.76 ºC, 1.53 and 0.28 ºC for A2a and 0.99 ºC, 0.54 ºC, 1.21ºC and 0.22 ºC for the case of B2a emission scenarios will be expected in Wukro, Mekele Airport And Atsbi stations respectively. There will be an overall increase by 0.99ºC and 0.72ºC for A2a and B2a emission scenarios respectively.

Mekelle Airport and Atsbi stations will not have such big difference in the trend pattern of temperature for both scenarios where as Wukro and Hagereselam stations will show an increasing trend for both emission scenarios. The average annual maximum temperature of the study area in 2020s, 2050s, and 2080s will be increased by 0.32 ºC, 0.60 ºC and 0.99 ºC for A2a and by 0.32 ºC, 0.52 ºC and 0.72 ºC in 2080s for B2a emission scenario respectively. The overall change for both scenarios of stations have been listed (Table 4.3).

Minimum Temperature

As presented in Figure 4.5, the downscaled minimum temperature in all stations, except Mekelle, show an increasing trend in all future periods for the cases of A2a and B2a emission scenarios when compared with the observed baseline.

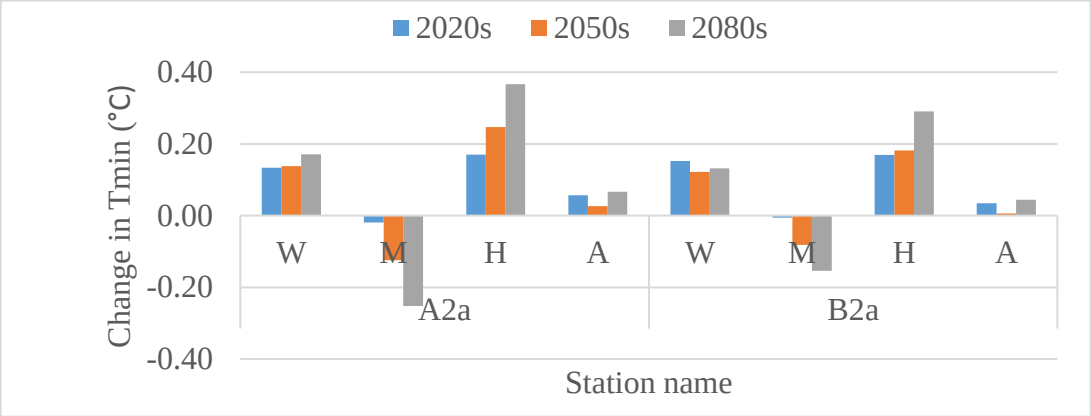

Figure **4. 5**. Change in Tmin for Future A2a and B2a Scenarios.

In Atsbi meteorological station, the average annual minimum temperature in all future time horizons will not show significant change for both of A2a and B2a emission scenarios. The increment in Hagereselam station in case of 2080s period is higher than that of 2020s and 2050s time period in bothA2a and B2a emission scenario. The average annual minimum temperature in Wukro, Hagereselam and Atsbi stations will increase by 0.15ºC, 0.26ºC, 0.05ºC and 0.14 ºC, 0.21ºC, 0.03ºC for the cases of A2a and B2a emission scenarios

respectively. Mean minimum temperature in Mekelle Airport station will decrease by 0.13 for A2a and 0.08 for B2a scenario (Table 4.3).

Precipitation

For all stations, the precipitation projection shows in many of months an increasing trend as well as decreasing (underestimation) trend also expected in a few months in an average mean precipitation in all periods (2020s, 2050s and 2080s). This is due to GCMs usually generate an estimate of the average rainfall over a large grid square for the GCM time step, but they fail to take into account localized temporal and spatial variations in rainfall which, on a smaller scale, can produce highly significant result variations (Calder, 2005). The second reason is there is an intermediate process between regional forcing and local weather (e.g., local precipitation amounts depend on wet–/dry–day occurrence, which in turn depend on regional–scale predictors such as humidity and atmospheric pressure, this results to variation (Wilby and Dawson 2004). The third reason is precipitation varies based on topography but GCM considers the pixel or grid value as an average therefore, due to this all reasons precipitation shows both an increase trend value as well as underestimation trend in a few months in all stations. This result agrees with East Africa report IPCC Projected Climate Change (Hulme et al., 2001; IPCC, 2001).

In the 2020s, precipitation in Wukro, Mekele Airport and Atsbi stations will increase by 1.8%, 0.83% and 2.05% forA2a scenario and by 4.41%, 1.12% and 2.27% for B2a scenario. Precipitation in Hagereselam will decrease for A2a scenario by 0.32% and increase for B2a scenario by 0.27%. For the 2050s, Wukro and Atsbi will increase in annual mean precipitation by 5.69%, and 2.86%for A2a scenario and 6.5% and 5.46% for B2a scenario. Precipitation in Mekelle Airport and Hagereselam stations will decrease by 0.14% and 3.19% for A2a and 0.26% and 0.96% for B2a emission scenarios.

In the 2080s, the annual mean precipitation will show an increasing trend in Wukro and Atsbi stations by 6.32%and 3.87% forA2a and 7.37% and 1.5% for B2a emission scenarios. Precipitation in Mekelle airport will increase by 1.79% for A2a scenario and no change for B2a scenario. In Hagereselam, Precipitation will be decreased by 4.0% for A2a and 0.84%for B2a scenario. The overall effect in 2020s, 2050s and 2080s will have an increase of average annual precipitation by 1.03%, 0.8% and 1.05% for the A2a scenario and 1.94%, 3.06% and 1.35% for the B2a scenario respectively (Table 4.3).The magnitude values of the emission scenarios for the future periods have been listed under (Appendix Table 4).

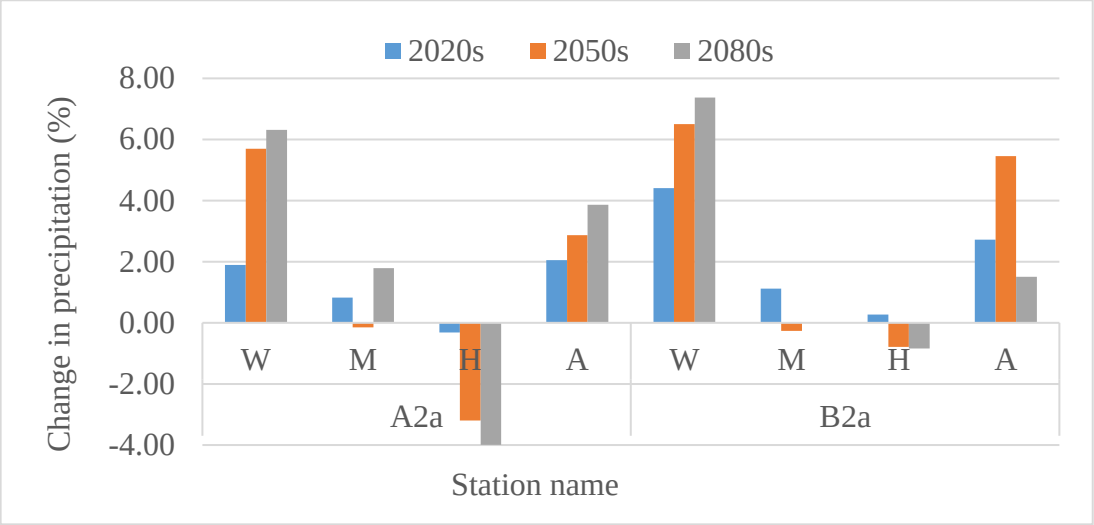

Figure**4. 6**. Change in Precipitation for Future A2a and B2a Scenarios.

Table **4. 3**. Change in Climate for Future Periods A2a and B2a Scenarios

Parameter	Period	A2a				B2a				Aerial mean	
		W	M	H	A	W	M	H	A	A2a	B2a
Precipitation change (%)	2020s	1.89	0.83	-0.32	2.05	4.41	1.12	0.27	2.72	1.03	1.94
	2050s	5.69	-0.14	-3.19	2.86	6.50	-0.26	-0.79	5.46	0.80	3.06
	2080s	6.32	1.79	-4.00	3.87	7.37	0.01	-0.84	1.50	1.05	1.35
	mean	4.63	0.82	-2.50	2.93	6.09	0.29	-0.45	3.23	0.96	2.12
PET Change (%)	2020s	2.48	1.19	4.12	0.39	2.43	1.25	4.10	0.59	2.08	2.14
	2050s	4.21	2.68	5.69	0.76	3.73	2.29	5.24	0.91	3.13	2.95
	2080s	6.55	4.86	8.03	1.33	4.95	3.43	6.43	1.04	4.64	3.65
	mean	4.41	2.91	5.94	0.83	3.71	2.32	5.26	0.84	3.28	2.91
Change in Tmax(°C)	2020s	0.46	0.19	0.75	0.12	0.46	0.21	0.74	0.13	0.32	0.32
	2050s	0.83	0.42	1.07	0.17	0.73	0.36	0.94	0.18	0.60	0.52
	2080s	1.34	0.76	1.53	0.28	0.99	0.54	1.21	0.22	0.99	0.72
	mean	0.88	0.46	1.11	0.19	0.72	0.37	0.96	0.18	0.64	0.52
Change in Tmin(°C)	2020s	0.13	-0.02	0.17	0.06	0.15	-0.01	0.17	0.03	0.07	0.08
	2050s	0.14	-0.12	0.25	0.03	0.12	-0.08	0.18	0.01	0.03	0.03
	2080s	0.17	-0.25	0.37	0.07	0.13	-0.15	0.29	0.04	0.01	0.02
	mean	0.15	-0.13	0.26	0.05	0.14	-0.08	0.21	0.03	0.04	0.04

Potential Evapotranspiration

The potential evapotranspiration of the study area will generally have an increasing trend with an average value of % for A2a and % for B2a emission scenarios in 2020s, 2050s and 2080s respectively (Figure 4.7).

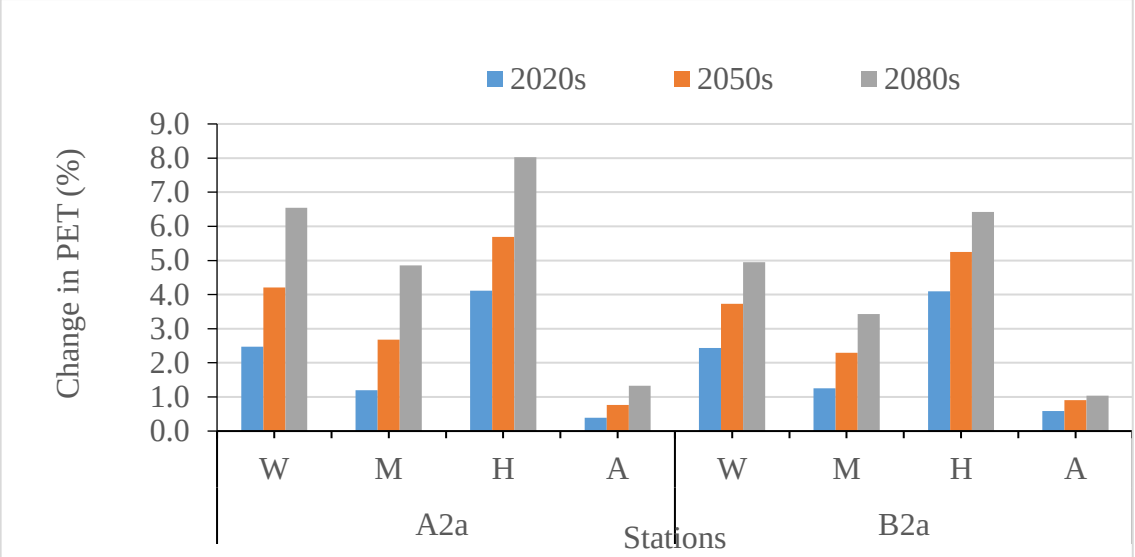

Figure 4. 7. Change in PET for A2a and B2a of the Future Time Horizons

4.2 WetSpa Model Results

4.2.1 Sensitivity Analysis for WetSpa Model Parameters

WetSpa model has eleven global model parameters. Three of them (base temperature, degree day coefficient for estimating snow melt and rainfall degree day coefficient) were not considered in this study as there is no snow in the study area. The eight parameters have observed to show to which parts of the hydrograph were the global parameters sensitive in the calibration process. Hence, the interflow scaling parameter (K_i) and Threshold for rainfall intensity (P_{max}) were very sensitive to the peak discharge used to calibrate the high flows. Whereas, the groundwater recession coefficient (K_g) and maximum groundwater storage (G_max) were sensitive to the low flow volume and used to calibrate the base flow of the hydrograph. The initial groundwater storage (Go) was sensitive to the first year of the calibration period, in this case, 1993 and the relative soil moisture (k_ss) was sensitive to the last year of the calibration period. The surface runoff coefficient (K_run) and potential evapotranspiration correction factor (K_ep) parameters were sensitive to the total discharge of the watershed.

4.2.2 WetSpa Model Calibration and Validation

The most useful list of main calibration global parameters and corresponding measurement units of WetSpa model were given in Table 4.4.

Table**4. 4.**The WetSpa Model Global Parameters Calibration Results

Parameter description	Symbol	Unit	Value range	Calibration Value
Interflow scaling parameter	k_i	-	0–12	2.515
Groundwater recession coefficient	k_g	-	0–0.06	0.00095
Relative soil moisture	k_ss	-	0-2	0.912
Correction coefficient for pet	k_ep	-	0-5	2.265
Initial groundwater storage	G0	mm	0-100	45.2
Maximum groundwater storage	G_max	mm	0-3000	2650
Base temperature	TO	°C	-	-1.0
Degree day coefficient	k_snow	mm$°C^{-1}d^{-1}$	-	-1.0
Rainfall degree day coefficient	k_rain	$°C^{-1}d^{-1}$	-	-1.0
Surface runoff coefficient	k_run	-	0-10	7.267
Threshold for rainfall intensity	Pmax	mmd^{-1}	0-500	123.4

Interflow scaling factor (ki) is a parameter for reflecting the organic matter in plants root zone associated with soil hydraulic conductivity. Groundwater flow recession coefficient (Kg) is a global parameter for reflecting catchment's groundwater recession regime. Relative soil moisture parameter (k_ss) is related to field capacity for soil moisture content. Similarly, potential evapotranspiration is associated with a correction factor k_ep and G0 is the depth of initial groundwater storage. The maximum groundwater storage parameter (G_max) is dependent on groundwater depth and k_run is an exponent for reflecting the effect of small rainfall intensity on surface runoff. Pmax is a modelling time dependent threshold for rainfall intensity.

Temperature data was not taken as input for the modelling process as snow melting and accumulation is not occurred in the watershed. Hence, the global parameters as base temperature (TO), degree day coefficient (K_snow) for estimating snow melt as well as rainfall degree day coefficient (K_rain) were set to negative one (-1) to make it nonsense by the model (Table 4.4).

The calibration and validation of WetSpa model was implemented by observing the graphical fitness between simulated and observed discharges (Figure 4.8) and through use of model performance evaluation criteria (Appendix Table 11). In both cases, the statistical and graphical comparisons of the observed and simulated discharge hydrographs have confirmed that WetSpa model was calibrated well in the modeling process. This calibration result was obtained with a repetitive trial and error method to fine-tune the global parameters within the range. Table 4.6 reveals the best fit agreement values created between observed and simulated discharges for the watershed.

The calculated model bias (C_1), model determination confidence (C_2) and Nash- Sutcliffe efficiency (C_3) results showed acceptable range when compared with the model performance evaluating measures. Based on this, the calculated values of these model performance criteria have shown very close to their optimum best fit values (Table 4.6).

So far, the hydrograph (Figure 4.8) of the model evaluation criteria of the observed and simulated discharges have showed the model has well calibrated. This ensures that model can then be used to simulate future water balance change in the watershed.

Table **4. 5.** Calibration and Validation Periods Water balance (mm)

(a) Calibration period water balance components

Component	symbol	**Calibration period (1993-1999)**					
		Observed value			Simulated value		
		sum	mean	max	sum	mean	max
Precipitation	P	4955.5	1.94	44.6	4930.8	1.93	44.45
Interception	I				533.3	0.21	1.86
Soil water storage	SD				-65.9	172.2	282.1
Infiltration (F)	F				3946.9	1.54	33.78
Evapotranspiration	ET	9552.6	3.74	5.36	4482 (actual)	1.75	8.56
Percolation	PERC				287.5	0.11	8.89
Surface runoff	SR				370.6	0.15	10.33
Interflow	IR				51.2	0.02	1.94
Groundwater flow	GR				80.9	0.03	0.12
Discharge	R	490.1	0.19	9.29	502.7	0.20	10.57
Groundwater storage	GD				17.4	31.92	121.1

(b) Validation period water balance components

Component	symbol	Validation Period (2000-2003)					
		Observed value			Simulated value		
		Sum	mean	max	sum	mean	max
Precipitation	P	2647.1	1.812	41.74	2633	1.80	41.44
Interception	I				283.3	0.19	1.86
Soil water storage	SD				-64.4	170.1	279.4
Infiltration (F)	F				2112	1.45	37.23
Evapotranspiration	ET	5651.1	3.868	5.162	2444 (actual)	1.67	8.75
Percolation	PERC				181.9	0.13	8.69
Surface runoff	SR				196.5	0.14	10.31
Interflow	IR				33	0.02	1.82
Groundwater flow	GR				59.3	0.04	0.1
Discharge	R	250	0.171	9.82	288.8	0.20	10.87
Groundwater storage	GD				-29.7	40.93	102.8

Table **4. 6.** Calibration and Validation Periods Model Performance Evaluation Results (%)

Evaluating criteria	Symbol	calibration value	validation value	Acceptable value
Model Bias	C_1	2.58	15.34	0-20
Model Confidence	C_2	88.61	96.48	50-100
Nash & Sutcliffe efficiency	C_3	82.45	93.02	50-100

Based on the values in the calibration period in Table 4.5 (a), the actual evapotranspiration, total discharge and percolation were simulated as 4482 mm, 502.7 mm and 287.5 mm which are 91%, 10.2% and 5.8% of the total precipitation (4930.8 mm) respectively and this is consistent with the findings of (Tesfamichael *et al*., 2010; Beyene *et al*., 2011) at Geba catchment, Tekeze basin of Ethiopia.

The base flow in the calibration period was produced from groundwater flow. The sum of simulated surface runoff (370.6mm), interflow (51mm) and groundwater flow (80.9 mm) produced total runoff (502.7 mm), which is nearly similar with the observed discharge value. The simulated total runoff in the dry season is almost contributed by the base flow.

The result obtained during validation also indicate the same trend except slight overestimation on total discharge (Table 4.5 (b)).

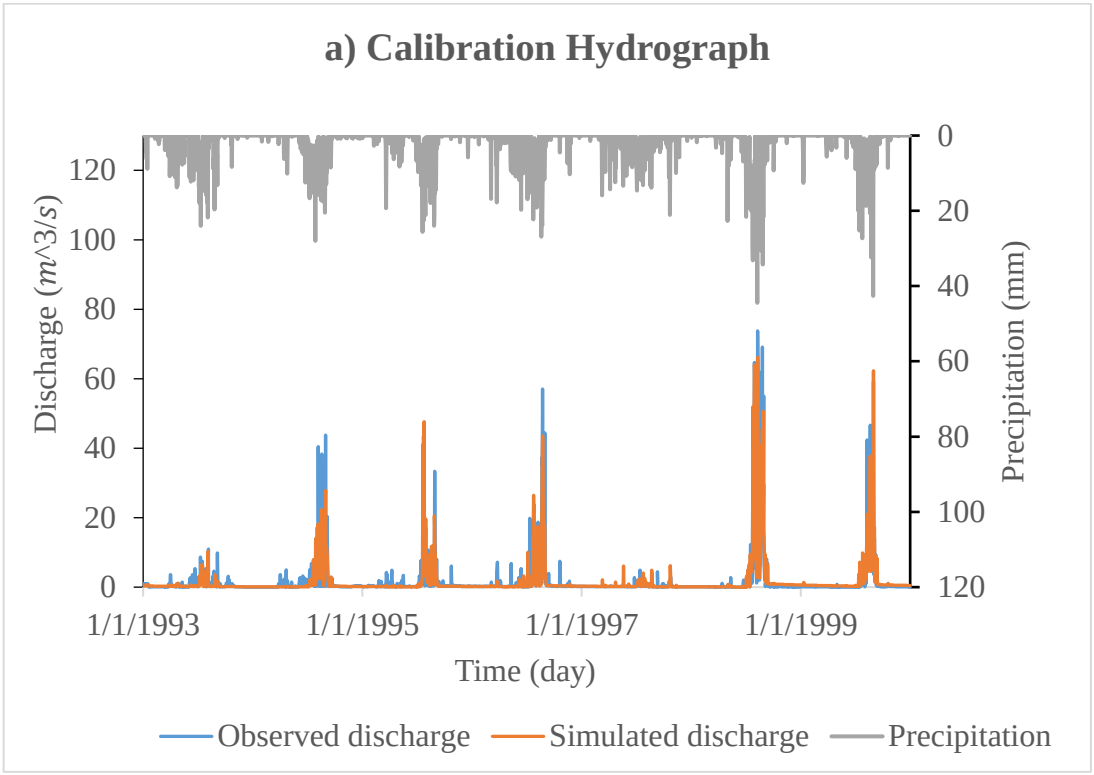

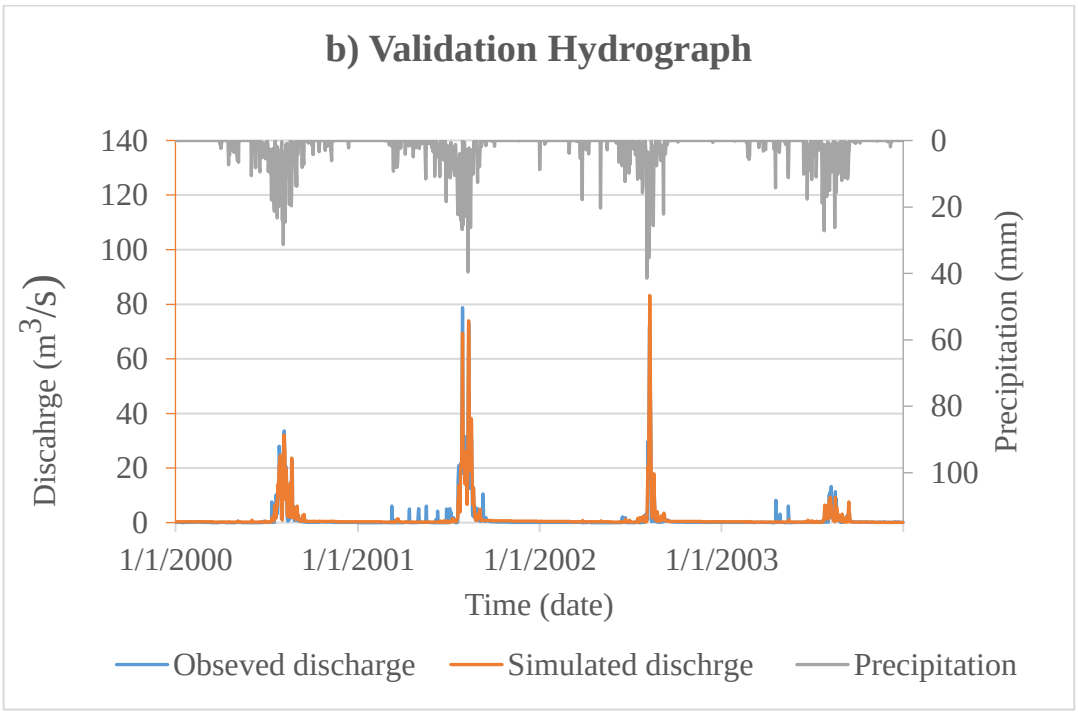

Figure **4. 8**. (a) Model Calibration Hydrograph (1/1/1993 – 1/31/1999) and (b) Model Validation Hydrograph (1/1/2000 - 1/1/2003) for Agula'e Watershed.

4.2.3 Simulation of Base Period Water Balance of Agula'e Watershed

The baseline water balance components of Agula'e watershed were estimated based on the measured and downscaled (A2a and B2a scenarios) input parameters to the model after having calibrated WetSpa model with a proper global model parameters. The measured and downscaled daily precipitation and potential evapotranspiration for the base period were used as input hydro-meteorological parameters together with the spatial watershed gridded maps of topography, land use, soil type and climatic stations from which the water balance parameters and spatial grid maps were simulated.

Total precipitation, interception, infiltration, percolation, actual evapotranspiration, surface runoff, interflow, groundwater drainage, soil moisture storage and groundwater storage were then simulated for the watershed. Hence, sum of each time step water balance components for present period were simulated. The total volume and mean values of the water balance components have been presented in Table 4.7.

Table **4. 7.**Base Period Measured and Simulated (A2a and B2a) Water Balance (mm)

Water balance components	Measured value		A2a Scenario		B2a Scenario	
	sum	mean	sum	mean	total	mean
Precipitation	13903.8	1.609	14091.1	1.631	13871.1	1.605
Interception	1434.5	0.17	3406	0.39	3369.3	0.39
Soil moist storage	-62.7	168	-64.3	167.5	-59.3	167.1
Infiltration	11418	1.322	10138.4	1.17	9974.9	1.154
Evapotranspiration	12887.5	1.492	13885	1.61	13676	1.583
Percolation	568.5	0.066	58.6	0.01	53.9	0.006
Surface runoff	840.4	0.097	289.6	0.03	275.7	0.032
Interflow	111.4	0.013	0.3	0	0.5	0
Groundwater flow	173.5	0.02	29.3	0.003	28.3	0.003
Total runoff	1125.3	0.13	319.5	0.037	304.8	0.035
Groundwater storage	-42	20.05	-42.5	3.376	-45.1	3.28

In addition to that, total runoff, actual evapotranspiration, groundwater recharge, interflow and soil moisture values were simulated as spatial distribution grid maps during the simulation. Based on the values in Table 4.7, the actual evapotranspiration and precipitation

for the baseline, and present A2a and B2a scenarios were simulated, which shows the same result as the observed value. Surface runoff and percolation of the A2a and B2a result is less than the result obtained from measured data and this is consistent with the findings of (Tesfamichael *et al*., 2010; Beyene *et al*., 2011) at Geba catchment, Tekeze basin of Ethiopia.

Total discharge values was produced from surface runoff, interflow and from groundwater flow. The sum of simulated discharge for the A2a and B2a result show underestimation when compared with the baseline value, which has similar trend with (Nyenje and Batelaan, 2009).

4.3 Climate Change Impact on Future Water Availability

The basic water balance components obtained by running the WetSpa model are stored in text and spatial grid file formats. Thus, total actual evapotranspiration, groundwater recharge, surface runoff, interflow and soil moisture contents at the outlet were simulated on a current and future time scale basis in grid formats while the remained water balances outputs were provided in text format only.

The simulated baseline (1992–2015) and future periods (2020s, 2050s, and 2080s) precipitation, actual evapotranspiration and surface runoff water balance components of bothA2a and B2aemission scenarios were illustrated in Table 4.8. These components were analyzed and presented in annual average basis. Hence, list of the main water balance components were provided and their future changes were analyzed based on the A2a and B2a emission scenarios.

From the simulated result of the WetSpa model, the future precipitation of the study area is expected to averagely increase by 0.95% for A2a and 2.12% for B2aemission scenarios. This result is consistent with the climatic projections produced by SDSM model for each of the stations in this study. The actual evapotranspiration will also increase by 7.13% for A2a and 8.89 % for B2a which showed similar projections as precipitation and temperature. This indicates as temperature and precipitation increase, actual evapotranspiration will also increase with similar trend in the time horizons keeping other conditions constant.

The surface runoff decrement in the future from the reference period is expected to be 71% for A2a and 70% for B2a SRES emission scenarios. This will occur as the increment in evapotranspiration is greater than that of precipitation in the selected time horizons. The change in temporal distribution of the total precipitation, actual evapotranspiration and surface runoff for A2a and B2a scenarios for the 2020s, 2050s and 2080s are presented in

Figures 4.8 (a), (b) and (c). The higher change for precipitation and actual evapotranspiration will be observed in2050s for B2a emission scenarios.

Generally, the precipitation and actual evapotranspiration produced for both scenarios will increase with higher change for B2a than A2a emission scenario. This result is consistent with findings of (Nyenje and Batelaan, 2009) which indicated these components will increase in the future. Hence, risk of annual flooding is limited in the watershed due to decreased amount of surface runoff in the future.

It can be concluded that the future hydrological water balance changes will happen in the watershed for the emission scenarios considered in this study. The precipitation and actual evapotranspiration will show positive increment. The surface runoff, however, will decrease due to high increase in actual evapotranspiration. The increment of actual evapotranspiration inforce to have high infiltration rate, which minimizes the surface runoff, and decrease the percolation rate, that in turn, limits the interflow and groundwater flow. As a result, there will be less discharge and flooding problems will not treat the watershed.

Table **4. 8**. Baseline and Future Period Mean Annual P, ET and SR for A2a and B2a Scenarios

Description	period	A2a			B2a		
		P	ET	SR	P	ET	SR
Observed (mm)	baseline	579.3	537	35.02	579.3	537	35.02
Simulated (mm)	2020s	585.3	577.3	11.38	590.5	582.5	11.24
	2050s	583.9	577.5	10	597	590.2	10.62
	2080s	585.3	579.9	9.1	587.1	581.3	9.671
Change (mm)	2020s	5.9	40.3	-23.6	11.2	45.6	-23.8
	2050s	4.5	40.5	-25.0	17.7	53.2	-24.4
	2080s	5.9	43.0	-25.9	7.7	44.3	-25.3
Change (%)	2020s	1.0	7.5	-67.5	1.9	8.5	-67.9
	2050s	0.8	7.5	-71.4	3.0	9.9	-69.7
	2080s	1.0	8.0	-74.0	1.3	8.3	-72.4
	Mean	0.9	7.7	-71.0	2.1	8.9	-70.0

P = Precipitation, ET = Actual evapotranspiration, SR = Surface runoff

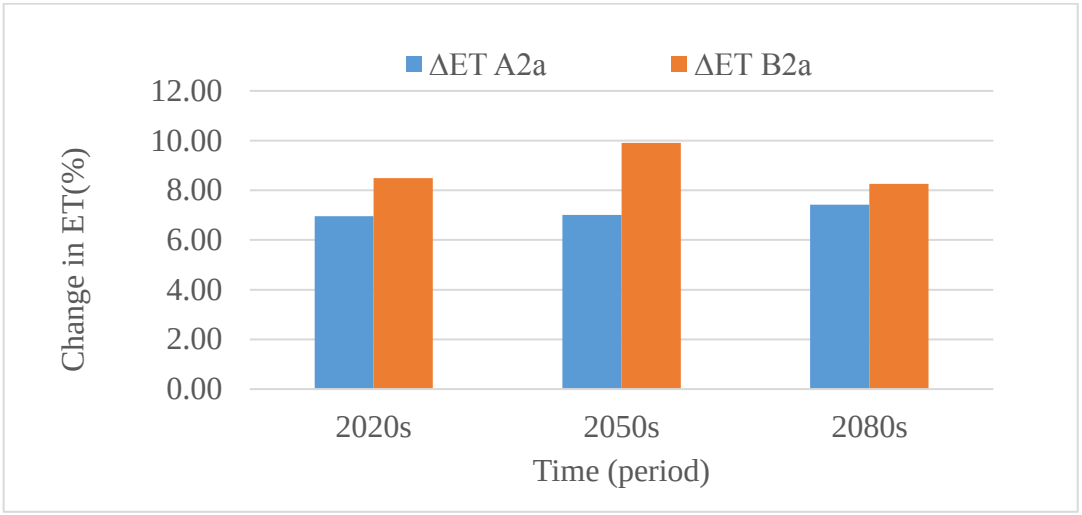

(a)

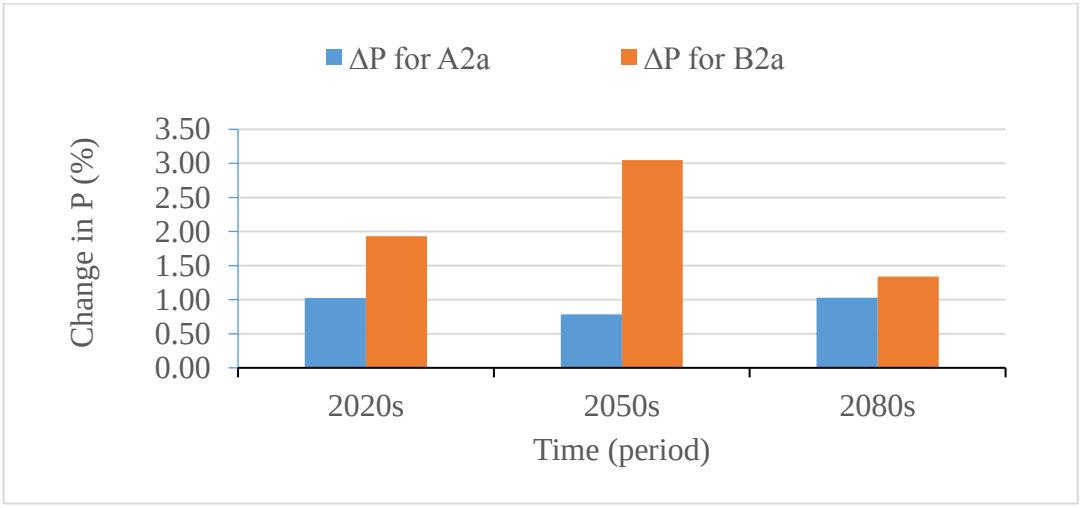

(b)

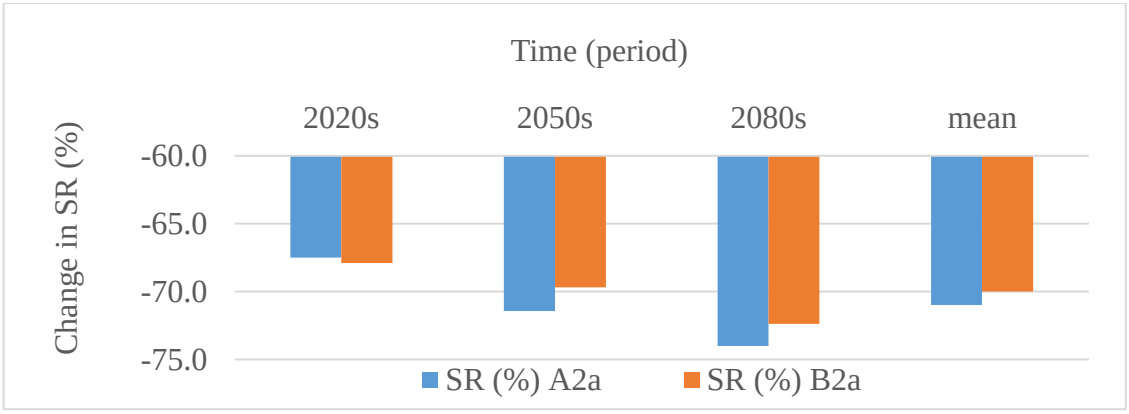

(c)

Figure **4. 9**: Change in (a) P, (b) ET, and (c) SR for A2a & B2a for Future Time Horizons.

5 CONCLUSIONS AND RECOMMENDATIONS

5.1 Conclusions

The overall objective of this thesis work was to estimate the impact of climate change on local water availability in Agula'e watershed. Based on data availability and proximity to the watershed, Wukro, Hagereselam & Mekelle Airport and Atsbi stations were used from the available meteorological stations. To investigate the future climate change impacts for the separate meteorological stations, a statistical downscaling model (SDSM) was employed to downscale the large scale GCM outputs to local scale parameters. Hence, available data of (1992-2006) and (2007-2015) of the selected stations were used separately for model calibration and validation processes respectively. Using SDSM model, precipitation, minimum and maximum temperature projections were investigated by taking large scale climatic data from HadCM3 GCM outputs. The future potential evapotranspiration was estimated based on the downscaled future maximum and minimum temperature.

A spatially distributed and grid based WetSpa hydrological model was used for investigating the spatial and temporal water balance components of the study area.

Downscaling climatic data is mainly needed to investigate present climate situations and future climate change occurred due to greenhouse gases emissions through converting coarse resolution climate data from GCM output to point or watershed level. So that, based on the local climate variables (predictands) a regional climate model GCM outputs were downscaled as predictor variables. The rainfall and maximum and minimum temperature changes that will likely occur due to changes in climate for the future periods (2020s, 2050s, and 2080s) were estimated. These projections were based on the SRES emission scenarios of A2a and B2a scenario output data for rainfall and temperature in the time defined time horizons. Hence, rainfall and temperature change projections were forecasted for Agula'e watershed based on the emission scenarios considered as indicator treatments.

When the downscaled future likely precipitation for each of the meteorological stations were compared with the present value, maximum change was observed in Wukro station (4.63 % and 6.1%) and Atsbi station (2.93% and 3.23 %)for A2a and B2a scenarios respectively. Minimum rainfall change was also observed in Mekelle station for A2a (0.84%) and B2a (0.29 %). Future precipitation in Hagereselam station will decrease by 2.5% for A2a and 0.45% for B2a emission scenario. The overall precipitation change in the study area is expected to be 0.96% for A2a and 2.12% for B2a emission scenarios. In the

future climate system, negative change in rainfall is seldom but expected to increase. In case of the change in projected maximum temperature, maximum change will be observed in Wukro station for A2a (0.88°C) and B2a (0.72°C) and Hagereselam station 1.11% (for A2a) and 0.96% (for B2a). Smaller change in maximum temperature, however, is investigated at Atsbi stations. Generally, the change in maximum temperature is expected to be in the range of 0.18°C to 1.11°Cwith average increment by 0.64°C for A2a and 0.52°C for B2a emission scenarios in the watershed.

Future change in minimum temperature were also estimated based on the calibration results for the emission scenarios. As a result, maximum change in minimum temperature is observed in Hagereselam station for A2a (0.26°c) and B2a (0.21°c). Similarly, change were investigated in Wukro and Atsbi stations for both emission scenarios. Negative change in minimum temperature will be observed in Mekelle Airport station in the future range of the study time. Generally, minimum temperature will not have significant change in the future for A2 and B2a emission scenarios.

An investigation of the available water potentials at present and future time was quantified by water balance components determination model. The main concern is to investigate the present (1992-2015) and future three time horizons (2020s, 2050s and 2080s) water resource potential of Agula'e watershed. The future change in water resource potentials was investigated after downscaling future rainfall and temperature obtained from HadCM3 GCM model.

Due to the effect of climate change, precipitation and actual evapotranspiration will averagely increase by 0.95% and 7.13% for A2a and 2.11% and 8.9% for B2ascenarios respectively. But surface runoff will decrease by71% for A2a and 70% for B2a emission scenarios.

Generally, precipitation and actual evapotranspiration will show positive increment. Whereas, the surface runoff will decrease and flooding problems will not threat the watershed.

5.2 Recommendations

- Since precipitation and temperature show positive increment in the three periods (2020s, 2050s and 2080s) people have to be aware of it and take actions as per necessary.
- The water resources potentially available in Agula'e watershed is useful for irrigation use, livestock consumption and potable water for the resident people. Wise use of these

water resources have paramount importance. Hence, exploitation of these water resources which is parallel to the water resources increment is recommended.

- The model simulation considered only future climate change scenarios assuming all other conditions constant. But change in land use scenarios, soil, management activities and other climate variables will also contribute to evapotranspiration and surface runoff variability. Therefore, it is better if consider these changes for future climate change predictions.
- Policy and technical measures should be taken to avoid or reduce the negative effect of climate change on the natural environment and also the adaptation options for minimizing the impact of climate change consequences should be developed.

REFERENCES

Adem G. and Bateman O. 2006. Modeling Groundwater-Surface Water Interaction by coupling MODFLOW with WetSpa, Geophysical Research, Vol. 8, 03181.

Allen, G. R., Pereira, L. S., Raes, D and Smith, M. 1998. ‘’Crop Evapotranspiration-Guidelines for computing crop water requirement.’’ FAO Irrigation and Drainage Paper 56. FAO, Rome, Italy, 78-86

Awulachew, S. B.; Yilma, A. D.; Loulseged, M.; Loiskandl, W., Ayana, M.; Alamirew, T. 2007.Water Resources and Irrigation Development in Ethiopia. Colombo, Sri Lanka: International Water Management Institute. 78p (Working Paper 123).

Bahremand A. & F. De Smedt, 2008. Distributed Hydrological Modeling and Sensitivity Analysis in Torysa Watershed, Slovakia, and Water Resource Manage 22:393–408

Batelaan, O., Wang, Z.M. & De Smedt, F., 1996. An adaptive GIS toolbox for hydrological modelling 3-9, eds., Kovar, K. & Nachtnebel, H.P., Application of geographic information systems in hydrology and water resources management, IAHS Publ.

Bates, B.C., Z.W. Kundzewicz, S.Wu and J.P. Palutik of, Eds., 2008: Climate Change and Water. Technical Paper of the Intergovernmental Panel on Climate Change, IPCC Secretariat, Geneva, 210 pp.

Beyene Y. Alemu, O.Batelaan and H. Goitom. 2011. Spatial and Temporal Simulation of Groundwater Recharge for Geba Catchment, Northern Ethiopia Using WetSpa, MSc. Thesis, Universiteit Gent, Vrije Universiteit Brussel, Belgium

Brooks, R. H. & Corey, A.T.1966. Properties of porous media affecting fluid flow, J. Irrig. Drain, ASCE IR2, 61–88.

Calder, I. R. (2005) Blue Revolution: *Integrated Land and Water Resource Management*, Earth scan, London.

Casper J. K., 2010. Climate Management: Solving the Problem, Bang Printing, and Brainerd, MN, United States of America.

Cunderlik M. Jurai, October 2003. Hydrologic model selection fort the CFCAS project: Assessment of Water Resource Risk and Vulnerability to Changing Climatic Conditions, Project Report I, 40pp.

De Smedt, D., 1997. Development of a continuous model for sewer system using MATLAB, MSc. Thesis, Laboratory of Hydrology, Vrije Universiteit Brussel, Belgium.

Drogue G., A. El Idrissi, L. Pfister, T. Leviandier, J.F. Iffly & L. Hoffmann, 2002. Calibration of a parsimonious rainfall-runoff model: a sensitivity analysis from local to regional scale, eds., Rizzoli A.E. & Jakeman A.J., 464-469, Integrated Assessment and Decision Support, Proceedings of the First biennal meeting of the International Environmental Modelling and Software Society, Switzerland, Vol. 1.

Eagleson, P.S, 1970. Dynamic Hydrology, 364, McGraw-Hill Pub.

Ezana, 1999. Hydrogeology and water resources development of Agula'e and Genfel catchments. EZANA Mining development private company, Tigray, Ethiopia.

FAO, 1998: Richard G. Allen, Luis S. Pereira, Dirk Raes, and Martin Smith: Crop evapotranspiration - Guidelines for computing crop water requirements - FAO Irrigation and drainage paper 56, FAO - Food and Agriculture Organization of the United Nations Rome.

George Estefan, Rolf Sammer and John Ryon, 2013. Methods of soil, plant and water analysis. A manual for the west Asia and North Africa region.

Goosse H., P.Y. Barriat, W. Lefebvre, M.F. Loutre and V. Zunz, 2013. Introduction to climate dynamics and climate modeling. Online textbook available at http://www.climate.be/textbook.

Hailemariam, Kinfe, 1999. Impact of Climate Change on the Water Resources of Awash River Basin, Ethiopia, Climate Research, International and Multidisciplinary Journal, Vol. 12: 91-96pp.

Haan, C.T., Johnson, H.P., Brakensiek, D.L. 1982. Hydrologic modeling of small watersheds. ASAE, 533 p.

Herrera-Pantoja M. and K. M. Hiscock, 2008. The effects of climate change on potential groundwater recharge in Great Britain, Hydrol. Process. 22, 73 – 86.

Holman I. P. 2006, Climate change impacts on groundwater recharge-uncertainty, short comings, and the way forward, Hydrogeology Journal, 14, 637–647.

Henderson, F.M., 1966. Open Channel Flow, 522, McMillan, New York.

Hulme, M., R. Doherty, T. Ngara, M. New, D. Lister. 2001. African climate change: 1900 – 2100. Climate Research 17: 145-168.

IPCC, 1990: *Climate Change: The IPCC Scientific Assessment*. [Houghton, J.T., G.J. Jenkins, and J.J.Ephraums (eds.)]. Cambridge University Press, Cambridge, 365 pp.

IPCC, 1996: Climate Change 1995. The Science of Climate Change. Contribution of Working Group I to the Second Assessment Report of the Intergovernmental Panel

on Climate Change. [Houghton, J.T., L.G.M.Filho, B.A. Callander, N. Harris, A. Kattenberg, and K. Maskell (eds.)]. Cambridge University Press, Cambridge, 572 pp

IPCC, Intergovernmental Panel on Climate Change (2001). Climate Change 2001. The Scientific Basis. Contribution of Working Group I to the Third Assessment Report of the Intergovernmental Panel on Climate Change. Houghton, J. T., Ding, Y., Griggs, D. J., Noguer, M., van der Linden, P. J. Dai, X., Maskell, K. and Johnson, C. A. (eds.). Cambridge, United Kingdom and New York City, NY, USA.

IPCC, Intergovernmental Panel on Climate Change (2007). Climate Change 2007: The Physical Science Basis. Contribution of Working Group I to the Fourth Assessment Report of the Intergovernmental Panel on Climate Change. Solomon, S., Qin, D., Manning, M., Chen, Z., Marquis, M., Averyt, K. B., Tignor, M. and Miller, H. L. (eds.). Cambridge, United Kingdom and New York City, NY, USA.

IPCC, 2013: Climate Change 2013: The Physical Science Basis. Contribution of Working Group I to the Fifth Assessment Report of the Inter govern-mental Panel on Climate Change [Stocker, T. F., D. Qin, G.-K. Plattner, M. Tignor, S.K. Allen, J. Boschung, A. Nauels, Y. Xia, V. Bex and P.M. Midgley (eds.)]. Cambridge University Press, Cambridge, United Kingdom and New York, NY, USA, 1535 pp.

IPCC, 2014: Climate Change 2014: Synthesis Report. Contribution of Working Groups I, II and III to the Fifth Assessment Report of the Intergovernmental Panel on Climate Change [Core Writing Team, R.K. Pachauri and L.A. Meyer (Eds.)]. IPCC, Geneva, Switzerland, 151pp.

IPCC-TGICA, 2007: General Guidelines on the Use of Scenario Data for Climate Impact and Adaptation Assessment. Version 2. Prepared by T.R. Carter on behalf of the Intergovernmental Panel on Climate Change, Task Group on Data and Scenario Support for Impact and Climate Assessment, 66 pp.

Jaroslaw Chormański, Okke Batelaan, 2011. Application of the WetSpa distributed hydrological model for catchment with significant contribution of organic soil. Upper Biebrza case study, Ann. Warsaw Univ. of Life Sci. – SGGW, Land Reclaim. 43 (1), 25–35.

Karamouz Mohammad, Ferenc Szidarovsky, Banafsheh zhraie. 2003. Water Resources System Analysis. Lewis Publishers. A Crc Press Company, Boca Raton London New York Washington, D.C.

Kebede A, Diekkrüger B, Moges S. A. 2013. An Assessment of Temperature and Precipitation Change Projections using a Regional and a Global Climate Model for the Baro-Akobo Basin, Nile Basin, Ethiopia. Earth Science Climate Change, 4: 133.

Kebede A., Diekkrueger B., Moges S., 2014. Comparative study of a physically based distributed hydrological model versus a conceptual hydrological model for assessment of Climate Change response in the Upper Nile, Baro-Akobo Basin, a case study of Sore watershed Ethiopia, International Journal of River Basin Management DOI:10.1080/15715124.2014.917315

Kim U, J.J Kaluarachchi, & V.U Smakhtin, 2008: Climate Change Impacts on Hydrology and Water Resources of the Upper Blue Nile Basin, Ethiopia, IWMI RR 126.

Laprise, R. (2008). Regional climate modelling. Journal of Computational Physics, 227(7), 3641–3666.

Lenhart, T., K. Eckhardt, N. Fohrer, H.-G. Frede, 2002. Comparison of two different approaches of sensitivity analysis, Physics and Chemistry of the Earth 27 (2002), Elsevier Science Ltd., 645–654pp.

Linsley, R.K., Kohler, J., Max A. & Paulhus, J.L.H., 1982. Hydrology for Engineers, 237, 3rd Ed., McGraw-Hill, New York.

Liu YB (2004) Development and application of a GIS-based hydrological model for flood prediction and watershed management. PhD Thesis, Vrije Universiteit Brussel, Belgium

Liu, Y.B., Gebremeskel, S, De Smedt, F, Hoffmann, L. & Pfister, L., 2003. A diffusive transport for flow routing in GIS-based flood modelling, J. Hydrol., 283, 91-106.

Liu, Y.B.,F. De Smedt a, L. Hoffmannb and L. Pfister, L., 2004. Assessing land use impacts on flood processes in complex terrain by using GIS and modeling approach, Environmental Modeling and Assessment 9: 227–235.

Liu Y.B. and De Smedt. F. 2004. WetSpa Extension, A GIS-based Hydrologic Model for Flood Prediction and Watershed Management, Documentation and User Manual, Department of Hydrology and Hydraulic Engineering Vrije Universiteit Brussels Pleinlaan 2,1050 Brussels, Belgium.

Majewski D., 1991. The Europa-Modell of the Deutscher Wetterdienst. ECMWF Seminar on Numerical Methods in Atmospheric Models, Vol 2, 147-191.

Melesse Assefa M. (Editor). 2011. Nile River Basin Hydrology, Climate and Water Use Department of Earth and Environment, Florida International University, Modesto A. Maidique Campus, Miami, FL 33199, USA.

Miller, W.A. & J.A. Cunge, 1975. Simplified equations of unsteady flow, eds., K. Mahmood & V. Yevjevich, Unsteady flow in open channels, Water Resources Publications, Fort 124Collins, CO.

Molnar P. & Ramirez, J.A., 1998. Energy dissipation theories and optimal channel characteristics of river networks, Water Resource. Res., 34, 1809-1818,

Moss Richard H., Jae A. Edmonds, Kathy A. Hibbard, Martin R. Manning, Steven K. Rose, Detlef P. van Vuuren, Timothy R. Carter, Seita Emori, Mikiko Kainuma, Tom Kram, Gerald A. Meehl, John F. B. Mitchell, Nebojsa Nakicenovic, Keywan Riahi, Steven J. Smith, onald J. Stouffer, Allison M.Thomson, John P.Weyant and Thomas J. Wilbanks, 2010. The next generation of scenarios for climate change research and assessment, Nature, Vol463, 747–756.

Nash, J.E. and Sutcliffe, J.V., 1970. River flow forecasting through conceptual model, Journal of Hydrology, 10: 282–290.

Nyenje Philip M., Batelaan Okke. 2009. Estimating the effects of climate change on groundwater recharge and base flow in the upper Ssezibwa catchment, Uganda. Hydrological Sciences Journal, 54(4).

Paeth Heiko, Thamm Hans-Peter, 2007. Regional modeling of future African climate north of 15°S including greenhouse warming and land degradation, Climatic Change, 83:401–427.

Palmer, Richard N., Erin Clancy, Nathan T. Van Rheenen, and Matthew W. Wiley, 2004. The Impacts of Climate Change on the Tualatin River Basin Water Supply: An Investigation Projected Hydrologic and Management Impacts, Draft Report. Department of Civil and Environmental Engineering, University of Washington.

Raghunath H.M. 2006. Hydrology Principles, Analysis and Design: Revised edition. New Age International Publishers, New Delhi, India.

Refsgaard, J. C., and Storm, B., 1996. MIKESHE. In Computer Models in Watershed Hydrology, 809-846. [(ed.) Singh, V. J.], Highland Ranch, Colo.

Soliman Eman S.A., M. A. Aty Sayed and Marc Jeul and, 2009. Impact Assessment of Future Climate Change for the Blue Nile Basin, Using a RCM Nested in a GCM, Nile Basin Water Engineering Scientific Magazine, Vol.2.

Tekleab S., Y. Mohamed, S. Uhlenbrook, 2013. Hydro-climatic trends in the Abay /Upper Blue Nile basin, Ethiopia, Physics and Chemistry of the Earth, 61–62, 32–42.

Tesfamichael G., De Smedt F., Miruts H., Solomon G., Kassa A., Kurkura K., Abdulwassie H., Bauer H., Nyssen J., Moeyersons J., Deckers J., Mitiku H. And Nurhussen T. 2010. Large-Scale geological mapping of the Geba basin, northern Ethiopia. Tigray Livelihood Paper No 9, VLIR – Mekelle University IUC Program, 46 pp.

Thornthwaite, C.W. and Mather, J.R., 1955. The water balance. Publ. Climatol., 8(1). Wang Z.M., Batelaan, O. and De Smedt, F. 1997. A distributed model for water and energy transfer between soil, plants and atmosphere (WetSpa), Phys. Chem. Earth, 21(3): 189-193.

Wang Z.M., Batelaan, O. and De Smedt, F. 1997. A distributed model for water and energy transfer between soil, plants and atmosphere (WetSpa), *Phys. Chem. Earth, 21(3): 189-193.*

Wilby R.L., SP Charles, E Zorita, B Timbal, P Whetton, and LO Mears, 2004. Guidelines for use of climate scenarios developed from statistical downscaling methods.

Wilby Robert L. and Christian W. Dawson, 2007. SDSM 4.2 -A decision support tool for the assessment of regional climate change impacts User Manual.

Wittenberg, H. & Sivapalan, M. 1999, Watershed groundwater balance estimation using streamflow recession analysis and base flow separation, J. Hydrol., 219, 20-33,.

Xu C.Y, Widen E., and Halldin S., 2005. Modeling hydrological consequences of climate change progress and challenges, advances in atmospheric science, 22 (6), 789-798.

Yakob Mehammed, 2009. Climate change impact assessment on soil water availability and crop yield in Anjeni watershed, Blue Nile basin, Ethiopia, MSc. Thesis, Arbaminch University Institute of Technology.

Yazew E. 2005. Development and management of irrigated lands in Tigray, Ethiopia. PhD thesis, UNESCO-IHE Institute for Water Education, Delft, the Netherlands, 265pp.

Zenebe Abreha., 2009. Assessment of Spatial and temporal variability of river discharge, sediment yield and sediment fixed nutrient export transport in Geba catchment northern Ethiopia. Pp53-56.

Zeray Abraham., 2006. Climate Change Impact on Lake Ziway Watershed Water Availability, Ethiopia, MSc Thesis, Cologne, Germany. University of Applied Science Cologne Institute of Technology for Tropics.

APPENDICES

A) Appendix Tables.

Appendix Table**1**. Location and Data Availability of Hydro Meteorological Stations

ID	station name	GPS location (m)		Elevation (m.a.s.l)	data available		% of missed data (yr)	Location relative to watershed
		Easting	Northing		From	to		
1	Atsbi	581200	1534940	2716	2000	2015	10	inside
2	Hagereselam	533434	1505715	2608	1992	2015	5	outside
3	Mekelle Airport	551768	1494659	2267	1957	2015	0	outside
4	Wukro	566515	1525145	1995	1991	2015	2	outside
5	Agula'e outlet	544099	1506599	1975	1993	2003	1	at outlet

Appendix Table2. Mean Monthly Observed Hydro Climatic Inputs for WetSpa (1993-2003)

Description	Jan	Feb	Mar	Apr	May	Jun	Jul	Aug	Sep	Oct	Nov	Dec	mean
Precipitation (mm)													
Wukro	3.5	1.6	18.8	25.9	25.4	38.0	188.9	246.1	31.9	4.6	3.4	1.4	49.1
Mekelle Airport	3.8	3.5	23.7	25.0	24.3	35.1	175.8	213.4	29.6	8.5	5.8	1.9	45.9
Hagereselam	4.5	3.5	28.1	31.7	44.2	64.9	176.8	211.4	47.3	14.7	12.5	3.0	53.6
Atsbi	3.8	3.5	23.7	25.0	24.3	35.1	175.8	213.4	29.6	8.5	5.8	1.9	45.9
Maximum Temperature (°C)													
Wukro	27.4	28.5	29.0	29.4	30.1	30.2	26.6	26.3	27.6	27.1	26.2	26.4	27.9
Mekelle Airport	23.0	24.4	25.1	25.8	26.9	27.0	23.4	22.3	24.2	23.7	22.5	22.2	24.2
Hagereselam	21.7	23.1	23.7	24.0	24.5	23.7	19.6	19.3	21.5	21.5	21.1	21.0	22.1
Atsbi	19.2	20.1	20.6	20.9	21.7	22.1	19.4	19.9	19.9	19.0	18.4	18.9	20.0
Minimum Temperature (°C)													
Wukro	8.3	9.4	11.8	13.5	13.5	12.9	13.1	13.4	11.4	10.3	9.3	7.9	11.2
Mekelle Airport	9.4	10.4	11.9	13.2	13.8	13.5	13.1	13.0	11.6	11.0	10.4	9.5	11.7
Hagereselam	9.1	9.8	11.3	12.4	13.1	12.9	12.2	12.1	11.4	10.4	9.4	8.6	11.1
Atsbi	7.1	8.0	9.4	10.7	11.2	11.1	10.8	10.8	9.5	8.6	7.7	6.8	9.3
Potential Evapotranspiration (mm)													
Wukro	135	139.9	167.0	168	179	176.0	153.8	153.1	152.6	148	127	129	152.5
Mekelle Airport	108	113.7	137.4	139	151	147.0	124.1	117.2	129.5	121	103	101	124.4
Hagereselam	103	108.8	129.0	130	138	126.7	98.8	98.7	114.2	112	100	100	113.4
Atsbi	93.4	97.1	115.2	115	124	121.6	104.1	101.5	107.0	103	88.4	89.2	105.0
Discharge(m^3/s)	4.3	2.8	7.2	9.4	7.3	13.6	128.4	302.5	40.7	10.3	4.4	3.6	44.5

Appendix Table3. Mean Monthly Observed Hydro Climatic Data for SDSM Inputs (1992-2015)

Stations	Jan	Feb	Mar	Apr	May	Jun	Jul	Aug	Sep	Oct	Nov	Dec	Monthly mean	Annual mean
Mean Monthly Observed Maximum Temperature (°C))														
Wukro	27.3	28.5	29.0	29.4	30.1	30.4	26.7	26.3	27.6	27.1	26.2	26.4	27.92	27.92
Mekelle Airport	23.1	24.4	25.2	25.8	27.0	27.0	23.4	22.5	24.3	23.8	22.6	22.3	24.29	24.29
Hagereselam	21.7	23.1	23.7	24.1	24.6	23.7	19.8	19.4	21.6	21.6	21.1	21.0	22.12	22.12
Atsbi	19.5	20.2	20.6	20.9	21.5	22.0	19.5	19.2	19.9	19.2	18.5	18.6	19.89	19.89
Aerial mean	24.7	25.9	26.4	26.9	27.8	28.0	24.5	23.9	25.4	24.8	23.8	23.8	25.50	25.50
Mean Monthly Observed Minimum Temperature (°C))														
Wukro	8.3	9.3	11.8	13.4	13.5	12.9	13.2	13.3	11.5	10.4	9.3	7.9	11.23	11.23
Mekelle Airport	9.4	10.3	11.9	13.2	13.8	13.4	13.1	13.0	11.6	10.9	10.4	9.5	11.71	11.71
Hagereselam	9.1	9.8	11.2	12.4	13.1	13.0	12.2	12.1	11.4	10.4	9.4	8.5	11.04	11.04
Atsbi	7.1	7.9	9.4	10.7	11.2	11.1	10.8	10.7	9.6	8.6	7.7	6.8	9.31	9.31
Aerial mean	8.5	9.5	11.5	13.0	13.3	12.8	12.8	12.9	11.3	10.3	9.5	8.3	11.13	11.13
Mean Monthly Observed Precipitation (mm)														
Wukro	3.5	1.6	18.8	25.9	25.4	38.0	188.9	246.1	31.9	4.6	3.4	1.4	49.13	589.50
Mekelle Airport	3.8	3.5	23.7	25.0	24.3	35.1	175.8	213.4	29.6	8.5	5.8	1.9	45.87	550.39
Hagereselam	4.5	3.5	28.1	31.7	44.2	64.9	176.8	211.4	57.3	14.7	12.5	3.0	54.37	652.48
Atsbi	3.7	1.7	19.3	25.8	25.0	34.5	160.1	206.3	36.6	4.6	6.2	1.6	43.78	525.41
Aerial mean	3.6	2.3	20.6	25.6	25.0	36.6	180.2	228.8	31.9	6.0	4.7	1.6	48.52	582.20
Mean Monthly Observed Potential Evapotranspiration (mm)														
Wukro	131.2	149.3	160.5	167.2	173.2	176.2	148.0	143.2	153.8	141.9	125.6	122.4	149.38	1792.50
Mekelle Airport	106.9	123.6	134.7	141.6	148.8	149.7	123.8	115.6	130.8	120.0	103.9	98.9	124.86	1498.27
Hagereselam	99.8	117.0	126.6	131.7	133.3	125.9	98.9	96.4	112.2	107.6	97.9	94.6	111.81	1341.67
Atsbi	92.4	104.0	111.2	114.4	117.9	121.2	104.0	101.3	106.9	97.8	87.3	85.7	103.67	1244.03
Aerial mean	99.3	113.5	122.5	127.5	132.6	134.6	127.6	107.8	117.5	108.2	95.1	92.2	113.54	1362.40

Appendix Table**4**. Mean Annual Baseline and Future Time Horizons Climatic Values for A2a and B2a Scenarios of Agula'e Watershed

Parameters	Period	A2a				B2a				Aerial mean	
		W	M	H	A	W	M	H	A	A2a	B2a
Mean Annual Precipitation (mm)	Ob	589.5	550.4	652.5	525.4	589.5	550.4	652.5	525.4	582.2	582.2
	2020s	600.6	554.9	650.4	536.2	615.5	556.6	654.2	539.7	588.2	593.5
	2050s	623.1	549.6	631.6	540.5	627.8	549.0	647.3	554.1	586.9	600.1
	2080s	626.8	560.2	626.4	545.7	632.9	550.5	647.0	533.3	588.3	590.1
	mean	616.8	554.9	636.2	540.8	625.4	552.0	649.5	542.4	587.8	594.6
Mean Annual PET (mm)	Ob	1792.5	1498.3	1341.7	1244.0	1792.5	1498.3	1341.7	1244.0	1362.4	1362.4
	2020s	1836.9	1516.1	1396.9	1248.9	1836.1	1517.0	1396.6	1251.4	1390.7	1391.6
	2050s	1867.9	1538.4	1418.0	1253.5	1859.4	1532.6	1412.0	1255.3	1405.1	1402.6
	2080s	1909.8	1571.0	1449.3	1260.6	1881.3	1549.6	1427.9	1257.0	1425.7	1412.1
	mean	1871.6	1541.9	1421.4	1254.3	1858.9	1533.1	1412.2	1254.5	1407.2	1402.1
Mean Maximum temperature (°C)	Ob	27.92	24.29	22.12	19.97	27.92	24.29	22.12	19.97	25.50	25.50
	2020s	28.36	24.41	22.81	20.01	28.35	24.42	22.81	20.02	25.77	25.78
	2050s	28.73	24.63	23.13	20.06	28.62	24.57	23.01	20.06	26.05	25.97
	2080s	29.24	24.97	23.59	20.17	28.88	24.75	23.27	20.11	26.44	26.17
	mean	28.77	24.67	23.18	20.08	28.62	24.58	23.03	20.06	26.09	25.97
Mean Minimum temperature (°C)	Ob	11.23	11.73	11.05	9.32	11.23	11.73	11.05	9.32	11.14	11.14
	2020s	11.36	11.71	11.22	9.37	11.38	11.72	11.22	9.35	11.21	11.22
	2050s	11.37	11.61	11.30	9.34	11.35	11.65	11.24	9.32	11.17	11.17
	2080s	11.40	11.48	11.42	9.38	11.36	11.58	11.34	9.36	11.15	11.16
	mean	11.38	11.60	11.32	9.37	11.36	11.65	11.27	9.34	11.17	11.18

Where W= Wukro, M = Mekelle Airport, H = Hagereselam, A = Atsbi

Appendix Table**5**. Simulated Baseline and Future Period Water Balance Components (mm) for A2a Scenario of Agula'e Watershed

Water balance components	baseline output	Simulated from downscaled inputs				Change (mm)			Change (%)			
		base period	2020s	2050s	2080s	2020s	2050s	2080s	2020s	2050s	2080s	mean
Input values												
Precipitation	13973.2	14163.9	14117.1	14084.9	14120	143.9	111.7	146.8	1.03	0.80	1.05	0.96
Potential evapotranspiration	32698.3	33188	33377.1	33721.3	34216.5	678.8	1023	1518.2	2.08	3.13	4.64	3.28
Simulated results												
Precipitation	13903.8	14091.1	14046.1	14012.4	14046.3	142.3	108.6	142.5	1.02	0.78	1.02	0.94
Interception	1434.5	3406.3	3403.5	3420.9	3425.1	1969	1986.4	1990.6	137.26	138.47	138.77	138.17
Soil moisture storage	-62.7	-64.3	-62.1	-62.9	-64	0.6	-0.2	-1.3	-0.96	0.32	2.07	0.48
Infiltration	11417.9	10138.4	10116	10108.7	10171.5	-1301.9	-1309.2	-1246.4	-11.40	-11.47	-10.92	-11.26
Actual evapotranspiration	12887.5	13885.5	13854.4	13860.2	13918.3	966.9	972.7	1030.8	7.50	7.55	8.00	7.68
Percolation	568.5	58.6	50.3	42.5	38.8	-518.2	-526	-529.7	-91.15	-92.52	-93.18	-92.28
Surface runoff	840.4	289.6	273.2	240.1	218.4	-567.2	-600.3	-622	-67.49	-71.43	-74.01	-70.98
Interflow	111.4	0.3	0.1	0.3	0.2	-111.3	-111.1	-111.2	-99.91	-99.73	-99.82	-99.82
Groundwater flow	173.5	29.3	26.5	24.5	23.3	-147	-149	-150.2	-84.73	-85.88	-86.57	-85.73
Total Discharge	1125.3	319.5	300.3	265.2	242.2	-825	-860.1	-883.1	-73.31	-76.43	-78.48	-76.07
Groundwater storage	-42	-42.5	-42.2	-44.7	-43.8	-0.2	-2.7	-1.8	0.48	6.43	4.29	3.73

Note: The (-) sign indicates the decrement in the respective value

Appendix Table**6**. Simulated Baseline and Future Period Water Balance Components (mm) for B2a Scenarios of Agula'e Watershed

Water balance components	Baseline output	Simulated result from downscaled inputs				Change (mm)			Change (%)			
		base period	2020s	2050s	2080s	2020s	2050s	2080s	2020s	2050s	2080s	mean
Inputs values												
Precipitation	13973.2	13940.9	14244.6	14401.2	14162.2	271.4	428	189	1.94	3.06	1.35	2.12
Potential evapotranspiration	32698.3	33261.9	33397.9	33661.6	33890.5	699.6	963.3	1192.2	2.14	2.95	3.65	2.91
Simulated results												
Precipitation	13903.8	13871.1	14172.6	14327.6	14089.7	268.8	423.8	185.9	1.93	3.05	1.34	2.11
Interception	1434.5	3369.3	3423.8	3441	3419.4	1989.3	2006.5	1984.9	138.68	139.87	138.37	138.97
Soil moisture storage	-62.7	-59.3	-60.9	-64.4	-61.7	1.8	-1.7	1.0	-2.87	2.71	-1.59	-0.58
Infiltration	11417.9	9974.9	10222.8	10379.8	10195.3	-1195	-1038	-1223	-10.47	-9.09	-10.71	-10.09
Actual evapotranspiration	12887.5	13675.6	13981.1	14164.1	13951.2	1093.6	1276.6	1063.7	8.49	9.91	8.25	8.88
Percolation	568.5	53.9	54.6	36.8	20.5	-513.9	-531.7	-548	-90.4	-93.5	-96.4	-93.44
Surface runoff	840.4	275.7	269.8	254.8	232.1	-570.6	-585.6	-608.3	-67.9	-69.7	-72.4	-69.99
Interflow	111.4	0.5	0.6	0	0.7	-110.8	-111.4	-110.7	-99.5	-100.0	-99.4	-99.61
Groundwater flow	173.5	28.3	27.2	23	17.4	-146.3	-150.5	-156.1	-84.3	-86.7	-90.0	-87.01
Total Discharge	1125.3	304.8	298	278.4	250.5	-827.3	-846.9	-874.8	-73.5	-75.3	-77.7	-75.51
Groundwater storage	-42	-45.1	-41	-45.1	-44.2	1	-3.1	-2.2	-2.38	7.38	5.24	2.11

Note: The (-) sign indicates the decrement in the respective value

Appendix Table**7**. Default Values of Land Use Land Cover Parameters (Wilby and Dawson, 2004)

Category	Cover	Root depth	n	I_Max	I_Min	VF	LAI_Max	LAI_Min
		cm	%	mm	mm	%	-	-
1	Closed Shrublands	8	40	25	5	80	60	10
2	Croplands	8	35	20	5	85	60	5
3	Mixed Forest	10	55	30	5	83	60	30
4	Barren or Sparsely Vegetation	5	10	10	2	5	20	5
5	Grasslands	8	30	20	5	80	20	5
6	Evergreen Needleleaf Forest	10	40	20	5	80	60	50
7	Evergreen Broadleaf Forest	10	60	30	5	90	60	50
8	Deciduous Needleleaf Forest	10	40	20	5	80	60	10
9	Deciduous Broadleaf Forest	10	80	30	5	80	60	10
10	Open Shrublands	8	40	20	5	80	60	10
11	Woody Savannah	10	50	30	5	80	60	8
12	Savannahs	8	40	20	5	80	60	5
13	Permanent Wetlands	5	50	10	2	80	60	5
14	Urban and Built-Up	5	5	0	0	0	0	0
15	Cropland / Natural Vegetation	8	35	15	5	83	40	5
16	Snow and Ice	1	5	0	0	0	0	0
17	Water Bodies	1	5	0	0	0	0	0

Where n = Manning's Coefficient, I_MAX = Maximum Interception, I_MIN = Minimum Interception, VF = Vegetation Fraction, LAI_MAX = Maximum Leaf Area Index, LAI_MIN = Minimum Leaf Area Index

Appendix Table 8. Watershed Land Use Classification Determination

Row Id	FAO Grid Code	Count	WetSpa Model Cover Class Name	WetSpa Tabular Code	WetSpa Reclass Code	WetSpa Reclass Name
0	14	47762	Croplands	2	3	Crop
1	20	51043	Croplands	2	3	Crop
2	30	120881	Grasslands	5	2	Pasture
3	60	616	Deciduous Broadleaf Forest	9	1	Forest
4	110	4650	Closed Shrublands	1	1	Forest
5	120	108	Grasslands	5	2	Pasture
6	130	7313	Closed Shrublands	1	1	Forest
7	143	766	Grasslands	5	2	Pasture
8	150	42903	Barren or Sparsely Vegetation	4	1	Forest
9	200	216	Barren or Sparsely Vegetation	4	1	Forest

Appendix Table**9**. Default Values of Soil Parameters (Wilby and Dawson, 2004)

Value	Soil texture classes	Hydraulic conductivity	Porosity	Field capacity	Wilting point	Residual moisture	Pore size distribution index
		(mmh^{-1})	(m^3m^{-3})	(m^3m^{-3})	(m^3m^{-3})	(m^3m^{-3})	(-)
1	sand	208.80	0.437	0.062	0.024	0.020	3.39
2	loamy sand	61.20	0.437	0.105	0.047	0.035	3.86
3	sandy loam	25.92	0.453	0.190	0.085	0.041	4.50
4	silt loam	13.32	0.501	0.284	0.135	0.015	4.98
5	silt	6.84	0.482	0.258	0.126	0.015	3.71
6	loam	5.58	0.463	0.232	0.116	0.027	5.77
7	sandy clay loam	4.32	0.398	0.244	0.136	0.068	7.20
8	silt clay loam	2.30	0.471	0.342	0.210	0.040	8.32
9	clay loam	1.51	0.464	0.310	0.187	0.075	8.32
10	sandy clay	1.19	0.430	0.321	0.221	0.109	9.59
11	silt clay	0.90	0.479	0.371	0.251	0.056	10.38
12	clay	0.60	0.475	0.378	0.251	0.09	12.13

Appendix Table 10. Watershed Soil Classification Determination

ID	FAO Soil Code	Count	Coarse soil Classification	Textural Ratio in %			USDA Textural Soil Class	
				Sand	Silt	Clay	Code	Name
0	Bh/3-2/3c	66461	Medium/Fine	0	65	35	8	silty clay loam
1	Ne15-3c	173807	Fine	0	40	60	12	clay
2	Qc5-1c	35997	Coarse	50	50	0	3	Sandy loam

Appendix Table11. Model Performance Evaluation Criteria

Level	C_1	C_1- C_1
Excellent	< 0.05	> 0.85
Very good	0.05 to 0.10	0.65 to 0.85
good	0.10 to 0.20	0.50 to 0.65
Poor	0.20 to 0.40	0.20 to 0.50
Very poor	> 0.40	> 0.20

B) Appendix Figures

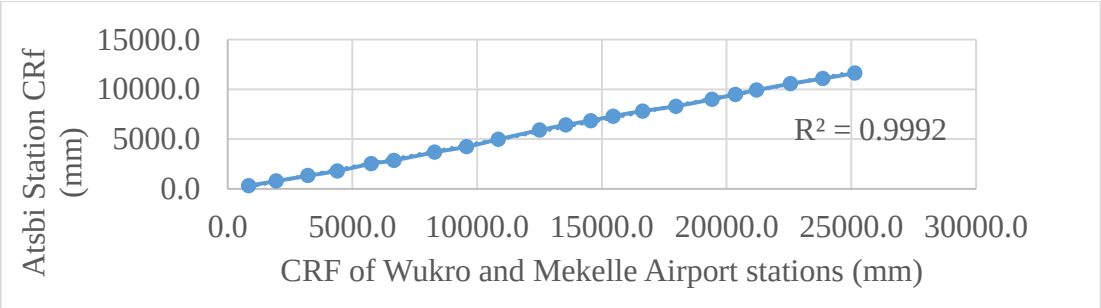

(a) Double Mass Curve of Atsbi station

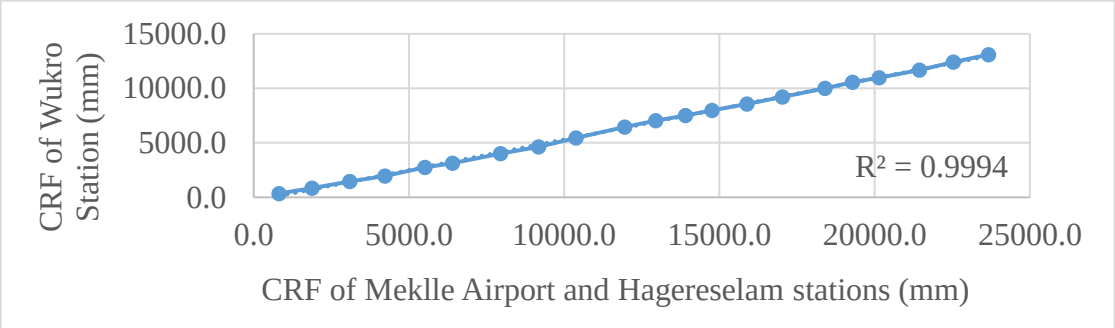

(b) Double Mass Curve of Wukro Station, CRF = Cumulative Rainfall.

Appendix Figure**1.** Double Mass Curve of Precipitation of Atsbi and Wukro.

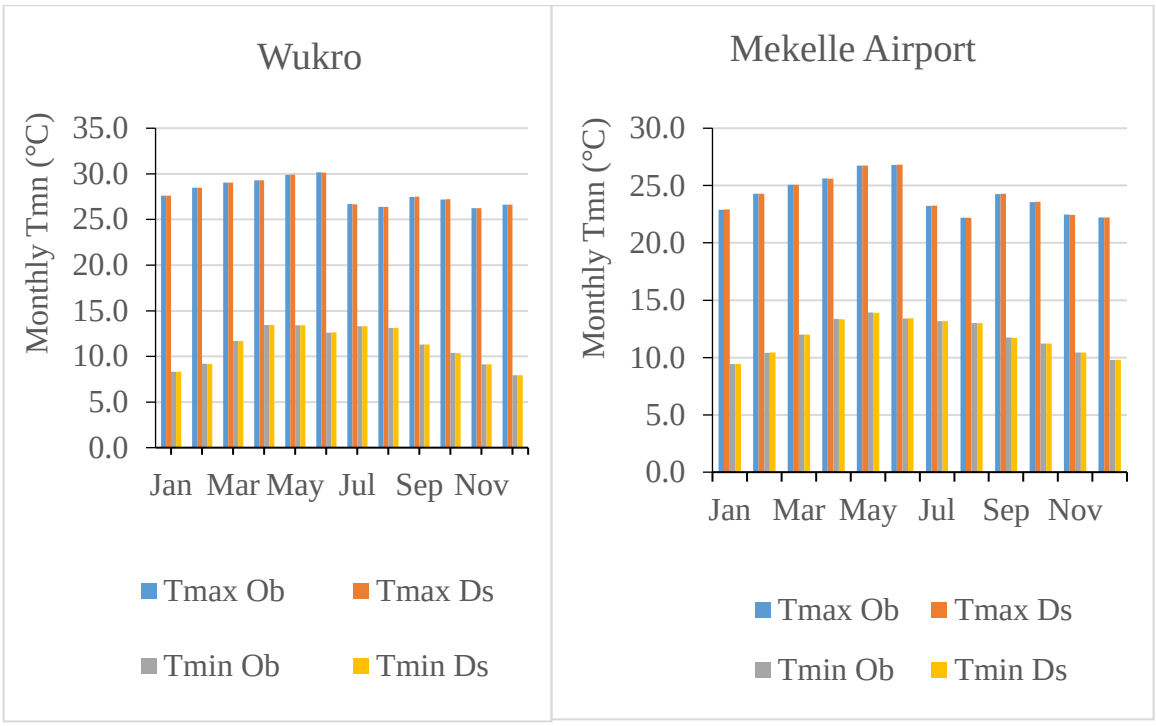

(a) Calibration Period (1992-2006)

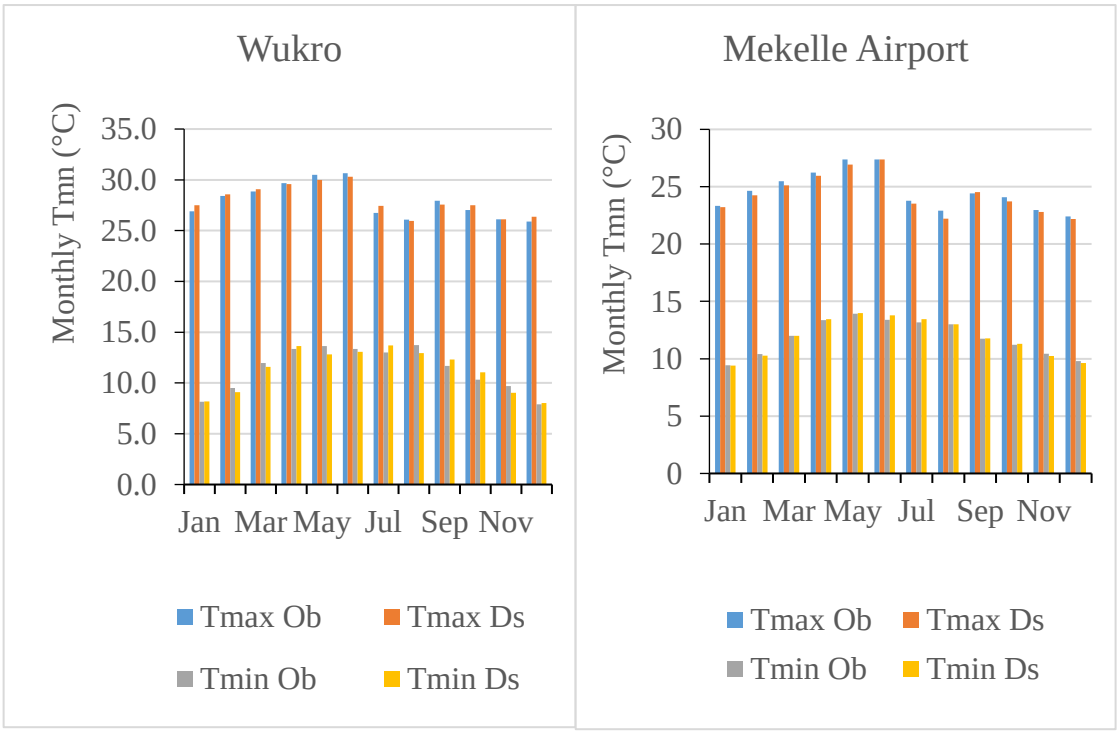

(b) Validation Period (2006-2015) Ob = Observed value, Ds = Downscaled value

Appendix Figure 2. (a) Calibration (1992-2006) and (b) Validation (2007-2015) Graph of SDSM for Tmax and Tmin for Wukro and Mekelle Airport Stations

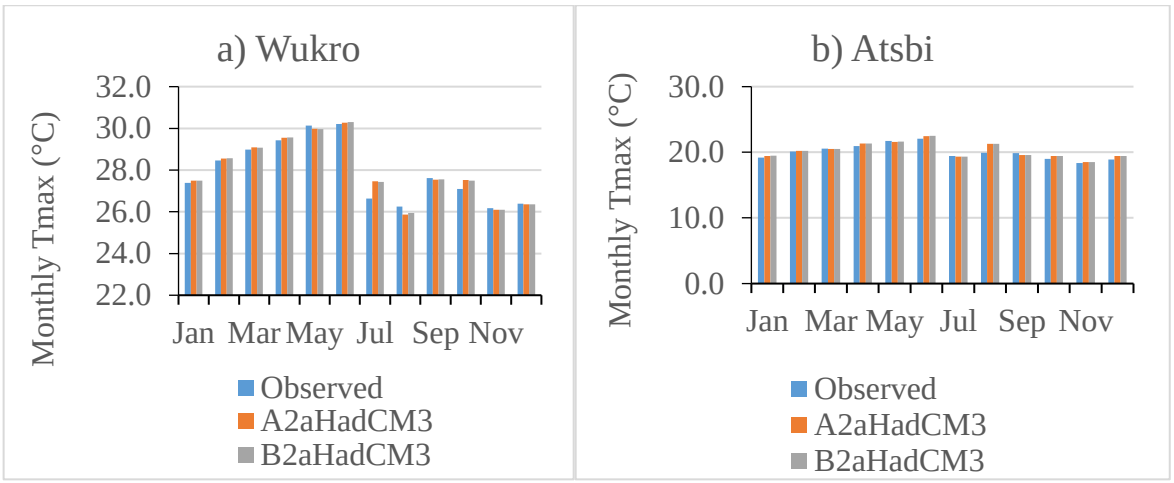

a) Mean Monthly Tmax (1992-2015)

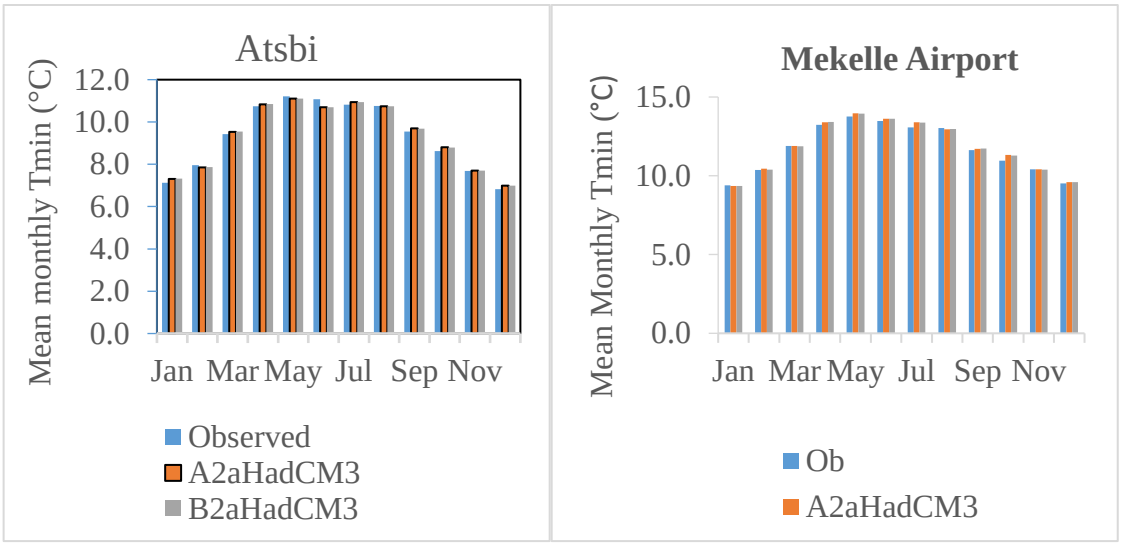

b) Mean Monthly Tmin (1992-2015)

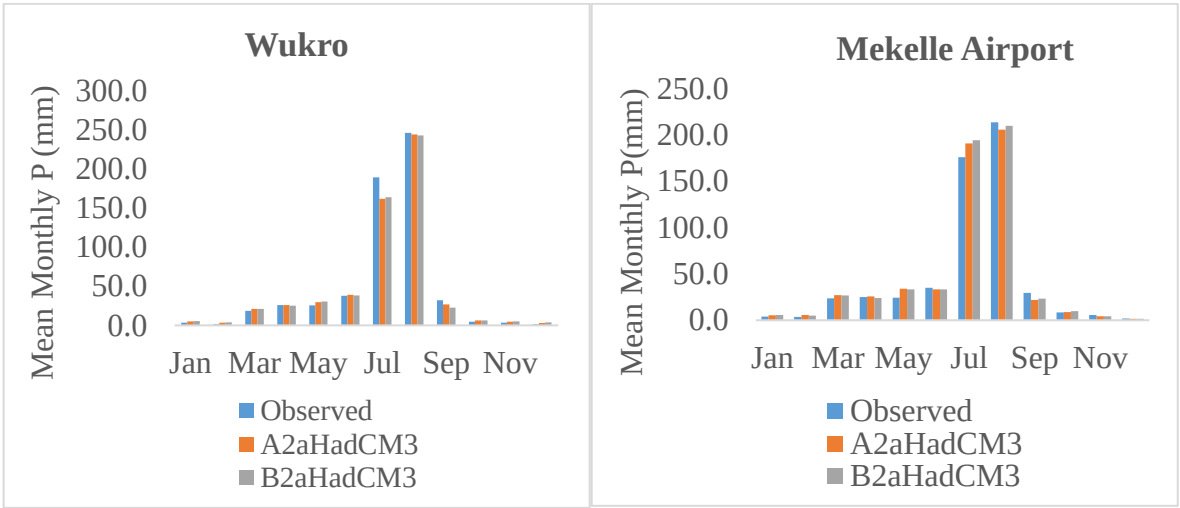

c) Mean Monthly Precipitation (1992-2015)

Appendix Figure 3. Observed and Downscaled Climatic Data (1992-2015)

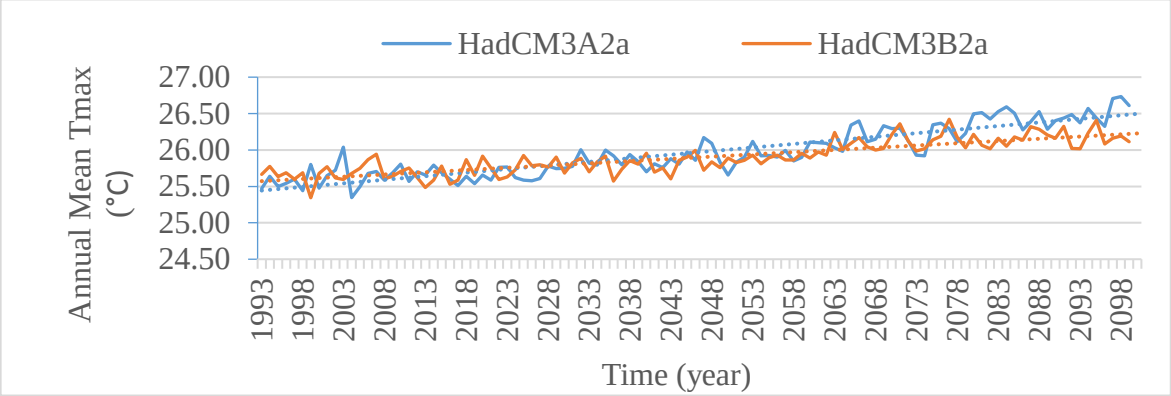

(a) Trend of Mean Annual Maximum Temperature (1992-2099)

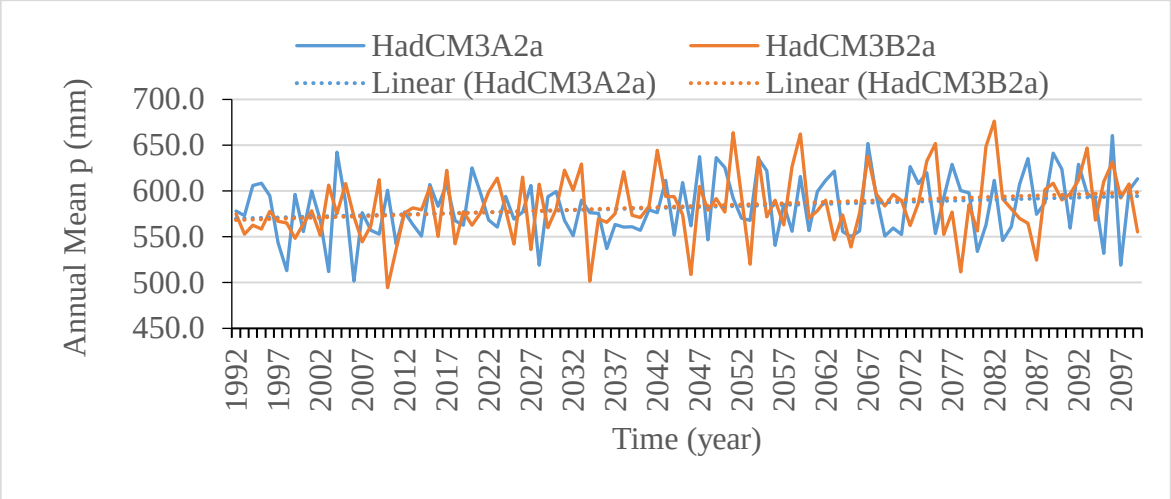

(b) Trend of Mean Annual Precipitation (1992-2099)

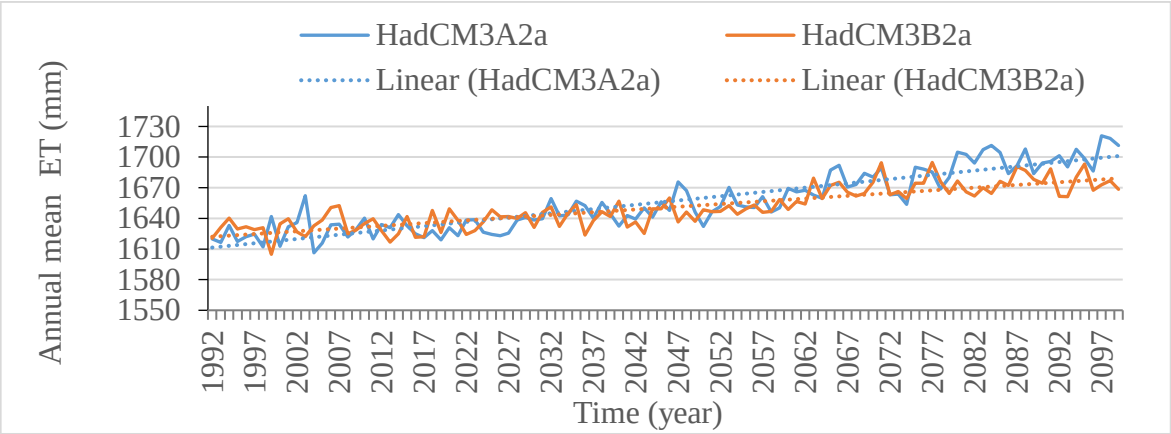

(C)Trend of Annual Mean Actual Evapotranspiration (1992-2099)

Appendix Figure4. Trends of (a) Precipitation, (b) Tmax and (C) ET for A2a and B2a Emission Scenarios for 1992-2099.

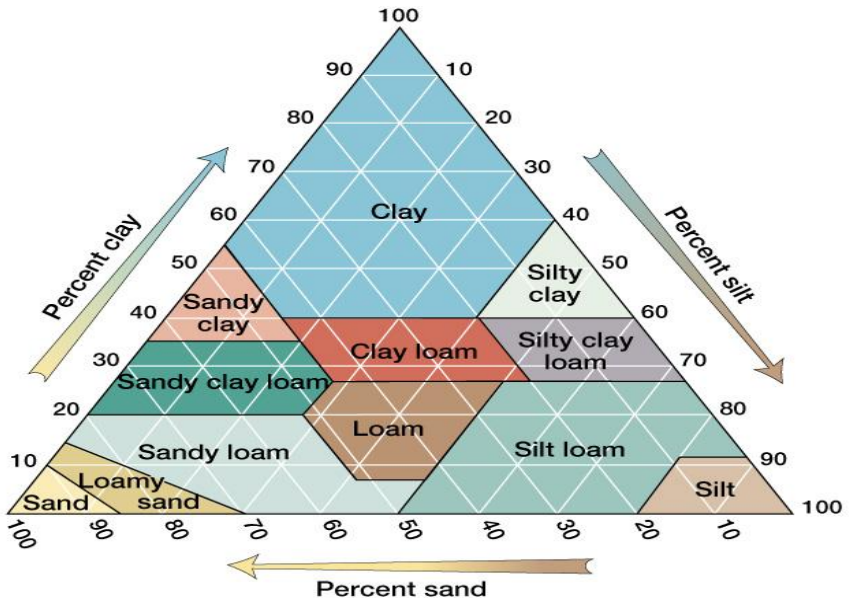

Appendix Figure5.USDA Triangular Soil Texture Classification (George et al, 2013))

C) Appendix Equations

Appendix Equation1. Estimation of Extraterrestrial Radiation (FAO56, 1998)

$$R_a = 0.408 * (\frac{24(60)}{\pi} G_s d_r [\omega_s \sin(\varphi)\sin(\delta) + \cos(\varphi)\cos(\delta)\sin(\omega_s)] \quad \text{eqn .1}$$

$$d_r = 1 + 0.033 \cos(\frac{2 * \pi * J}{365}) \quad \text{eqn .2}$$

$$\omega_s = A\cos(-\tan(\varphi) * \tan(\delta)) \quad \text{eqn .3}$$

$$\delta = 0.409 * \sin(\frac{2 * \pi * J}{365 - 1.39}) \quad \text{eqn .4}$$

$$\varphi = \frac{\pi}{180}[Latitudina \quad l\ decimal \quad \deg ree\ of\ the\ study\ site] \quad \text{eqn .5}$$

Where R_a= extraterrestrial radiation (mm/day),G_s= Solar constant = $0.082 MJm^{-2}min^{-1}$, d_r= Inverse relative distance Earth-Sun, ω_s= Sunset hour angle [rad], δ= Solar declination [rad], φ = Latitude [rad), which has positive for the northern hemisphere, J = Day of the year. The value 0.408 is the factor used to convert the unit of R_a from $MJ/m^2/day$ to mm/day.